

SOLID STATE EMISSIVE BODIPY DYES WITH BULKY SUBSTITUENTS
AS SPACERS AND
A SENSITIVE AND SELECTIVE RATIOMETRIC NEAR IR
FLUORESCENT PROBE FOR ZINC IONS BASED ON THE DISTYRYL-
BODIPY FLUOROPHORE

A THESIS
SUBMITTED TO THE MATERIALS SCIENCE AND NANOTECHNOLOGY
PROGRAM OF THE INSTITUTE OF ENGINEERING AND SCIENCES
OF BILKENT UNIVERSITY
IN PARTIAL FULFILLMENT OF THE REQUIREMENTS
FOR THE DEGREE OF
MASTER OF SCIENCE

By
TUĞBA ÖZDEMİR
July 2010

I certify that I have read this thesis and that in my opinion it is fully adequate, in scope and in quality, as a thesis of the degree of Master of Science.

.....

Prof. Dr. Engin U. Akkaya (Principal Advisor)

I certify that I have read this thesis and that in my opinion it is fully adequate, in scope and in quality, as a thesis of the degree of Master of Science.

.....

Assist. Prof. Dr. Mehmet Bayındır

I certify that I have read this thesis and that in my opinion it is fully adequate, in scope and in quality, as a thesis of the degree of Master of Science.

.....

Assist. Prof. Dr. Neslihan Şaki

Approved for the Institute of Engineering and Science:

.....

Prof. Dr. Levent Onural

Director of the Institute of Engineering and Science

ABSTRACT

SOLID STATE EMISSIVE BODIPY DYES WITH BULKY SUBSTITUENTS AS SPACERS AND A SENSITIVE AND SELECTIVE RATIOMETRIC NEAR IR FLUORESCENT PROBE FOR ZINC IONS BASED ON THE DISTYRYL-BODIPY FLUOROPHORE

Tuğba Özdemir
M.S. in Materials Science and Nanotechnology
Supervisor: Prof. Dr. Engin U. Akkaya
July, 2010

Dyes having solid state fluorescence are playing an important role for organic light emitting devices (OLED), optoelectronic devices and photoelectric conversion. However, emissive solids are not common because of the quenching resulting from the packing. With these considerations, we have synthesized and characterized novel boradiazaindacene BODIPY-based dye with bulky substituents (3,5-di-*tert*-butylphenyl) to prevent π - π stacking of the chromophore. We have successfully demonstrated that by simple modulation of BODIPY core with very bulky groups lead us to have a bright emissive compounds in solid state. In the second part of this research, we developed BODIPY based near-IR dye as a selective, ratiometric and water-soluble fluorophore for Zn (II) cation. We functionalized the versatile BODIPY from its 3 and 5 positions for long wavelength emission the zinc selective chemosensor.

Keywords: Solid state fluorescence, Stokes' shift, π - π stacking, Near-IR dyes, boradiazaindacene, chemosensor.

ÖZET

HACİMLİ GRUPLAR KULLANILARAK KATI HAL EMİSYONU OLAN BODİPY BOYARMADDELERİ VE DİSİTİRİL BOYAR MADDE BAZLI ÇİNKO İYONLARI İÇİN SEÇİCİ VE DUYARLI ORANTISAL YAKIN INFRARED FLORESANS PROBU

Tuğba Özdemir
M.S. in Materials Science and Nanotechnology
Supervisor: Prof. Dr. Engin U. Akkaya
July, 2010

Emisyonu olan katı maddeler fotoelektrik çevrim ve OLED uygulamalarını da içeren çeşitli uygulamalarından dolayı ilgi çekmektedirler. Ancak katı halde emisyon özelliği olan çok az sayıda organik bileşik vardır. Bu fikir doğrultusunda, ortogonal büyük hacimli grupların (3,5-di-*tert*-butil) BODIPY çekirdeğine yerleştirilmesi π -yüzeyleri arasındaki örtüşmeyi azaltarak sönümlenmeyi de en aza indiren bileşikler sentezlemiş bulunmaktayız. Farklı dalgaboylarında emisyonları olan bir seri katı halde emisyonlu bileşikler sentezlenmiştir. Çalışmanın ikinci kısmında, yakın-IR bölgesinde emisyonu olan, seçici, orantılamalı ve suda çözünebilen BODIPY-temelli Zn(II) katyonuna duyarlı boya geliştirmiş bulunuyoruz. BODIPY yi 3 ve 5 pozisyonlarından türevlendirerek uzun dalga boyunda emisyonu olan çinkoya duyarlı kemosensör sentezlenmiştir.

Anahtar Kelimeler: Katı hal emisyonu, Stokes kayması, π - π istiflenmesi, yakın kızılötesi boyalar, boradiazaindasen, kemosensör.

ACKNOWLEDGEMENT

I would like to express my sincere gratitudes to my supervisor Prof. Dr. Engin U. Akkaya for invaluable guidance, support, and patience during the course of this research. One of the most important and right decisions in my life is joining Prof. Akkaya's lab and being a member of such a beautiful team. I will never forget experience that I have benefited from greatly throughout my life.

I would like to thank to Dr. Serdar Atilgan for being a brother for me and for the great contribution to everything present in this thesis. I am very lucky to have a chance to work with him. His lab experience, motivation and encouragement forced me to become a good scientist. He will be in my life with her wife Neslihan and her beautiful son Eymen Kaan in perpetuity.

Also, I want to thank Dr. Leyla T. Yıldırım (Hacettepe University) for gathering the X-ray data and Dr. Abdullah Tülek and Assist. Prof. Dr. Mehmet Bayındır for providing absorption and emission spectra in thin films.

I owe a special thank to Dr. Ö. Altan Bozdemir, Dr. Ali Coşkun, Deniz Yılmaz ve Erhan Deniz for his support and guidance to improve my skills in the field of supramolecular chemistry.

I am obliged to thank each and every member of Supramolecular Chemistry Laboratory, Ruslan Guliyev, Yusuf Çakmak, Onur Büyükçakır, Sündüs Erbaş Çakmak, Barbaros Reis, Safacan Kölemen, Sencer Selçuk, Ziya Köstereli, Fazlı Sözmen, Dr. Cihan Gündüz, Bilal Kılıç, Nisa Yeşilgül, Merve Türkşanlı, Eser İden, Hande Boyacı, Yiğit Altay, Tuba Yaşar and Tuğçe Durgut for the great atmosphere in the laboratory. It is my pleasure to work with them.

My special thanks are due to Bora Bilgiç, Oya Bilgiç, Tamer Tezel, Asuman Durmuş, Görkem Günbaş and Abidin Balan for their help, support and friendships. Finally, I want to express my gratitude to my family and İlker Kütük for their love, support, and understanding.

TABLE OF CONTENTS

ABSTRACT	iii
ÖZET	iv
ACKNOWLEDGEMENT	v
TABLE OF CONTENTS	vi
LIST OF FIGURES	ix
LIST OF TABLES	xv
INTRODUCTION	1
1.1 Fluorescence	1
1.2 Stokes shift.....	4
1.3 BODIPY as a Fluorophore.....	5
1.4 Suzuki reaction	6
1.4.1 Mechanism of Suzuki coupling	7
1.4.2 Applications of Suzuki coupling	10
1.5 Sonogashira coupling.....	12
1.5.1 Mechanism of Sonogashira Reaction	14
1.5.2 Applications of the Sonogashira Reaction	15
1.6 Fluorescence in the Solid State.....	17
1.7 Fluorescent chemosensors	20
1.8 Mechanism of Sensing.....	21
1.8.1 Photoinduced Electron Transfer (PET)	22
1.8.2 Internal Charge Transfer (ICT)	23
1.9 Importance of Ratiometric Analysis	26
1.10 Di-2-picolyamine (DPA) as a selective ligand	27

1.11	Importance of Zn ²⁺ ion	27
1.12	Fluorescent Zn ²⁺ chemosensors	28
EXPERIMENTAL PROCEDURES		30
2.1	General.....	30
2.2	Experimental Part-I.....	31
2.2.1	Synthesis of Compound (3).....	31
2.2.2	Synthesis of Compound (6).....	32
2.2.3	Synthesis of Compound (7).....	33
2.2.4	Synthesis of Compound (9).....	34
2.2.5	Synthesis of Compound (10).....	35
2.2.6	Synthesis of Compound (11).....	36
2.2.7	Synthesis of Compound (13).....	37
2.2.8	Synthesis of Compound (14).....	38
2.2.9	Synthesis of Compound (15).....	39
2.3	Experimental Part-II	40
2.3.1	Synthesis of Compound (17).....	40
2.3.2	Synthesis of Compound (19).....	41
2.3.3	Synthesis of Compound (20).....	41
2.3.4	Synthesis of the Compound (21)	42
2.3.5	Synthesis of compound (22).....	43
2.3.6	Synthesis of Compound (23).....	44
2.3.7	Synthesis of Compound (26).....	45
2.3.8	Synthesis of Compound (27).....	46
2.3.9	Synthesis of Compound (28).....	47
2.3.10	Synthesis of Compound (29).....	48
RESULTS AND DISCUSSIONS		50

3.1	Solid state emissive BODIPY dyes with bulky substituents as spacers ⁷²	50
3.2	A Sensitive and Selective Ratiometric Near IR Fluorescent Probe for Zinc Ions Based on the Distyryl-Bodipy Fluorophore ⁷⁴ ,.....	61
	CONCLUSION	73
	REFERENCES	74
	APPENDIX A- NMR SPECTRA	78
	APPENDIX B- MASS SPECTRA.....	91
	APPENDIX C- X-RAY DIFFRACTION STRUCTURE ANALYSIS	97

LIST OF FIGURES

Figure 1. Types of de-activation processes of an excited fluorophore.....	1
Figure 2. Jablonski diagram ⁴	2
Figure 3. Schematic representation of Stokes shift.	5
Figure 4. The structure and numbering system of BODIPY.....	5
Figure 5. Schematic representation of Suzuki coupling.....	7
Figure 6. Advantages of Suzuki coupling.....	7
Figure 7. Mechanism of Suzuki coupling.....	8
Figure 8. Example of functionalization on carbon nanotubes with Suzuki coupling	10
Figure 9. Example of application of Suzuki coupling in the synthesis of solar cell sensitizers.....	11
Figure 10. Example of using Suzuki coupling in NLO.....	11
Figure 11. Reaction conditions of Sonogashira coupling.....	12
Figure 12. Reaction conditions of Sonogashira coupling presented by Stephens and Castro.....	12
Figure 13. Reaction conditions of Stephens and Castro, Heck and Sonogashira coupling reactions.....	13
Figure 14. Mechanism of Sonogashira coupling.....	14
Figure 15. Example of application of Sonagashira coupling in energy transfer systems reported by Akkaya <i>et al.</i>	16
Figure 16. Example of application of Sonagashira coupling in biologically active compounds.....	16
Figure 17. Example of application of Sonagashira coupling in conjugated polymers.....	17
Figure 18. Example of hindering quenching of dyes in the solid state with using of bulky groups.....	18

Figure 19. Example of hindering quenching of dyes in the solid state with organic salt with primary amine.	19
Figure 20. Example of hindered quenching of dyes in the solid state with inclusion of guest molecules in the crystalline state.	19
Figure 21. Schematic representations for the types of fluorescent molecular sensors.	21
Figure 22. Molecular orbital diagrams for reductive PET.	22
Figure 23. Some examples of PET chemosensors.	23
Figure 24. Band gap changes on interactions with cations of ICT type sensors.	25
Figure 25. Some examples of ICT chemosensors.	26
Figure 26. Some examples of DPA- based chemosensors.	29
Figure 27. Synthesis of compound 3.	31
Figure 28. Synthesis of compound 6.	32
Figure 29. Synthesis of compound 7.	33
Figure 30. Synthesis of compound 9.	34
Figure 31. Synthesis of compound 10.	35
Figure 32. Synthesis of compound 11.	36
Figure 33. Synthesis of compound 13.	37
Figure 34. Synthesis of compound 14.	38
Figure 35. Synthesis of compound 15.	39
Figure 36. Synthesis of compound 17.	40
Figure 37. Synthesis of compound 19.	41
Figure 38. Synthesis of compound 20.	41
Figure 39. Synthesis of compound 21.	42
Figure 40. Synthesis of compound 22.	43
Figure 41. Synthesis of compound 23.	44
Figure 42. Synthesis of compound 26.	45

Figure 43. Synthesis of compound 27.	46
Figure 44. Synthesis of compound 28.	47
Figure 45. Synthesis of compound 29.	48
Figure 46. Absorption spectra of the thin films (top) and the emission spectra (bottom) of the dyes 3 and 6 in solution and as thin films. The inset shows the powder form of the compounds under UV irradiation at 360 nm.	51
Figure 47. Absorbance and emission spectra of Compound 3 and 6 in CHCl ₃	53
Figure 48. ORTEP drawings of compounds 3 (top) and 6 (bottom).	54
Figure 49. Packing diagram for Compound 3.	55
Figure 50. Packing diagram for Compound 6.	56
Figure 51. Structural representations of targeted dyes.	57
Figure 52. Absorption spectra of dyes 9, 11 and 15 in CHCl ₃	58
Figure 53. Absorption spectra of dyes 9, 11 and 15 in CHCl ₃	59
Figure 54. Representation of the modulated BODIPY fluorophore as a Zn ²⁺ selective chemosensor.	61
Figure 55. Absorbance change of the dye 56 (2.5 μM) in response to different metal ions (5.0 μM) in aqueous solutions. The solutions are buffered with 0.1 M HEPES pH 7.2. 5% EtOH was added as cosolvent.	63
Figure 56. Change in the emission spectrum in response to different cations (100 μM) in aqueous medium at pH 7.2. Excitation was done at 630 nm. The solutions are buffered with 0.1 M HEPES pH 7.2. 5% EtOH was added as cosolvent.	64
Figure 57. The change in absorption spectrum of the dye 29 (2.5 μM) as a function of increasing Zn(II) concentration. Concentration of Zn(II) is varied between 0 to 100 μM.	65
Figure 58. Change in the emission spectrum of the dye 29 (2.5 μM) in response to increasing concentrations of Zn(II) in ethanol-water mixture (%5 in ethanol). Zinc concentrations were varied in the following order: 0, 0.25, 0.5, 1, 2, 5, 10, 20, 50, 100 μM. Excitation was at 630 nm, with slit widths of 5 nm.	66

Figure 59. Fluorescence intensity ratio (F_{675}/F_{730}) of 29 versus $\log [Zn^{2+}]$. The concentration of 56 was 2.5 μ M. Hill plot analysis yielded to 1:1 stoichiometry with a slope 0.97.....	67
Figure 60. Logarithmic values for the fluorescence intensity of dye at 675 nm versus $\log[Zn^{2+}]$. Hill coefficients (0.938) fits with 1:1 coordination of dye- Zn^{2+}	68
Figure 61. Curve of fluorescence intensity at 675 nm of the dye versus increasing concentration of Zn^{2+} . The concentration of the dye was 5.0 μ M. Dissociation constant was calculated as 2.0×10^{-5} M.....	68
Figure 62. Curve of fluorescence ratio of the dye at 675 nm and 730 nm (5.0 μ M) versus increasing concentration of Zn^{2+}	69
Figure 63. Digital photographs of the chemosensor solutions (5.0 μ M) in the presence of different metal ions at 100 μ M concentration. The upper plate is taken under ambient light, and the bottom one under UV illumination at 360 nm. Solvent: ethanol-aqueous buffer mixture (5% in ethanol, HEPES 0.1 M, pH=7.2).....	69
Figure 64. Normalized emission intensities at 680 nm (the emission intensity of the free dye= 1) of the chemosensor (1.2 μ M) in the presence of selected metal ions (1.0 mM). Excitation was done at 630 nm with 5 nm slit widths. Solvent: ethanol-aqueous buffer mixture (5% in ethanol, HEPES 0.1 M, pH= 7.2).	71
Figure 65. Results of the competition experiments between Zn (II) and selected metal ions. The free dye 29 (chemosensor) concentrations were set at 2.5 μ M. Excitation was at 630 nm; emission intensity values at 680 nm were collected; and all metal ions were added at 200 μ M concentration. Solvent: ethanol-aqueous buffer mixture (5% in ethanol, HEPES 0.1 M, pH=7.2).	71
Figure 66. 1H spectrum of Compound 3.....	78
Figure 67. ^{13}C spectrum of Compound 3.	78
Figure 68. 1H spectrum of Compound 6.....	79
Figure 69. ^{13}C spectrum of Compound 6.	79
Figure 70. 1H spectrum of Compound 7.....	80
Figure 71. ^{13}C spectrum of Compound 7.	80
Figure 72. 1H spectrum of Compound 9.....	81

Figure 73. ^{13}C spectrum of Compound 9.	81
Figure 74. ^1H spectrum of Compound 11.....	82
Figure 75. ^{13}C spectrum of Compound 11.	82
Figure 76. ^1H spectrum of Compound 13.....	83
Figure 77. ^1H spectrum of Compound 14.....	83
Figure 78. ^1H spectrum of Compound 15.....	84
Figure 79. ^{13}C spectrum of Compound 15.	84
Figure 80. ^1H spectrum of Compound 17.....	85
Figure 81. ^1H spectrum of Compound 19.....	85
Figure 82. ^1H spectrum of Compound 20.....	86
Figure 83. ^1H spectrum of Compound 21.....	86
Figure 84. ^1H spectrum of Compound 22.....	87
Figure 85. ^{13}C spectrum of Compound 22.	87
Figure 86. ^1H spectrum of Compound 23.....	88
Figure 87. ^{13}C spectrum of Compound 23.	88
Figure 88. ^1H spectrum of Compound 26.....	89
Figure 89. ^1H spectrum of Compound 27.....	89
Figure 90. ^1H spectrum of Compound 29.....	90
Figure 91. ^{13}C spectrum of Compound 29.	90
Figure 92. Mass spectrum of Compound 6.	91
Figure 93. Mass spectrum of Compound 9.	92
Figure 94. Mass spectrum of Compound 11.	93
Figure 95. Mass spectrum of Compound 15.	94
Figure 96. Mass spectrum of Compound 23.	95
Figure 97. Mass spectrum of Compound 28.	95
Figure 98. Mass spectrum of Compound 29.	96

Figure 99. ORTEP drawing of the molecular structure of the title compounds with the atomic numbering scheme. a) Compound 3, b) Compound 6.....	101
Figure 100. Two different views of the packing diagram of the title compound 3. Planes A, B and C are the closest near parallel π -surfaces defined as the boradiazaindacene framework.....	103
Figure 101. Packing diagram of the title compound 6. Planes A, B and C are the closest near parallel π -surfaces defined as the boradiazaindacene framework.	105
Figure 102. View of the plane defined by the bodipy π -surfaces (A) and 8-phenyl substituent (P), dihedral angle between the A and P is 84.35° and 79.56° for compound 3 and 6 respectively.	106
Figure 103. Packing diagram of the of the bodipy dye with no meso substituent studied as a reference. Dihedral angle between the A and B group planes is 17.90°	107
Figure 104. Hydrogen bonding geometry in compound 6.	108

LIST OF TABLES

Table 1. Timescale of some possible excited state processes.	3
Table 2. Quantum yield, max. absorbance, max. emission and Stokes shifts of Compound 3 and 6.	53
Table 3. Quantum yield, max. absorbance, max. emission and Stokes shifts of Compound 9, 11 and 15.	59
Table 4. Crystal data and experimental details of the title compounds.	98
Table 5. Atomic coordinates and equivalent isotropic displacement parameters for non-hydrogen atoms of compound 3.	99
Table 6. Atomic coordinates and equivalent isotropic displacement parameters for non-hydrogen atoms of compound 6.	100
Table 7. Selected bond lengths (Å) and bond angles (°).	102
Table 8. Structural parameters of hydrogen bonds between donor (D), acceptor (A) and hydrogen (H).	103
Table 9. The distance between the closest near parallel π -surfaces for compound 3.	104
Table 10. The distance between the closest near parallel π -surfaces for compound 6.	104
Table 11. The distance between the closest near parallel π -surfaces for the reference compound.	107

CHAPTER 1

INTRODUCTION

1.1 Fluorescence

At room temperature, most elementary particles are in their ground states. However, the electrons are promoted to a higher energy state namely excited state, with the irradiation by photons with proper energies of these elementary particles. There are many pathways that an excited molecule can undergo as seen in Figure 1.

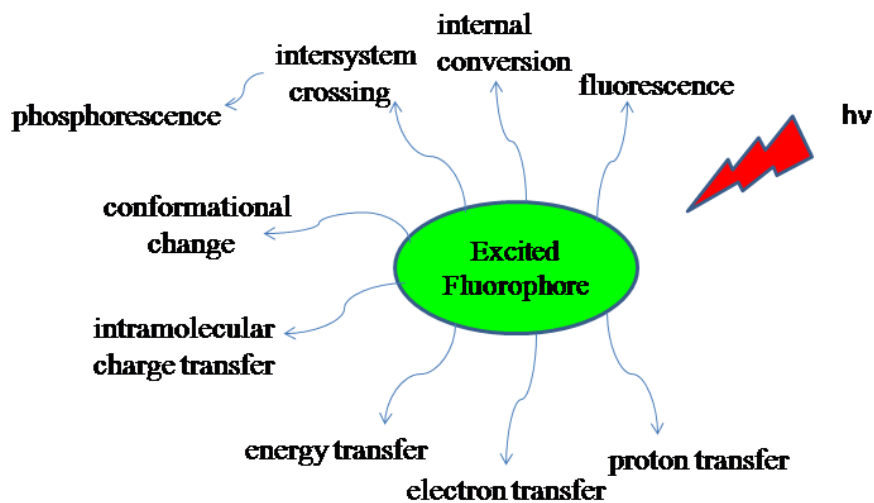


Figure 1. Types of de-activation processes of an excited fluorophore.

During the seventeenth and eighteenth centuries, luminescence phenomena was reported by several investigators but British scientist George G. Stokes was the first to describe in 1852¹ and he used the term “fluorescence” as “to denote the general appearance of a solution of sulphate of quinine and similar media”.²

If photon emission occurs as comeback of an electron from a singlet excited state to ground state, this process is termed as fluorescence. However, there are other processes for de-excitation like intersystem crossing, intramolecular charge transfer, and internal conversion. Furthermore, the excited state molecule can interact with another molecule and transfer its energy or electron or may form excimer.³

The Perrin-Jablonski diagram (Figure 2) explains possible pathways that photon absorption can cause. When a molecule absorbs light, it is promoted to one of the vibrational levels of the singlet electronic states (S_1 , S_2). If this excited molecule relaxes and turns to the vibrational state of a lower electronic state, this non-radiative transition is called as internal conversion.

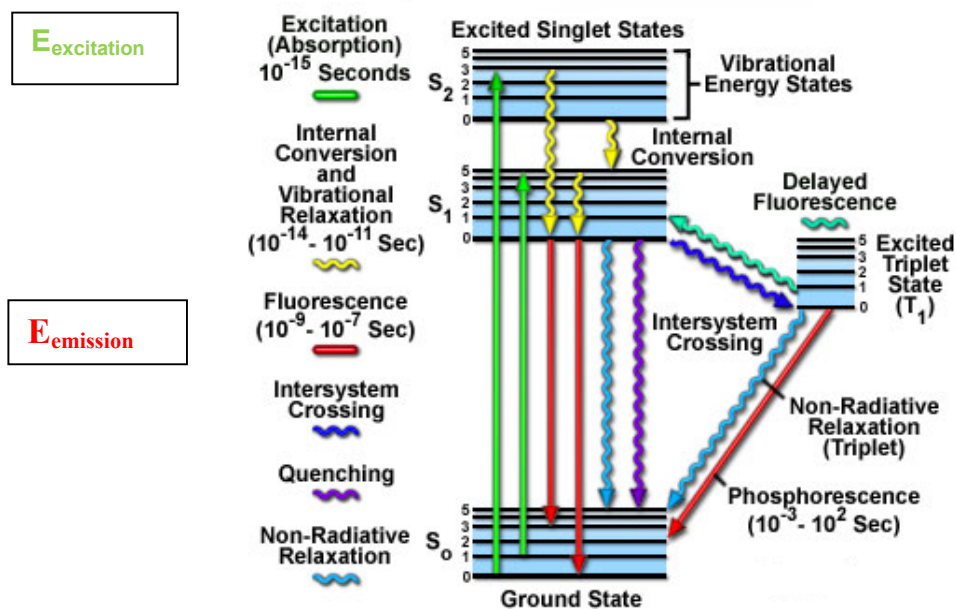


Figure 2. Jablonski diagram⁴

Internal conversion is less efficient from S_1 to S_0 , since the energy gap between S_1 and S_0 is much larger compared to S_2 and S_1 . Therefore, from S_1 to S_0 transition results emission of photons so it is called fluorescence. Another radiationless transition is intersystem crossing which occurs from excited singlet state (S_1) to the excited triplet state (T_1).

From excited triplet state (T_1), there are three possible pathways. First one is phosphorescence. This process occurs since non-radiative de-activation from the triplet state T_1 is dominant than radiative relaxation in solution at room temperature. Actually, T_1 to S_0 transition is forbidden but spin-orbit coupling allows the observation of this process. Second pathway is delayed fluorescence which is reverse intersystem crossing. The third path is the triplet-triplet transition. Since the triplet-triplet transition is spin allowed if the population of excited molecule in T_1 state is large enough, absorption occurs at a distinct wavelength by another photon.

In Table 1, timescale for fluorescence processes are given. The reason why the time of the phosphorescence is so long is the longer excited state lifetime.

Table 1. Timescale of some possible excited state processes.

Transition	Processes	Rate Constant	Timescale (s)
$S(0) \Rightarrow S(1)$ or $S(n)$	Absorption (Excitation)	Instantaneous	10^{-15}
$S(n) \Rightarrow S(1)$	Internal Conversion	$k(ic)$	10^{-14} to 10^{-10}
$S(1) \Rightarrow S(1)$	Vibrational Relaxation	$k(vr)$	10^{-12} to 10^{-10}
$S(1) \Rightarrow S(0)$	Fluorescence	$k(f)$	10^{-9} to 10^{-7}
$S(1) \Rightarrow T(1)$	Intersystem Crossing	$k(pT)$	10^{-10} to 10^{-8}
$S(1) \Rightarrow S(0)$	Non-Radiative Relaxation Quenching	$k(nr), k(q)$	10^{-7} to 10^{-5}
$T(1) \Rightarrow S(0)$	Phosphorescence	$k(p)$	10^{-3} to 100
$T(1) \Rightarrow S(0)$	Non-Radiative Relaxation Quenching	$k(nr), k(qT)$	10^{-3} to 100

1.2 Stokes shift

As stated above, when light is absorbed by a fluorophore, its electrons turn out to be excited and promoted from a ground state to the excited electronic singlet state. Every fluorophore requires different amount of energy and shown in Figure 2 as $E_{\text{excitation}}$ ⁵. Since the fluorophore is exposed to internal conformational change and releases some of its absorbed energy as heat, this state is only 1–10 nanoseconds long.

The electrons immediately after go to relaxed electronic singlet state which is a lower and more stable energy level. When the electrons in relaxed electronic singlet state turn back to their ground state, they give off the energy (E_{emission}) as fluorescence.

The distinction between the maximas of the excitation and emission wavelengths of a fluorophore is called Stokes shift (Figure 3). The reason why Stokes shift occurs is that energy of emission is fewer than the energy of absorption. In other words, fluorescence happens at lower energies.⁶ Almost all fluorophores exhibit this property when they are studied in solution. Also, molecular structure determines the magnitude of the shift and this shift can be up to several hundred nanometers.

The fall of excited electrons to the lowest vibrational energy level of the S_1 excited state, is the essential reason of the Stokes shift. Besides, excitation energy can diminish the excess vibrational energy, thermally. Resonance energy transfer, excited-state reactions and complex formation are other possible reasons of longer emission wavelengths.⁵

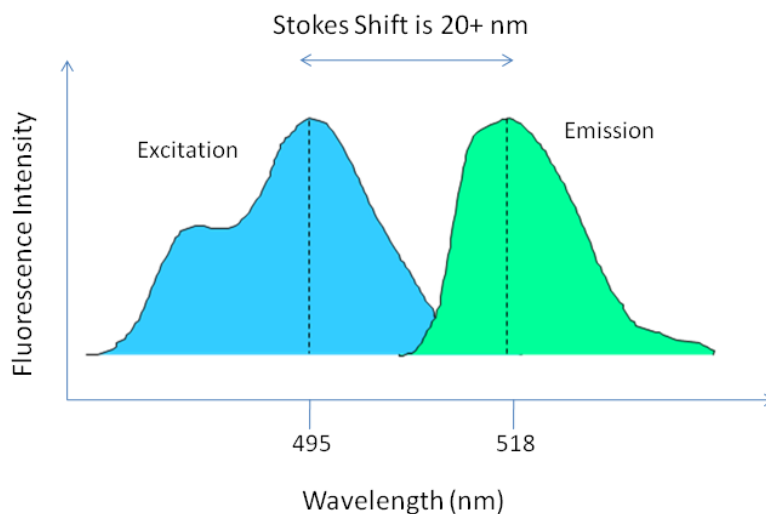


Figure 3. Schematic representation of Stokes shift.

Large Stokes shift has undeniable importance for fluorescence imaging. It allows more sensitive measurements. Also, increasing Stokes shift is very important to get solid-state emissive dyes used for different applications since it prevents self-quenching.

1.3 BODIPY as a Fluorophore

BODIPY is abbreviation of the 4,4-difluoro-4-bora-3a-aza-4a-aza-*s*-indacene. The structure and the numbering of the BODIPY core are given in Figure 4.

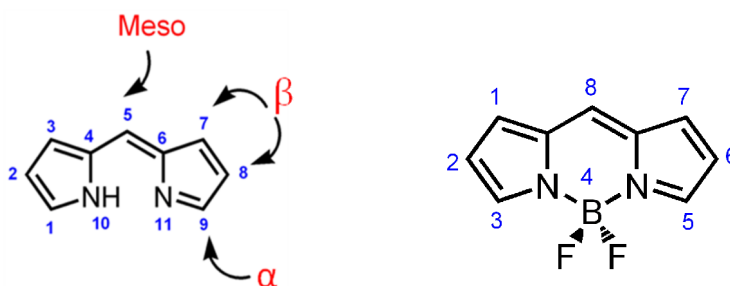


Figure 4. The structure and numbering system of BODIPY.

It is extremely useful fluorophore in many applications and Treibs and Kreuzer first discovered in 1968⁷. Last three decades, BODIPY has been used widely and it still maintains its popularity. This popularity arises because of the superior characteristics of BODIPY. To begin with, it has strong absorption and fluorescence in the visible and near-IR region⁸. Modification on the BODIPY core leads the variation on the emission range. Akkaya *et al.* reported and showed that by modification on the 1 and 7 positions with 3 and 5 positions with Knoevenagel reactions (tetra-stryryl BODIPY) allows almost 840 nm emission wavelength.⁹ In addition, BODIPY dyes can be functionalized in order for solubilization not only in organic solvents, but also in water. In other words, derivatization on the BODIPY core, which has seven positions susceptible to functionalization, provides versatile characteristics. Moreover, they have high quantum yields and large extinction coefficients and are stable under continuous illumination and almost insensitive to solvent polarity and pH of the medium^{10,11}. Furthermore, BODIPY dyes have narrow absorption and emission bandwidths, and so they give sharp peaks on emission spectra compared to other fluorophores such as fluorescein.⁵

1.4 Suzuki reaction

A useful and general methodology for the formation of carbon-carbon bonds (Figure 5) is obtained from the reaction between organoboron compounds and organic halides or triflates under the catalysis of palladium. This reaction is called Suzuki coupling.¹² In Figure 6, the advantages of Suzuki coupling reactions are shown.¹³ There are a plenty of advantages of this reactions. To illustrate, the reaction conditions are mild, unaffected by the presence of water and reagents are available. Moreover, it permits the usage of broad range of functional groups and small amount of catalyst and it is applied in one pot synthesis and gives non-toxic by-products. In addition, the waste products can be distracted readily and so it can be used both in laboratory and industrial

applications. Furthermore, it shows regio- and stereoselectivity and is not affected by the effect of steric hindrance.



Figure 5. Schematic representation of Suzuki coupling.

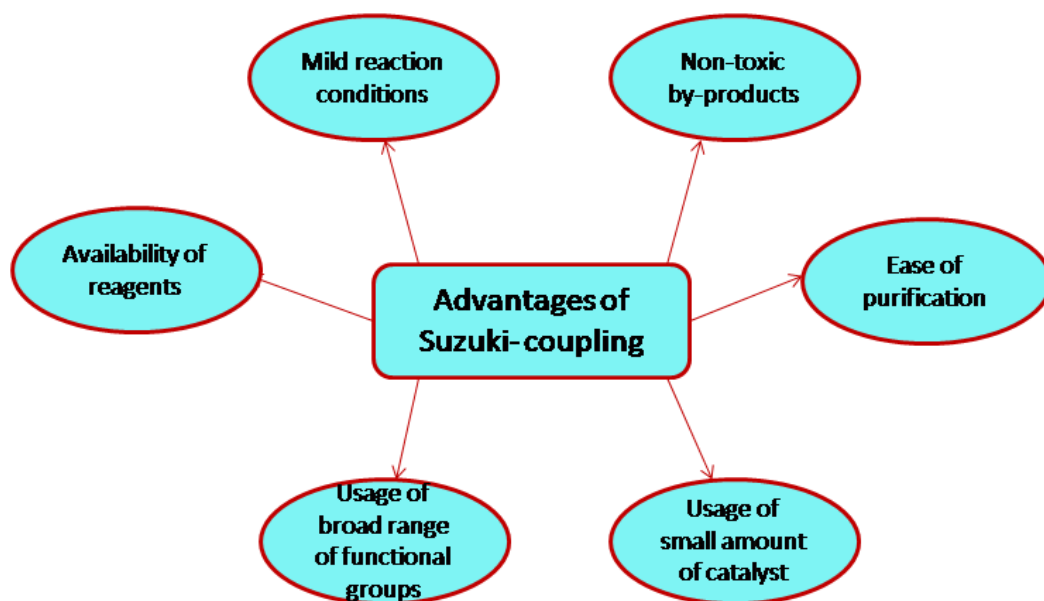


Figure 6. Advantages of Suzuki coupling.

1.4.1 Mechanism of Suzuki coupling

A widely used mechanism for Suzuki coupling reaction includes three steps which are oxidative addition, transmetalation and reductive elimination (Figure

7)¹⁴. Even though, the steps are difficult operations such as ligand exchanges, the presence of the intermediates **3** and **8** are proven by isolation or spectroscopic analyses¹⁵.

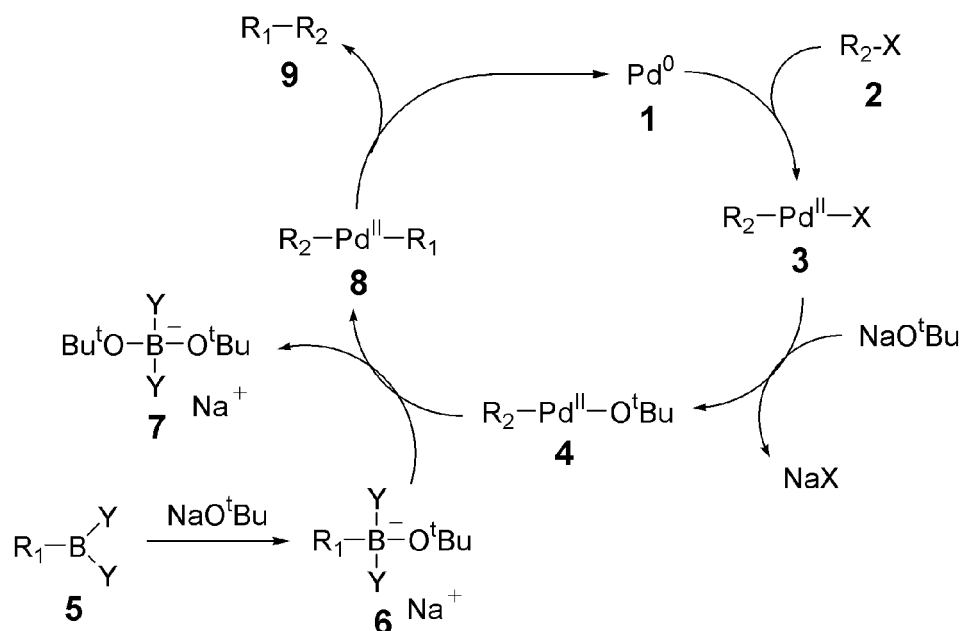


Figure 7. Mechanism of Suzuki coupling.

In Suzuki coupling reactions, various palladium (0) catalysts can be used since it can activate carbon-halogen bonds. A large number of palladium (0) catalysts can be useful in cross-coupling reaction. The most frequently employed palladium(0) catalysts are Pd(PPh₃), on the other hand, PdCl₂(PPh₃)₂, Pd(OAc)₂ and PPh₃ or phosphine derived ligands are suitable because they show resistance to air.¹⁶

Oxidation addition step 1-alkenyl, 1-alkynyl, allyl, benzyl, and aryl halides to a palladium (0) complex results a stable trans- σ -palladium (II) complex.¹⁷ In catalytic cycle, oxidative addition is generally rate-determining step.⁵ The relative reactivity order of halides is $I > OTf > Br \gg Cl$. Electron acceptors are more susceptible to the oxidative addition than electron releasing groups for activation of aryl and 1-alkenyl halides. Also, characterization of oxidative addition which involves oxidation of metal is performed by electrochemical techniques (steady state voltametry, cyclic voltametry).¹⁸

Due to being inert to the organopalladium(II) halides, organoboron compounds do not generally take part in catalytic cycle, but, low nucleophile strength of organic group on boron atom can be overcome by negatively charged bases such as sodium or potassium carbonate, phosphate, hydroxide, and alkoxide¹⁹ since these bases allow quaternization of the boron giving the corresponding “ate” complex which is more likely to undergo Suzuki coupling with organic halide.²⁰ Transmetalation step is less known since the mechanism depends on the media and environment where the reaction takes place.⁵

As mentioned above, third step in catalytic cycle of Suzuki coupling is reductive elimination. In this step, the palladium(0) complex is reproduced and the reaction occurs from *cis* complex and the *trans* complex is converted to *cis*-complex. The reactivity decreases in the order of diaryl- > (alkyl) aryl- > dipropyl- > diethyl- > dimethylpalladium(II). This can be explained by involvement by the π -orbital of aryl group while the bond is forming.²¹

The difference between the Suzuki and Stille couplings, in which both couplings allows C-C bond formation, is that the boronic acid must be activated with a base since the base converts the borane (BR_3) into boronate ($BR_3(OH)^-$) which is more reactive. Hence, activation of the boron atom promotes the transmetalation step by increasing the polarization of the organic ligand.

1.4.2 Applications of Suzuki coupling

Suzuki coupling reactions have high impact on chemistry and there are lots of application areas. Some of the examples are given to realize the importance of Suzuki coupling reactions.

To begin with, Suzuki coupling is used to functionalize carbon nanotubes which have excellent electronic and mechanical characteristics. With carbon nanotubes, non-covalent and covalent functionalizations are possible. For covalent modulations, Suzuki coupling can be used the derivatization of the walls of carbon nanotubes. As seen in the below (Figure 8), carbon nanotubes are functionalized with chromophores (Ar groups in the Figure 8) by using Suzuki coupling²².

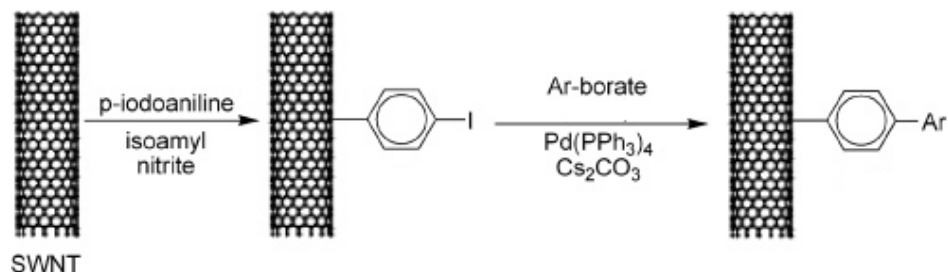


Figure 8. Example of functionalization on carbon nanotubes with Suzuki coupling.

Another application area of Suzuki coupling is in solar cell. This technology is crucial for being alternative to petroleum-based energy which is subject to depletion. In photovoltaic devices, poly(2,7-carbazole) derivatives are utilized as active constituents and Suzuki coupling is used for the synthesis of this polymer (Figure 9).²³

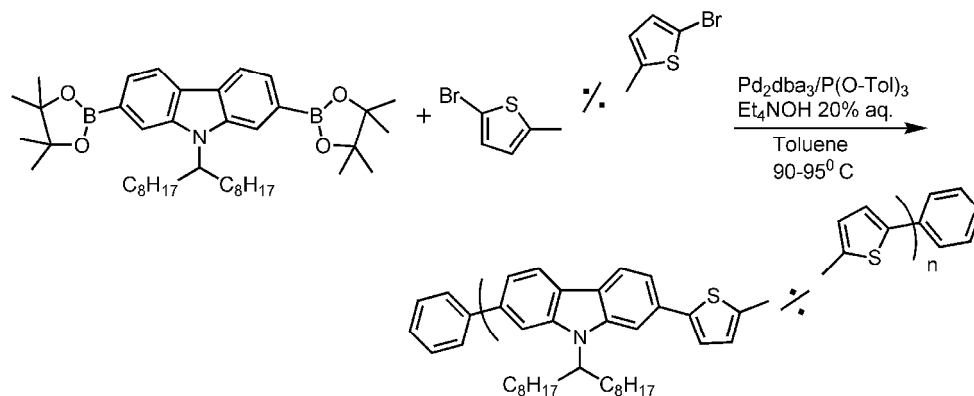


Figure 9. Example of application of Suzuki coupling in the synthesis of solar cell sensitizers.

Nonlinear optics (NLO) is the other application of Suzuki coupling reactions. NLO is the field of optics and deals with the action of light in non-linear media. NLO is very important since in the future, photonics might replace electronics. Therefore, connecting electron donor group with electron-withdrawing group can be achieved by Suzuki coupling reactions as in the example of 1,8-di(hetero)arylnaphthalene derivative (Figure 10).²⁴

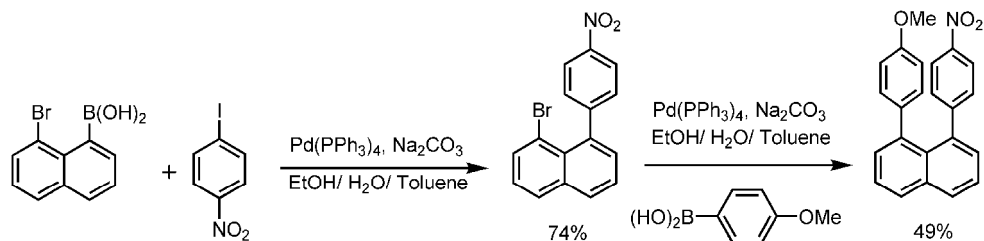


Figure 10. Example of using Suzuki coupling in NLO.

1.5 Sonogashira coupling

Sonogashira reaction is the coupling of terminal alkynes with aryl or vinyl halides by catalysis of palladium (Figure 11). Like Suzuki coupling, a base is required for the progression of the reaction, but, a co-catalyst such as copper iodide is used in sonogashira coupling which is not the case in Suzuki coupling.

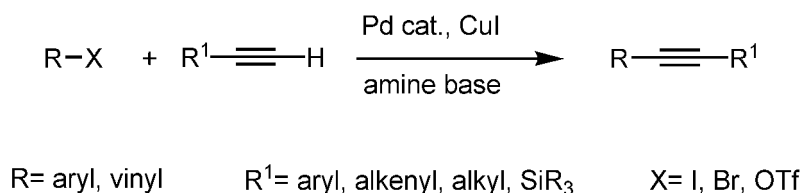


Figure 11. Reaction conditions of Sonogashira coupling.

Sonogashira coupling has been improved in 1975 by different groups as shown in Stephens and Castro²⁵ indicated under reflux in pyridine Pd catalyzed Stephens-Castro cross-coupling reaction of aryl halides with alkynylcopper to prepare internal arylacetylenes known as the Stephens-Castro reaction.

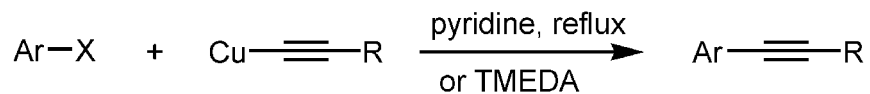


Figure 12. Reaction conditions of Sonogashira coupling presented by Stephens and Castro.

Cassar²⁶ demonstrated that the Pd-catalyzed cross-coupling reaction of aryl bromides and iodides with sodium acetylides generated in situ by mixing terminal alkynes with NaOMe in DMF (Figure 13). After that, Heck²⁷ showed

that by using Pd-complex and a base, aryl and vinyl halides undergo cross-coupling with terminal acetylenes (Figure 13). Then, Sonogashira²⁸ used CuI as a co-catalyst and an amine base as a solvent and reactant to make conditions milder and perform the reaction smoothly and now it is called as Sonogashira reaction (Figure 13). This coupling reaction is very useful for alkyne cross-coupling since it is simple to prepare starting material and conditions are mild even it gets more milder conditions for unactivated organic electrophiles. Furthermore, Sonogashira coupling is capable of tolerating various functional groups and modifications can be done to improve yields and to overcome difficulties with the cross-coupling reactions.

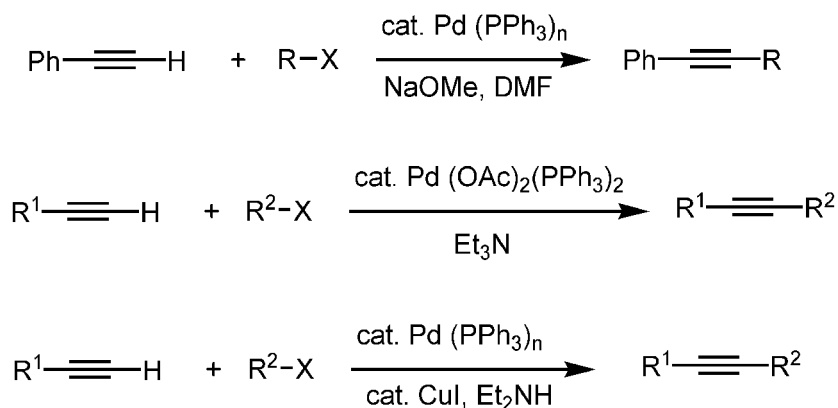


Figure 13. Reaction conditions of Stephens and Castro, Heck and Sonogashira coupling reactions.

1.5.1 Mechanism of Sonogashira Reaction

The mechanism of Sonogashira coupling (Figure 14) is similar to Suzuki coupling. It has three main steps: oxidative addition, transmetalation and reductive elimination. Since the steps are given in details above, these steps are not explained here deeply. Organic halide gives oxidative addition to form Pd(II) complex and this intermediate undergoes transmetalation with alkynyl copper which is formed by from the terminal alkyne, base, and copper iodide. With the coupling of two organic ligands, Pd(0) catalyst is obtained and so reductive elimination step is terminated.

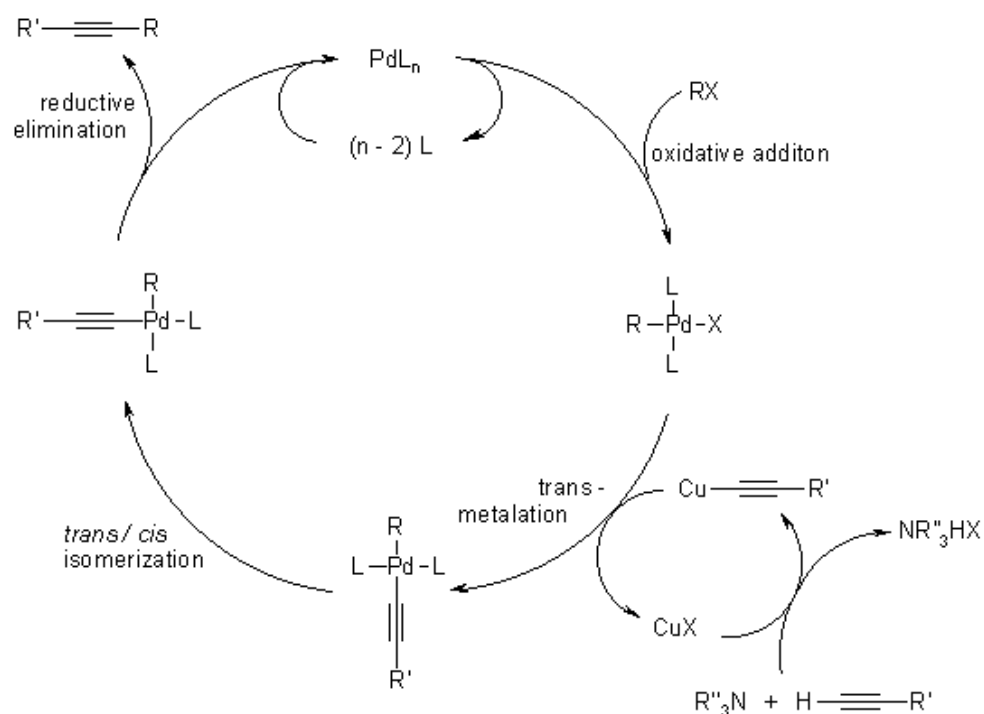


Figure 14. Mechanism of Sonogashira coupling.

One of the important parameters in Sonogashira coupling is the palladium catalyst. Most commonly used ones are Pd(PPh₃)₂Cl₂ and Pd(PPh₃)₄. They are

very similar to each other but $\text{Pd}(\text{PPh}_3)_4$ is more reactive and smaller reaction times is needed. Besides, this catalyst can decompose easily when exposed to air and temperature above 0° and it is more expensive compared to $\text{Pd}(\text{PPh}_3)_2\text{Cl}_2$. Also, $\text{Pd}(\text{PPh}_3)_4$ reduces the formation of by-product which is diacetylene formed by reduction of the Pd(II) complex. This formation can be reduced by bubbling argon or nitrogen gases to purge the oxygen from reaction medium. Generally, the amount of CuI used in Sonogashira coupling is twice of palladium catalyst (2-5 mol %).

The other vital parameter for Sonogashira coupling is the amine which is not only used as for a base but also for reaction solvent. Most commonly used bases are Et_3N , Et_2NH , $i\text{Pr}_2\text{NH}$. On the other hand, stronger bases like piperidine and pyrrolidine are used and increase in reaction rate is observed.

To get milder reaction conditions and to get rid of the difficulties faced with Sonogashira coupling, much effort has been spent by scientists and many articles were publishing.

1.5.2 Applications of the Sonogashira Reaction

There are numerous applications of the Sonogashira coupling such as light harvesting molecules, synthesis of natural products and conjugated polymers. To begin with, Sonogashira coupling can be used in the design of light harvesters. As shown in Figure 15, Akkaya *et al.* presented that BODIPY units can be linked to ethynyl- substituted benzene at (1,4), (1,3,5), and (1,2,4,5) positions. In this type of energy transfer cassettes are highly efficient because of both through-space and through-bond interactions.²⁹

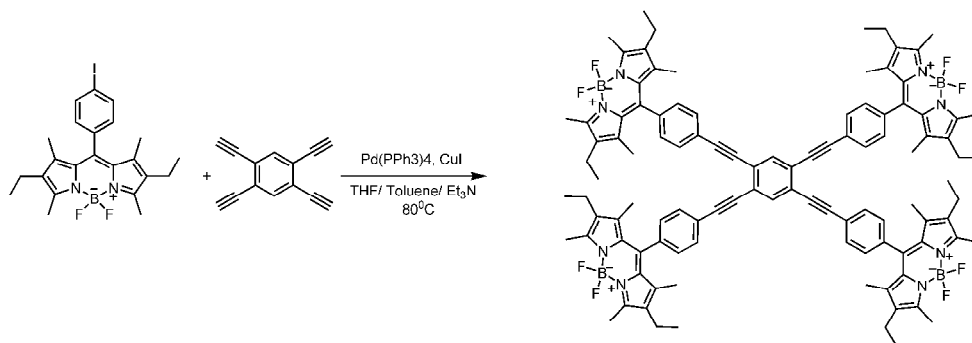


Figure 15. Example of application of Sonagashira coupling in energy transfer systems reported by Akkaya *et al.*

Sonogashira coupling is seen in the synthesis of a derivative of (+)- and (-)-harveynone, which have reported to be phytotoxin and have antitumor activity (inhibitor of spindle formation), and (-)-tricholomenyn A, which have shown antimitotic activity. By using Sonogashira coupling, they have got good yields of the desired coupled product (74-97%) (Figure 16)³⁰.

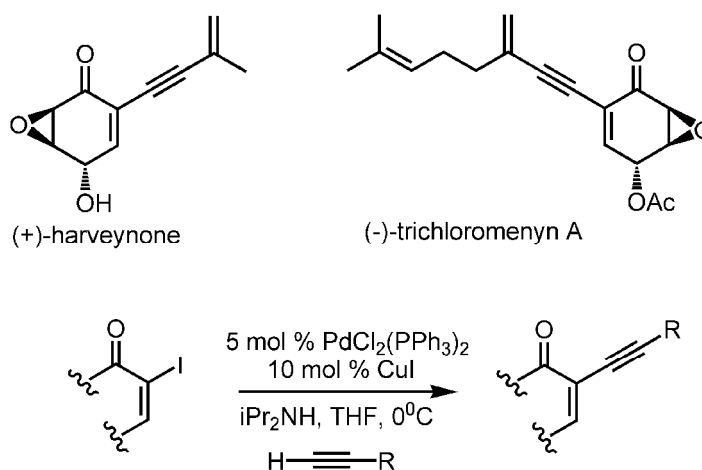


Figure 16. Example of application of Sonogashira coupling in biologically active compounds.

Conjugated polymers and oligomers are very important since they are functional materials for electronics, photonics, advanced coatings, and related applications. The characteristics of conjugated polymers are significantly sensitive to the presence of impurities, acting as uncontrolled dopants, quenchers of excited states.³¹ Sonogashira coupling is generally useful for getting polyaryleneethynyls (Figure 17) and fluorene polymers and copolymers by catalytic versions of chemical polymerization.

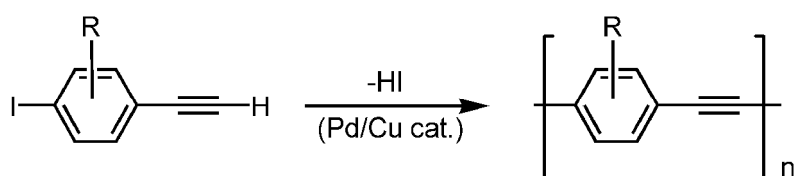


Figure 17. Example of application of Sonogashira coupling in conjugated polymers.

1.6 Fluorescence in the Solid State

π - π stacking is a non-covalent and intermolecular interaction and arises from the stacked arrangement of the aromatic moieties. However, even though some explanations have been made, the theoretical explanation of π - π stacking for larger molecules is not well explained.³²

π - π stacking is generally meant as π - π interaction because the interactions are the result of presence of π -orbitals. In other words, intermolecular overlapping of π -orbitals in π -conjugated systems causes π - π interactions. Therefore, as the number of π -electrons increases, the interactions become more stronger.³³

Fluorophores can show bright fluorescence in solution, however, in the solid-state, they become quenched due to π - π stacking. Hence, in the aggregation state, most of the fluorophores are exposed to fluorescence quenching and so having

fluorescence in the solid state becomes crucial for the fluorophores. Ultimately, the most important element for the design of novel, highly bright solid-state emissive dye is to hinder the quenching and prevent the π - π stacking in the solid-state.

There are some methods to reduce the π - π stacking in molecules. Introducing bulky groups is one of the methods used for separating π systems of fluorophores. With these considerations, Qian and coworkers³⁴ introduced two 4-tritylphenylethynyl and phenylethynyl groups into the 2,6-positions of the BODIPY core to inhibit the concentration of quenching and finally they got solid-state emissive dye with large Stokes shift (Figure 18).

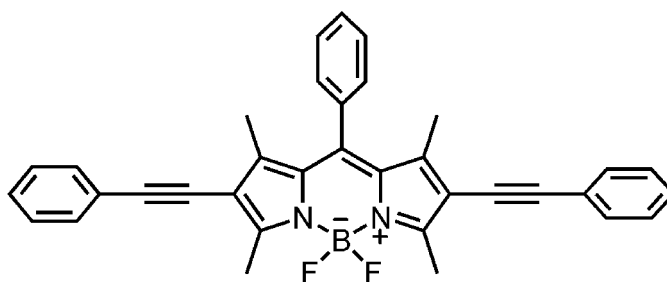


Figure 18. Example of hindering quenching of dyes in the solid state with using of bulky groups.

Another method for reducing π - π stacking in the molecules is using organic salt with a primary amine. In this method, the fluorescence intensity can be manipulated by changing the alkyl chain length of the amine. For example, as seen in the Figure 19, organic salts of anthracene-2,6-disulfonic acid (ADS) with linear alkylamines provide a tunable solid-state fluorescence system and the change in alkyl chain length of amines is interpreted as the arrangements and corresponding fluorescence properties.³⁵

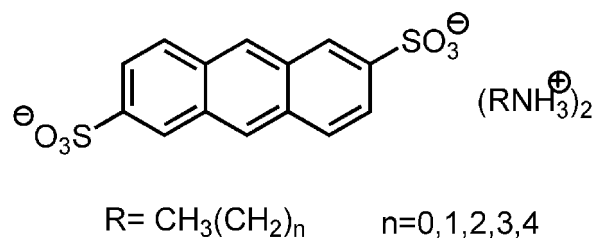


Figure 19. Example of hindering quenching of dyes in the solid state with organic salt with primary amine.

In the solid state, fluorescence enhancement can be obtained by inclusion of guest molecules in the crystalline state. Therefore, guest enclathration is the other method for the destruction of π - π interactions between the fluorophores³⁶. For fundamental research into solid state fluorescence and for the advancement of new intense solid-emissive materials, the benzofuranonaphthoquinol-type fluorophores which display dramatic fluorescence enhancement upon complexation with guest molecules will be convenient and so Yoshida *et al.* have developed the amine-inclusion (morpholine) derivatives of benzofuranonaphthoquinol fluorophores which have intense solid-fluorescence properties.³⁷ (Figure 20)

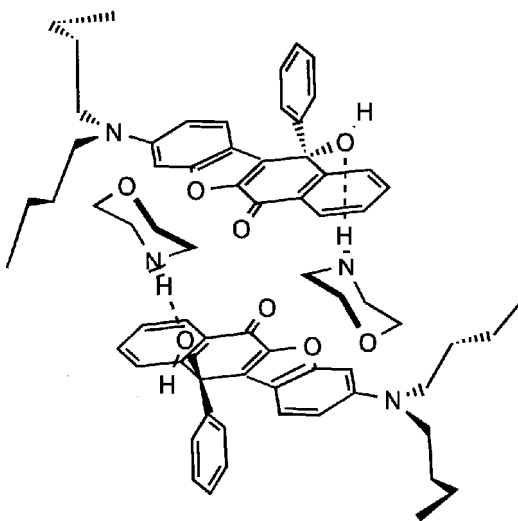


Figure 20. Example of hindered quenching of dyes in the solid state with inclusion of guest molecules in the crystalline state.

1.7 Fluorescent chemosensors

The fluorescent detection and biological imaging of the specific molecules which are crucial in living systems have aroused attention, since it is highly sensitive, cheap and processed easily compared to handling radioactive tracers for most biochemical measurements. Therefore, fluorescent chemosensors has a significant value for their simplicity and high sensitivity. In the design of the fluorescent sensors, the receptor (the recognition moiety) and fluorophore (signal source) are the substantial parts. The importance of the receptor arises from its impact on binding and selectivity³⁸. In other words, a receptor should have a strong affinity towards the target ion. The fluorophore is a signal transformer that transforms the information into an optical signal due to the analyte. Therefore, it should be stable under light and should not be affected by pH of the medium, temperature and polarity and so on. According to presence or concentration of the analyte when binds to sensor, there will be changes in the fluorescence intensity, lifetime or a shift of fluorescence wavelength will occur. Also, binding of the analyte to chemosensor will cause increase or decrease in the fluorescence that is observed with the help of the fluorophore³.

The fluorescent molecular sensors can operate in three different ways. First one depends on the collision of the analytes which causes fluorescence quenching like gas particles collision. Second methodology relies on the reversible binding of the analyte to fluorophore. In this probe, there can be fluorescence quenching known as chelation enhancement of quenching (CHEQ) or fluorescence enhancement known as chelation enhancement of fluorescence (CHEF). In the third approach, fluorophores can be attached to the receptor part with/without a spacer. If there is an alkyl chain as a spacer between receptor and fluorophore, the system is called fluorophore-spacer-receptor probe. However, if there is no spacer between receptor and the fluorophore, such probes are called integrated fluorescent probes (Figure 21). In other words, in integrated fluorescent probe, receptor is conjugated to the fluorophore via π -electron system³⁹. In this third way, fluorescence can be quenched or enhanced with the binding of analyte.

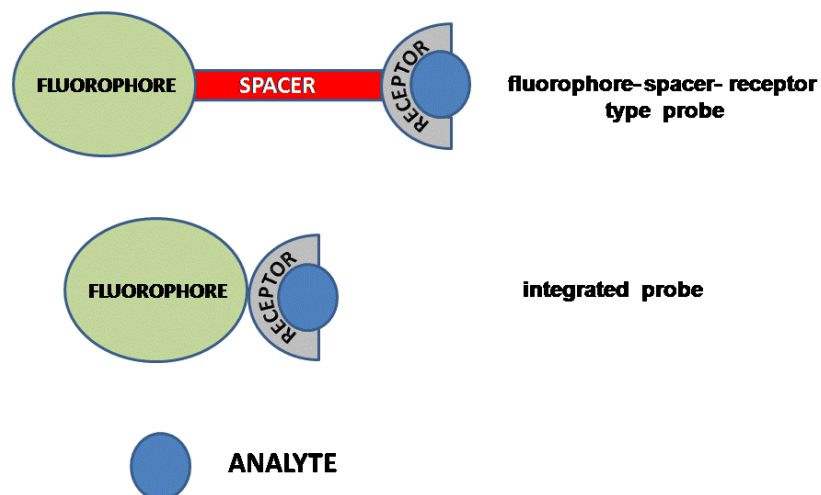


Figure 21. Schematic representations for the types of fluorescent molecular sensors.

1.8 Mechanism of Sensing

There are two main categories in the sensor design: electrochemical and optical sensor. The first type is based on the attachment of a redox active group to a receptor. Binding of guest molecule brings about the changes in the redox property of the receptor, and cyclic voltametry (CV) is used to detect these changes⁴⁰. However, there are some drawbacks of this design. For example, this method necessitates large amount of sample and it is expensive. Optical sensors can be colorimetric, electron-selective, path selective and fluorescent. The first two types are on the basis of the change in the absorbance.⁴¹ The most useful type of optical sensors is fluorescence-based sensors. They are more sensitive, fast, and more secure in terms of process, where samples are not demolished and no hazardous products are formed. These properties of fluorescence allow to detection of smaller concentration at pico or femtomolar levels.

There are two most commonly used mechanisms by fluorescence modulation in Zn(II) sensing. These are photoinduced electron transfer (PET)⁴² and internal charge transfer (ICT)⁴³.

1.8.1 Photoinduced Electron Transfer (PET)

In the idea of PET chemosensors, the fluorophore is attached to the receptor *via* a spacer and the receptor contains high energy non-bonding electron pair like on nitrogen atom. This atom can donate an electron to the excited fluorophore and so fluorescence quenching occurs. In this system, the excited fluorophore can be electron donor or acceptor.⁴⁴ Also, the redox potentials of the S_0 and excited states determine the direction of the electron transfer. As shown in Figure 22, when the fluorophore is excited, an electron of the fluorophore in the highest occupied molecular orbital (HOMO) is raised to the lowest unoccupied molecular orbital (LUMO). In other words, when an ion binds to the electron pair of the fluorophore, the oxidation-reduction potential of the receptor increases and so the HOMO of the receptor decreases in the energy fluorophore. As a result, PET process is blocked and fluorescence becomes enhanced.⁴⁵

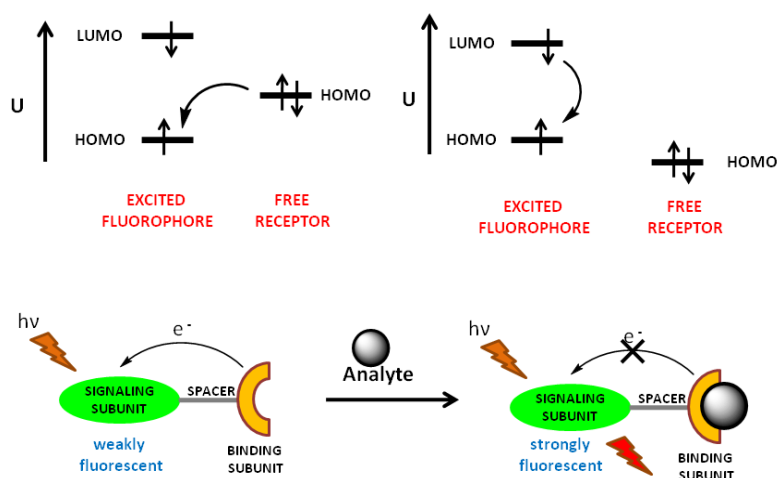


Figure 22. Molecular orbital diagrams for reductive PET.

In the literature, there are numerous examples of PET chemosensors as seen in Figure 23⁴⁶⁻⁴⁹. Moreover, large number of different receptor moieties can be used as a part PET sensor as selective ligands for alkali, alkaline earth and transition metal ions. By the coordination of cation, PET becomes thermodynamically unfavorable because of the decrease in HOMO energy of the ionophore, and so fluorescence quenching is suppressed.⁴⁷

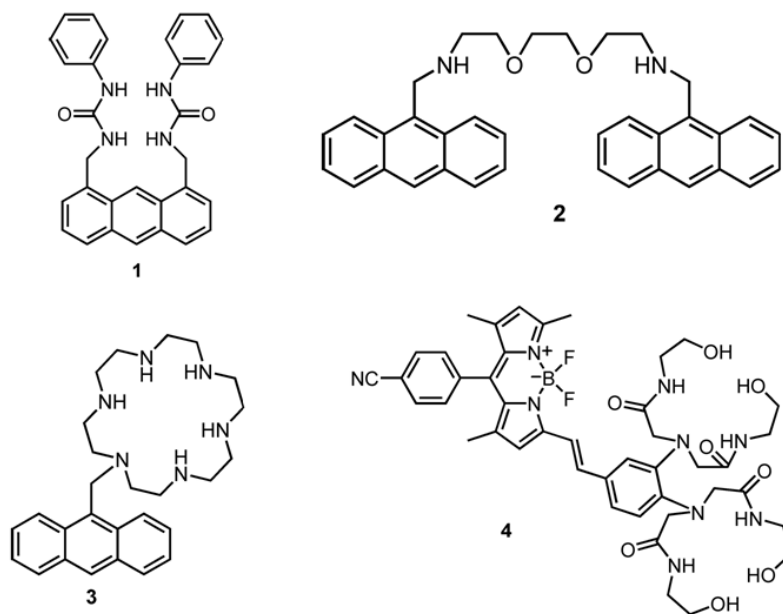


Figure 23. Some examples of PET chemosensors.

1.8.2 Internal Charge Transfer (ICT)

When there is no spacer between the fluorophore and receptor moieties in the design of the probe, in other words, receptor is directly attached to the fluorophore, it can be said that ICT mechanism is in action. In this design, receptor moiety is in conjunction with the π -electron system fluorophore moiety. To obtain an ICT type probe, fluorophore must contain an electron-donating

group such as -NH_2 and an electron-withdrawing group. By the excitation of the light, ICT occurs from donor to acceptor⁵⁰. When a receptor (electron-donating part) interacts with a cation, there will be a decrease in the electron-donating character of receptor. As a result, the conjugation will be affected and blue shift will be expected in the absorption spectrum. This mechanism can be explained as charge-dipole interactions. Amino group will be positively charged upon excitation and when this positively charged amino group interacts with the cation, the excited state will be destabilized. As seen in the Figure 24, energy gap between S_0 and S_1 will become larger at the end of this process so blue shift is anticipated. Another possible mechanism observed in the ICT processes is that the acceptor group (electron receptor) like carbonyl group can interact with the cation and increases electron-withdrawing property of that part. Again, charge-dipole interactions can be used to explain this mechanism. When the acceptor group is affected by the electron receptor, the excited state becomes more stable and as a result, red shift will be observed since the energy gap between S_0 and S_1 will decrease.⁵¹

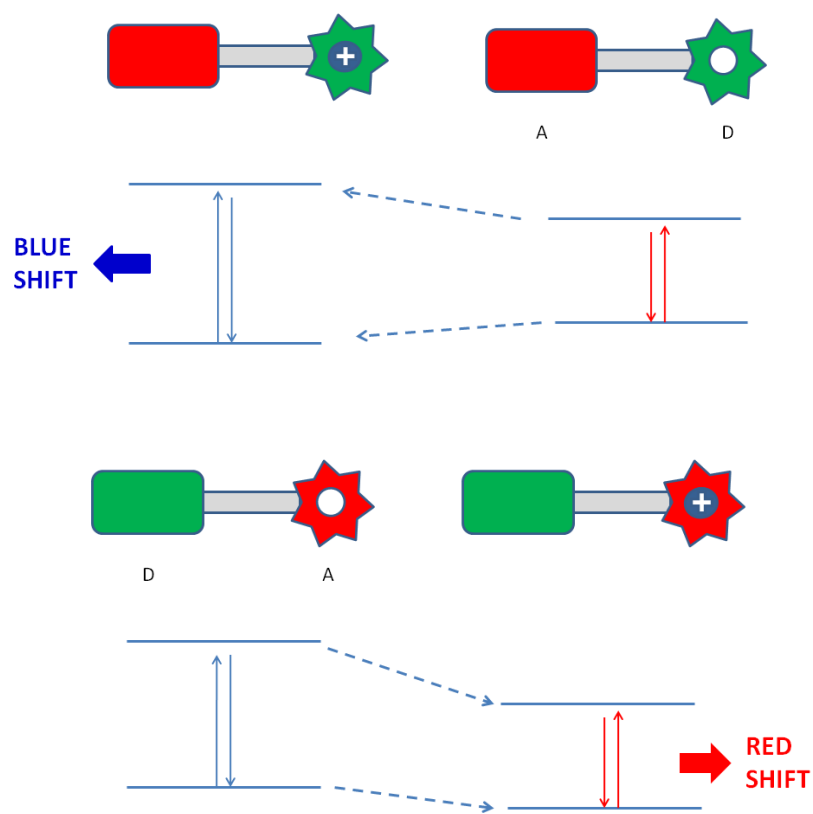


Figure 24. Band gap changes on interactions with cations of ICT type sensors.

As shown in the Figure 25, in the literature, there are lots of examples of ICT type chemosensors. These chemosensors are sensitive to different cations. Compound **5** is Cd^{2+} selective chemosensor with watersolubility. Also, *in vitro* studies with HK-2 cell lines showed its selectivity and sensitivity⁵². Another Hg^{2+} selective and sensitive and ICT type chemosensor is shown as compound **6**⁵³. The advance in the chemosensor design was presented by Akkaya group⁵⁴. Compound **7** is designed for the Hg^{2+} ion with modulation of resonance energy transfer, signal ratio was amplified.

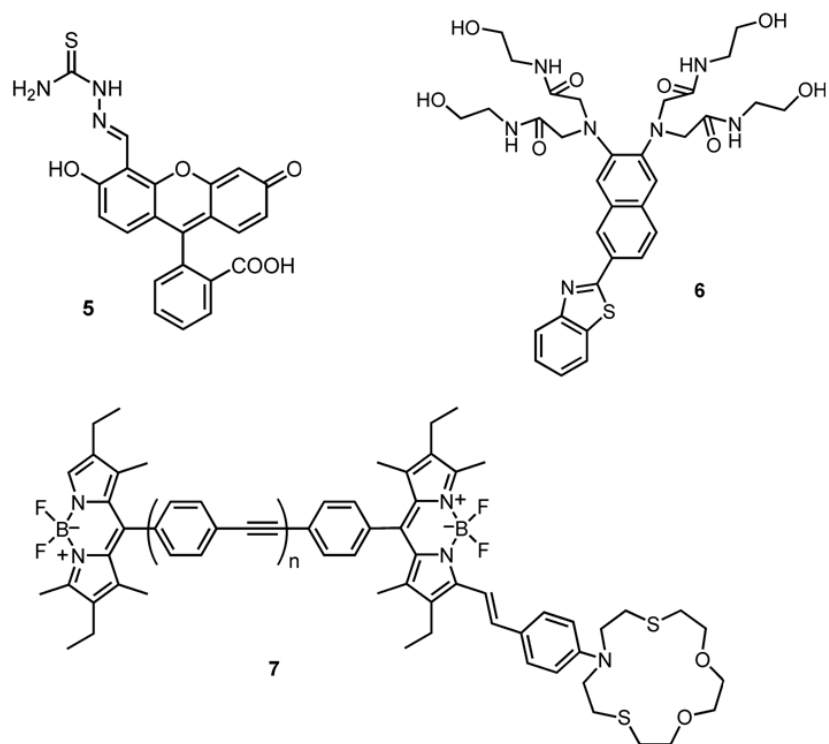


Figure 25. Some examples of ICT chemosensors.

1.9 Importance of Ratiometric Analysis

In chemosensors, ratiometric measurements are very important, since it allows high signal-selectivity.³⁷ Ratiometric analysis means that the ratio of the intensities at two suitable emission or absorption wavelengths. In this analysis, the signal ratio is independent of the concentration of the fluorophore, and also on the intensity of the incident light. In ICT mechanism, chemosensors can be designed in ratiometric manner because with cation binding, a shift can be observed not only in the absorption but also in emission wavelength, so we can observe larger changes in fluorescence intensity. Therefore, this measurement enables us to get more precise data and diminishes artifacts by reducing the

effect of extraneous factors (illumination, photobleaching) on the fluorescence probe.⁴⁶

1.10 Di-2-picolyamine (DPA) as a selective ligand

DPA was used firstly in 1996⁵⁵ and from then DPA was widely incorporated into many fluorophoroionophores to sense Zn^{2+} cations. There are other reasons why DPA is so common, such as its cell permeability and high selectivity against 1A and 2A metal ions. The latter property is very important since these metal ions are coexisting with Zn^{2+} ions in the biological environments.

Many examples have been published using DPA, which work according to either PET or ICT mechanisms. The amine on the DPA can be attached many different fluorophores by using a spacer or directly conjugated to the fluorophore. However, besides being capable of working through ICT and PET mechanisms, a chemosensor must meet some other requirements to be an effective sensor. To begin with, to prevent cell damage, excitation wavelength should be in the range of visible or near-IR region. Also, emission from near-IR fluorescent dyes are scattered much less than others and are crucial for *in vivo* imaging. Moreover, they should be water-soluble for biological applications and have high quantum yields and large extinction coefficients. As mentioned above, also it should allow ratiometric analysis and large Stokes shift.

1.11 Importance of Zn^{2+} ion

It is well-known that Zn^{2+} is the second most abundant transition metal ion in the body following iron. Zn^{2+} has vital role in biological processes⁵⁶ such as in the control of gene expression, programmed cell death, enzyme adjusting and synaptic transmission.⁵⁷ Also, it is known that Zn^{2+} is responsible for the

formation of amyloid plaques⁵⁸ which is related to the etiology of Alzheimer's disease.⁵⁹

An adult body holds more than a few grams of Zn(II)⁶⁰. Up to now, the protein bound form of Zn²⁺ have been presented but free or loosely bound, in other words, chetable Zn²⁺ maintains its ambiguity and its mechanism of action is still uncertain.⁶¹ Free Zn²⁺ exists in brain (in the amount of a few millimolars in the vesicles of the signal-passing neuron)⁶², pancreas and retina. Furthermore, since d-shell of Zn²⁺ is filled (d⁰ electron configuration), spectroscopic detection is not a viable option. Therefore, fluorescent sensor molecules have been studied enormously to make clearer the function of Zn²⁺.

1.12 Fluorescent Zn²⁺ chemosensors

Designing a chemosensor requires numerous parameters to controlled. To begin with, it should be simple, selective, show give response strongly and allow to study in aqueous environments⁶³.

According the hard and soft acids and bases theory,⁶⁴ Zn²⁺ cation which is a moderately soft acid should bond to moderate soft bases. As a result, for enhancement of the binding constant, most of the Zn²⁺ receptors contain nitrogen (N) which is a moderate soft donor atom.

In recent literature, a large number of fluorescent probes for zinc have been studied based on different fluorophores such as anthracene⁶⁵, 7-nitrobenz-2-oxa-1,3-diazole (NBD)⁶⁶, boradiazaindacene (bodipy),⁶⁷ and fluorescein⁶⁸. Unfortunately, for most of them, water solubility is limited, thus various solvent mixtures are used in characterization.

Although, there are lots of chemosensors based on DPA as a receptor, only few examples meet characteristics mentioned above. As shown in Figure 26, compound **8**⁶⁹ is a typical PET type Zn²⁺ ion sensitive probe. It is highly selective

but it does not allow ratiometric analysis, is not water-soluble and near-IR dye. Another ICT type, DPA receptor based chemosensor is compound **9**⁷⁰. In this chemosensor, the fluorophore is 7-nitrobenz-2-oxa-1,3-diazole (NBD) which has strongly electron-withdrawing character and so it shows relatively low affinity of DPA in for Zn^{2+} . Again, it does not show fluorescence alteration. Compound **10**⁷¹ is again ICT type and BODIPY-based Zn^{2+} selective chemosensor. It shows low dissociation constant and high quantum yield with the binding of Zn^{2+} . However as compound **8**, water- solubility is limited and it does not absorb in the near- IR region of the spectrum.

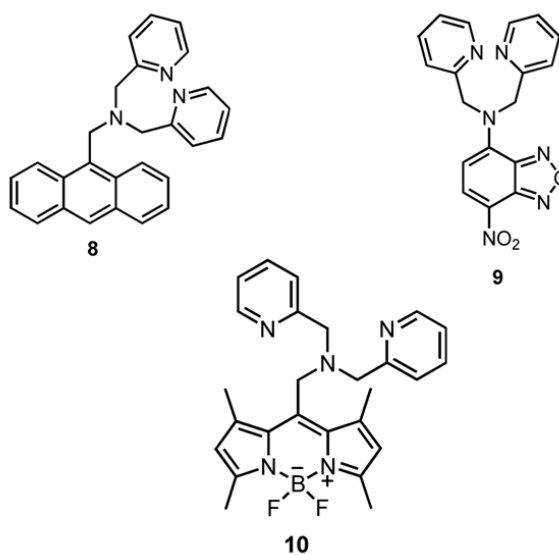


Figure 26. Some examples of DPA- based chemosensors.

CHAPTER 2

EXPERIMENTAL PROCEDURES

2.1 General

Without further purification, all chemicals and solvents purchased from Aldrich were used. ^1H NMR and ^{13}C NMR spectra were recorded using a Bruker DPX-400 in CDCl_3 or DMSO-d_6 with TMS as internal reference. Absorption spectrometry was performed using a Varian spectrophotometer. Steady state fluorescence measurements were conducted using a Varian Eclipse spectrofluorometer. Column chromatography of all products was performed using Merck Silica Gel 60 (particle size: 0.040–0.063 mm, 230–400 mesh ASTM). Reactions were monitored by thin layer chromatography using fluorescent coated aluminum sheets. Solvents used for spectroscopy experiments were spectrophotometric grade. Mass spectrometry measurements were done at the Ohio State University Mass Spectrometry and Proteomics Facility, Columbus, Ohio, U.S.A. and Bilkent University Agilent Technologies 6530 Accurate-Mass Q-TOF LC-MS. X-ray diffraction data were obtained on an Enraf-Nonius CAD4 (κ -geometry) diffractometer operating in $\omega/2\theta$ scan mode using graphite-monochromated MoK_α radiation ($\lambda = 0.71073 \text{ \AA}$) at room temperature.

2.2 Experimental Part-I

2.2.1 Synthesis of Compound (3)

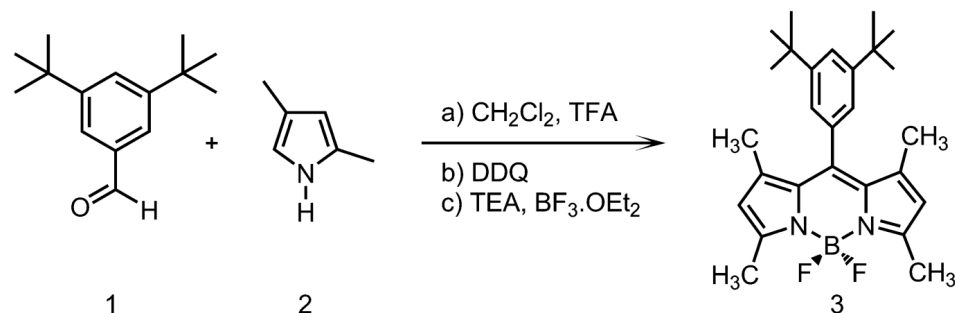


Figure 27. Synthesis of compound 3.

3,5-di-*tert*-butylbenzaldehyde (**1**) (1.83 mmol, 400 mg) and 2,4-dimethylpyrrole (**2**) (3.67 mmol, 348 mg) were dissolved in CH₂Cl₂ (350 mL) purged with argon in a 1000 mL flask. 1 drop of TFA was added and the mixture was stirred at room temperature for 3 hrs. When TLC showed consumption of the aldehyde was complete, a solution of 295 mg (1.83 mmol) of DDQ (2,3-Dichloro-5,6-dicyano-*p*-benzoquinone) in CH₂Cl₂ was added. After 3 h, Et₃N (4 ml) and BF₃.OEt₂ (4 ml) were added. Immediately after the addition of BF₃.OEt₂ bright green fluorescence was observed. Crude product was washed three times with water, dried over Na₂SO₄ and concentrated *in vacuo*. Then crude product purified by silica gel column chromatography using CHCl₃. The pale orange fraction which has bright green fluorescence was collected. Orange solid (0.476 mmol, 207 mg, 26 %).

¹H NMR (400 MHz, CDCl₃) δ 7.41 (s, 2H), 7.02 (s, 1H), 5.93 (s, 2H), 2.54 (s, 6H), 1.33 (s, 6H), 1.22 (s, 18H)

¹³C NMR (100 MHz, CDCl₃) δ 155.1, 152.0, 143.3, 143.2, 134.0, 131.5, 122.1, 121.9, 121.0, 35.0, 31.4, 14.5, 14.1.

ESI-HRMS calcd for M+Na 458.2795, found 458.2780, Δ= 3.3 ppm

2.2.2 Synthesis of Compound (6)

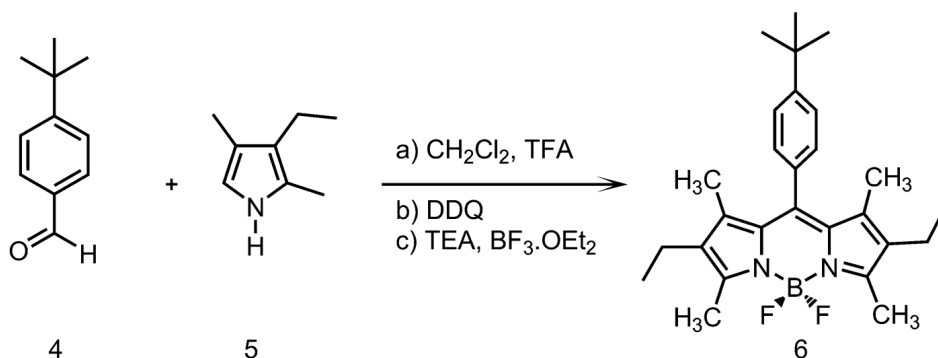


Figure 28. Synthesis of compound 6.

4-*tert*-butylbenzaldehyde (4) (3.10 mmol, 500 mg) and 2,4-dimethyl-3-diethylpyrrole (5) (6.2 mmol, 761.26 mg) were dissolved in CH₂Cl₂ (400 mL) purged with argon in a 1000 mL flask. 1 drop of TFA was added and the mixture was stirred at room temperature for 3 hrs. When TLC showed consumption of the aldehyde was complete, a solution of 500 mg (3.10 mmol) of DDQ (2,3-Dichloro-5,6-dicyano-*p*-benzoquinone) in CH₂Cl₂ was added. After 3 h, Et₃N (3 ml) and BF₃·OEt₂ (3 ml) were added. Immediately after the addition of BF₃·OEt₂ bright yellow fluorescence was observed. Crude product was washed three times with water, dried over Na₂SO₄ and concentrated *in vacuo*. Then crude product purified by silica gel column chromatography using CH₂Cl₂. The orange fraction which has bright yellow fluorescence was collected. Orange solid (0.147 mmol, 608 mg, 45 %).

¹H NMR (400 MHz, CDCl₃) δ 7.42 (d, 2H *J*=8.1 Hz), 7.15 (d, 2H *J*=8.1 Hz), 2.51 (s, 6H), 2.25-2.18 (q, 2H *J*=7.5 Hz), 1.29 (s, 9H), 1.2 (s, 6H), 0.93-0.96 (t, 3H, *J*=7.5 Hz)

¹³C NMR (100 MHz, CDCl₃) δ 152.9, 151.7, 140.2, 138.0, 132.2, 132.1, 130.5, 127.4, 125.3, 34.3, 30.9, 16.6, 14.1, 12.0, 11.0.

2.2.3 Synthesis of Compound (7)

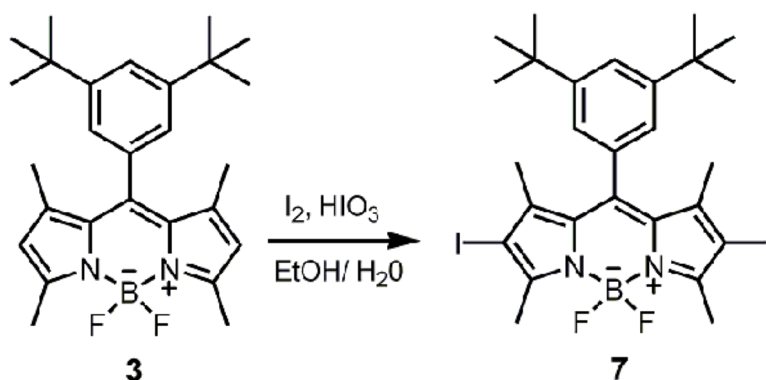


Figure 29. Synthesis of compound 7.

3 (0.92 mmol, 400 mg) and iodine (2.29 mmol, 582 mg) were added to a 500 mL round-bottomed flask containing 200 ml EtOH and iodic acid (1.83 mmol, 323 mg) dissolved in 2 mL of water was added to this solution. The reaction mixture was stirred at 60°C and was monitored by TLC chloroform. Saturated $\text{Na}_2\text{S}_2\text{O}_3$ solution in water was added to the solution, when all the starting material had been consumed, and the product was extracted into chloroform and dried over Na_2SO_4 . Then, the solvent was evaporated *in vacuo*. The residue was purified by silica gel column chromatography using chloroform as the eluant. Red solid (600 mg, 95%).

^1H NMR (400 MHz, CDCl_3) δ 7.51 (d, 1H, $J=1.7$ Hz.), 7.15 (d, 2H, $J=1.7$ Hz), 2.23 (s, 6H), 1.37 (s, 6H), 1.30 (s, 18H).

^{13}C NMR (100 MHz, CDCl_3) δ 152.5, 133.8, 122.5, 121.9, 35.1, 31.4, 16.7, 16.0.

2.2.4 Synthesis of Compound (9)

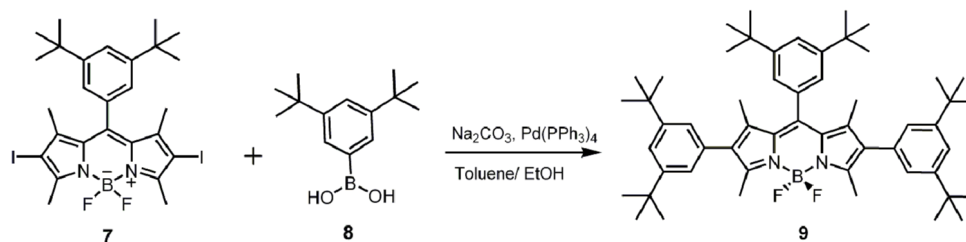


Figure 30. Synthesis of compound 9.

Compound 7 (0.073 mmol, 50 mg), 3,5-di-*tert*-butylphenylboronic acid (**8**) (0.14 mmol, 34 mg) and Pd(PPh₃)₄ (0.0073, 8.5 mg) were heated to reflux in toluene (10 ml), ethanol (5 ml) and 2 M Na₂CO₃ (2 ml) for 6 hours. Then, the mixture was cooled to room temperature and diluted with EtOAc (20 ml) and washed with water. Then, dried with Na₂SO₄ and evaporated to get crude product. Via silica gel chromatography (hexane/ CHCl₃: 2:1), product was purified. (51.4 mg, 87%)

¹H NMR (400 MHz, CDCl₃) δ 7.49 (s, 1H), 7.33 (t, 2H, J=1.7 Hz), 7.20 (d, 2H, J=0.86 Hz), 7.00 (d, 4H, J=0.88 Hz), 2.01 (s, 6H), 1.36 (s, 6H), 1.35 (s, 18H), 1.32 (s, 36H).

¹³C NMR (100 MHz, CDCl₃) δ 154.0, 152.0, 150.4, 138.9, 134.6, 132.6, 124.4, 122.2, 121.8, 120.6, 35.1, 34.8, 31.5, 31.4, 13.5, 12.5.

ESI-HRMS calcd for M+H⁺ 813.6070, found 813.6069, Δ= 0.1 ppm

2.2.5 Synthesis of Compound (10)

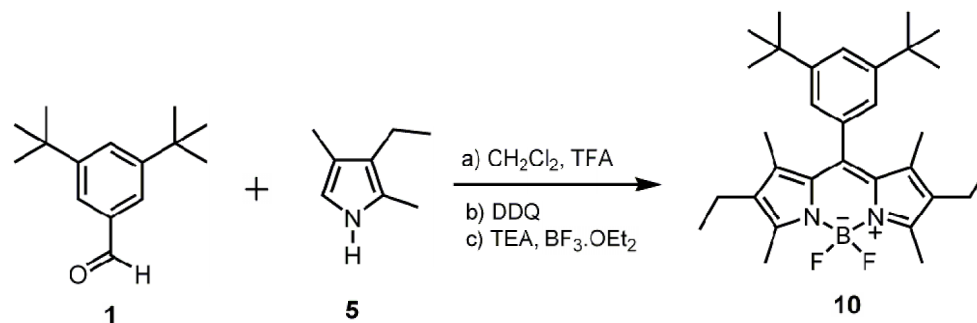


Figure 31. Synthesis of compound 10.

3,5-di-*tert*-butylbenzaldehyde (**1**) (2.3 mmol, 500 mg) and 2,4-dimethyl-3-diethyl pyrrole (**5**) (5.7 mmol, 706.4 mg) were dissolved in CH₂Cl₂ (400 mL) purged with argon in a 1000 mL flask. 1 drop of TFA was added and the mixture was stirred at room temperature for 3 hrs. When TLC showed consumption of the aldehyde was complete, a solution of 563 mg (2.3 mmol) of DDQ (2,3-Dichloro-5,6-dicyano-*p*-benzoquinone) in CH₂Cl₂ was added. After 3 h, Et₃N (3 ml) and BF₃·OEt₂ (3 ml) were added. Immediately after the addition of BF₃·OEt₂ bright yellow fluorescence was observed. Crude product was washed three times with water, dried over Na₂SO₄ and concentrated *in vacuo*. Then crude product purified by silica gel column chromatography using CHCl₃. The orange fraction which has bright yellow fluorescence was collected. Orange solid (207 mg, 42 %).

¹H NMR (400 MHz, CDCl₃) δ 7.49 (s, 1H), 7.11 (s, 2H), 2.14 (s, 6H), 2.31 (q, 4H, J=5.7 Hz), 1.34 (s, 18H), 1.28 (s, 6H), 1.01 (t, 6H, J=5.02 Hz).

¹³C NMR (100 MHz, CDCl₃) δ 153.3, 151.8, 138.5, 134.7, 132.5, 122.4, 120.6, 35.1, 31.4, 17.1, 14.6, 12.5, 11.4.

2.2.6 Synthesis of Compound (11)

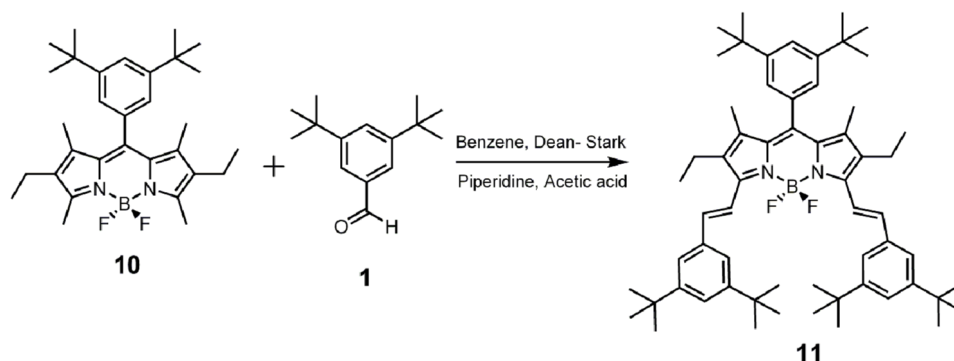


Figure 32. Synthesis of compound **11**.

Compound **10** (0.203 mmol, 100 mg) and **1** (0.406 mmol, 88 mg) were refluxed in a mixture of benzene (20 ml), glacial acetic acid (1.5 mL), and piperidine (2 mL). Any water formed during the reaction, was removed azeotropically in a Dean-Stark apparatus. By monitoring with TLC, when all the starting material had been consumed, the mixture was cooled to room temperature and solvent was evaporated. Water (100 mL) added to the residue and the product was extracted into the chloroform (100 mL). Organic phase dried over Na₂SO₄, evaporated and residue was purified by silica gel column chromatography using hexane/ CHCl₃ (5:1). The green colored fraction was collected then the solvent was removed under reduced pressure to yield compound **11** (148 mg, 82%).

¹H NMR (400 MHz, CDCl₃) δ 7.71 (d, 2H, J=16.7 Hz), 7.42 (s, 1H), 7.35 (s, 4H), 7.32 (s, 2H), 7.20 (d, 2H, J=16.7 Hz), 7.11 (s, 2H), 2.55 (q, 4H, J=7.4 Hz), 1.38 (s, 36H), 1.35 (s, 18H), 1.28 (s, 6H), 1.22 (t, 6H, J=5.5 Hz)

¹³C NMR (100 MHz, CDCl₃) δ 151.9, 151.1, 150.3, 138.9, 136.8, 136.7, 135.1, 133.5, 123.1, 122.8, 121.7, 121.6, 119.7, 35.1, 34.9, 31.5, 31.4, 29.7, 18.4, 14.1, 11.2

ESI-HRMS calcd for M-H⁺ 891.6539, found 891.6584, Δ= 5.05 ppm.

2.2.7 Synthesis of Compound (13)

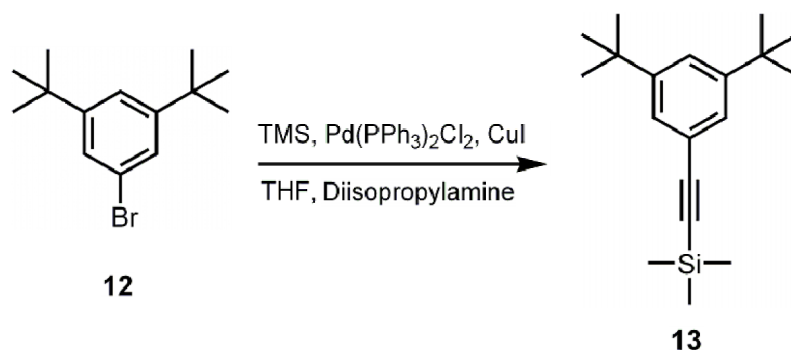


Figure 33. Synthesis of compound 13.

To 1-bromo-3,5-di-*tert*-butyl benzene (**12**) (0.93 mmol, 250 mg) in freshly distilled THF (10 ml) and diisopropylamine (5 ml), Pd(PPh₃)₂Cl₂ (0.056 mmol, 39 mg) and CuI (0.093 mmol, 17.6 mg) were added respectively. After 10 min., trimethylsilylacetylene (1.857 mmol, 184.4 mg) were added and the mixture was allowed to stand at 60°C overnight. The mixture was evaporated, washed with CH₂Cl₂ and water and organic phase was dried over Na₂SO₄. Then crude product purified by silica gel column chromatography using hexane. (216 mg, 87%)

¹H NMR (400 MHz, CDCl₃) δ 7.40 (d, 1H, J= 1.84 Hz), 7.35 (d, 2H, J= 1.88 Hz), 1.32 (s, 18H), 0.28 (s, 9H)

2.2.8 Synthesis of Compound (14)

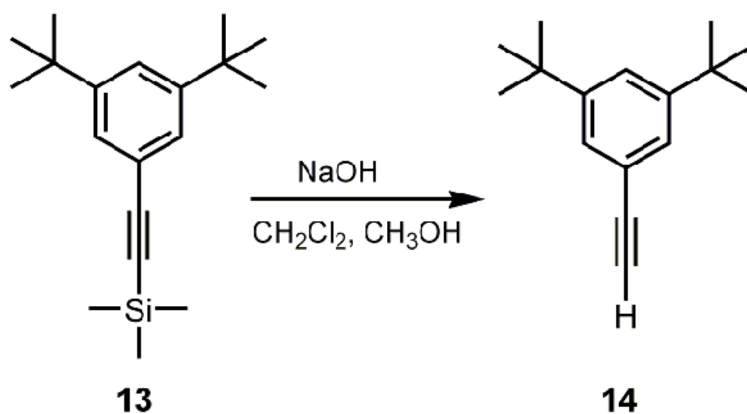


Figure 34. Synthesis of compound **14**.

Compound **13** (0.70 mmol, 200 mg) and NaOH (7 mmol, 279 mg) were added to a solution of DCM (10 ml) and MeOH (10 ml) and stirred about 15 min. Then, water (100 ml) was added to and the product was extracted into the CH₂Cl₂ (100 ml). The product was obtained after dried over Na₂SO₄ and evaporated. (147 mg, 98%)

¹H NMR (400 MHz, CDCl₃) δ 7.42 (d, 1H, J=1.88 Hz), 7.37 (d, 2H, J=1.80 Hz), 3.03 (s, 1H), 1.32 (s, 18H)

¹³C NMR (100 MHz, CDCl₃) δ 150.9, 126.4, 123.3, 121.0, 84.9, 75.8, 34.8, 31.3.

2.2.9 Synthesis of Compound (15)

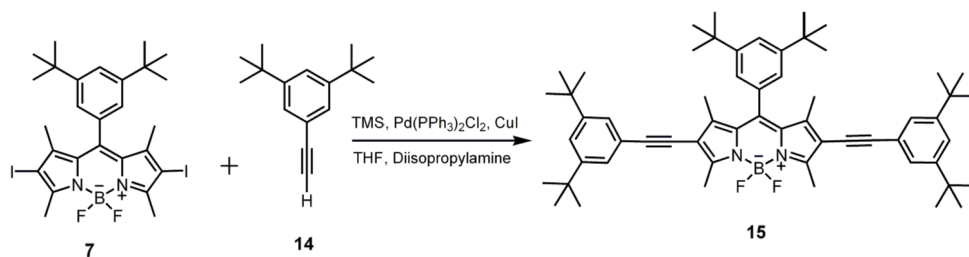


Figure 35. Synthesis of compound 15.

To Compound **7** (0.13 mmol, 89 mg) in freshly distilled THF (10 ml) and diisopropylamine (5 ml), Pd(PPh₃)₂Cl₂ (0.016 mmol, 10.9 mg) and CuI (0.026 mmol, 4.95 mg) were added respectively. After 10 min., Compound **14** (0.32 mmol, 69.2 mg) were added and the mixture was allowed to stand at 60°C overnight. The mixture was evaporated, washed with CH₂Cl₂ and water and organic phase was dried over Na₂SO₄. Then crude product purified by silica gel column chromatography using CHCl₃/hexane (2:1). (94 mg, 85%)

¹H NMR (400 MHz, CDCl₃) δ 7.40 (d, 1H, J= 1.84 Hz), 7.35 (d, 2H, J= 1.88 Hz), 1.32 (s, 18H), 0.28 (s, 9H)

¹³C NMR (100 MHz, CDCl₃) δ 158.1, 152.3, 150.9, 144.0, 143.8, 133.6, 131.3, 125.6, 122.7, 122.4, 122.2, 122.0, 97.4, 80.3, 35.2, 34.8, 31.4, 31.3, 13.8, 13.3.

ESI-HRMS calcd for M-H⁺ 859.5913, found 859.5694, Δ= 25.5 ppm

2.3 Experimental Part-II

2.3.1 Synthesis of Compound (17)

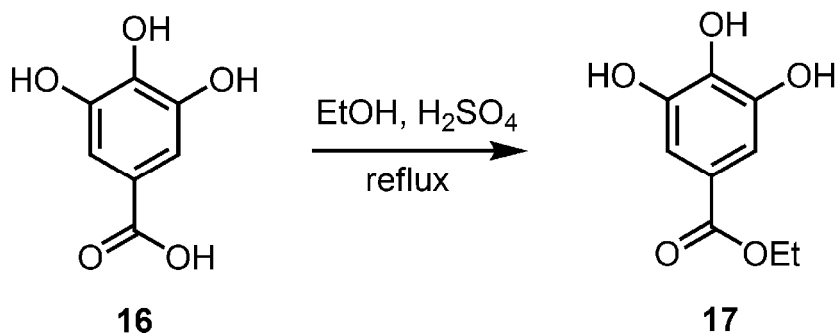


Figure 36. Synthesis of compound **17**.

3, 4, 5- trihydroxybenzoic acid (5.00 g, 29.4 mmol), **16**, was dissolved in 30 mL EtOH. 1 mL of 96% H₂SO₄ was carefully added in 10 min and the reaction mixture was refluxed overnight. The crude product was chromatographed on silica gel and eluted with chloroform-isopropanol 7:3 (v/v) to yield 3.20 g solid compound **17**. Yield was 55%. Without further purification **17** was used through next step.

¹H NMR (CDCl₃): δ (ppm) 6.95 (s, 2H, Ar-H), 4.20 (q, 2H, *J*=7.0 Hz, -CH₂), 1.25 (t, 3H, *J*=7.0 Hz, CH₃).

2.3.2 Synthesis of Compound (19)

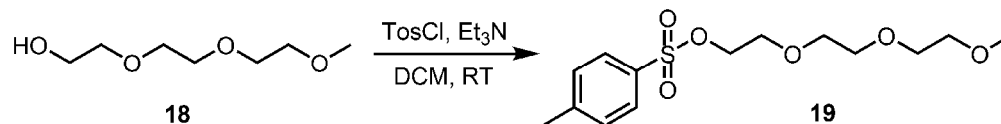


Figure 37. Synthesis of compound **19**.

Triethylene methyl ether, **18**, (3.00 g, 15.0 mmol) and 5 mL of Et₃N was dissolved in 150 mL of CH₂Cl₂. In a dropwise manner TsCl (3.20 g, 15.0 mmol) was added to the mixture. The reaction was completed after mixing one day at room temperature. The desired product was then collected with column chromatography in which the eluent was CHCl₃ to yield 3.32 g **19** in a liquid form. Yield 81%.^[6]

¹H NMR (CDCl₃): δ (ppm) 7.55 (d, 2H, *J* = 8.0 Hz, Ar-H), 7.15 (d, 2H, *J* = 8.0 Hz, Ar-H), 4.00 (m, 2H, CH₂), 3.60-3.30 (m, 10H), 3.20 (s, 3H, CH₃), 2.30 (s, 3H, CH₃).

2.3.3 Synthesis of Compound (20)

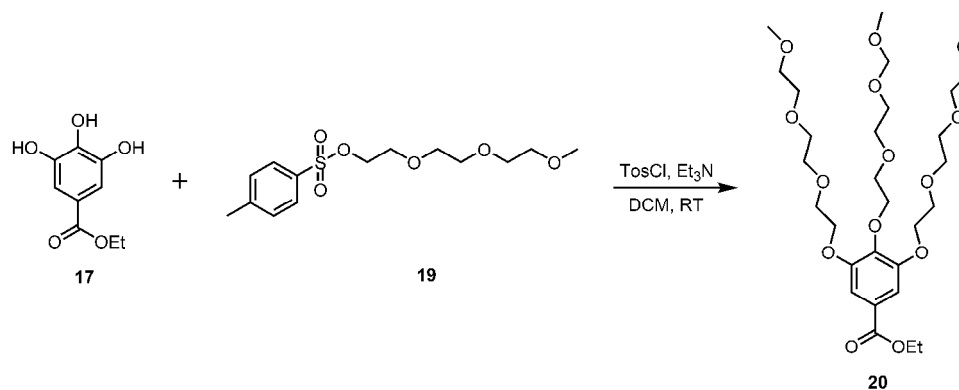


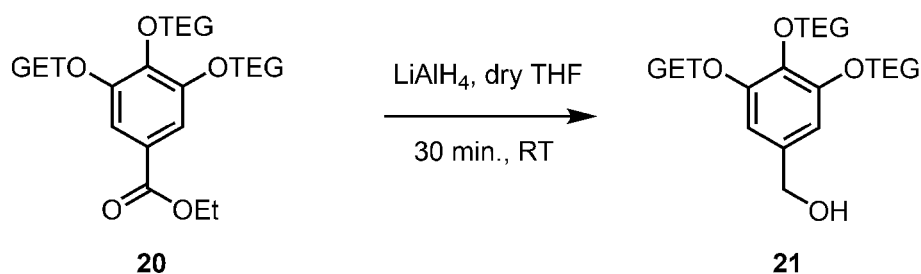
Figure 38. Synthesis of compound **20**.

A suspension of **17** (3.00 g, 15.0 mmol), **19** (12.4 g, 45.0 mmol), K₂CO₃ (8.10 g, 45.0 mmol) and catalyt amount of 18-crown-6 in 200 ml acetone was refluxed

overnight. Acetone was removed by evaporation, and the residue was redissolved in CHCl_3 and extracted with distilled water three times. The organic phase was taken and solvent was removed by evaporation. The expected product was taken without any further purification as brown oil (8.50 g, 92%).

$^1\text{H NMR}$ (CDCl_3): δ (ppm) 7.20 (s, 2H, Ar-H), 4.40- 3.10 (m, 45 H), 2.30 (q, 2H, $J=7.0$ Hz, $-\text{CH}_2$), 1.30 (t, 3H, $J=7.0$ Hz, CH_3).

2.3.4 Synthesis of the Compound (21)



TEG = $\text{CH}_2\text{CH}_2(\text{OCH}_2\text{CH}_2)_3\text{CH}_3$

Figure 39. Synthesis of compound **21**.

An excess amount of 2.0 g LiAlH_4 was dissolved in dry 20 ml of THF and **20** (8.00 g, 12.5 mmol) was added to the reaction mixture in a dropwise manner in 30 min. After reaction was completed which was monitored with TLC the excess amount of LiAlH_4 was killed with cold water. The crude reaction was filtered and washed with methanol. The solvent then was removed by evaporation and **21** was taken as an only product. (7.40 g, 100%)

$^1\text{H NMR}$ (CDCl_3): δ (ppm) 7.30 (s, 1H, $-\text{OH}$), 6.60 (s, 2H, Ar-H), 4.55 (s, 2H, $-\text{CH}_2$), 4.30- 3.30 (m, 45H).

2.3.5 Synthesis of compound (22)

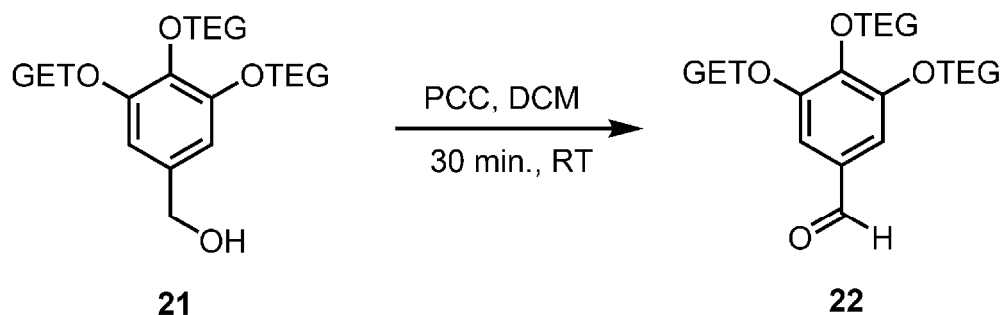


Figure 40. Synthesis of the compound **22**.

Compound **21** (7.00 g, 11.8 mmol) and excess amount of pyridinium chloro chromate (PCC) (5.00 g) were dissolved in CH_2Cl_2 . The reaction was monitored by TLC and when complete consumption of **21** was seen the reaction was completed. Crude reaction was extracted with basic aqueous solution one times, then three times with acidic aqueous solution. The organic phase was collected and solvent removed by evaporation. **22** was taken as only product after workup steps (6.90 g, 100%)

^1H NMR (400 MHz, CDCl_3): δ (ppm) 9.80 (s, 1H), 7.10 (s, 2H, Ar-H), 4.30-3.30 (m, 45H)

2.3.6 Synthesis of Compound (23)

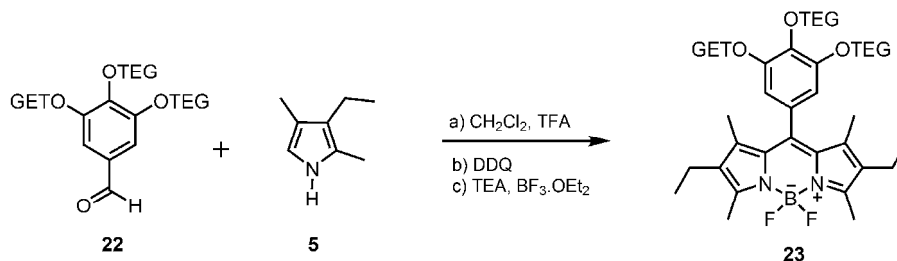


Figure 41. Synthesis of compound 23.

3,4,5-tris(2-(2-(2-methoxyethoxy)ethoxy)ethoxy)benzaldehyde (**22**) (0.34 mmol, 200 mg) and 2,4-dimethyl-3-ethyl pyrrole (**5**) (0.68 mmol, 84.0 mg) were dissolved in CH₂Cl₂ (250 mL) purged with argon in a 100 mL flask. 1 drop of TFA was added and the mixture was stirred at room temperature for 3 hrs. When TLC showed consumption of the aldehyde was complete, a solution of 166 mg (0.68 mmol) of DDQ (Tetrachloro-1,4-benzoquinone) in CH₂Cl₂ was added. After 3 h, Et₃N (3 ml) and BF₃.OEt₂ (3 ml) were added. Immediately after the addition of BF₃.OEt₂ bright yellow fluorescence was observed. Crude product washed three times with water, dried over Na₂SO₄ and concentrated in vacuo. Then crude product purified by silica gel column chromatography using CHCl₃/CH₃OH (99/1, v/v). The pale green fraction which has bright yellow fluorescence was collected. Orange solid (0.147 mmol, 120 mg, 43 %).

¹H NMR (400 MHz, CDCl₃) δ: 6.48 (s, 2H, Ar-H), 4.15 (t, *J*= 5.0 Hz, 2H), 4.06 (t, *J*= 5.0 Hz, 4H), 3.76 (t, *J*= 4.9 Hz, 4H), 3.70- 3.42 (m, 26H), 3.30 (s, 3H, -CH₃), 3.27 (s, 6H), 2.48 (s, 6H, -CH₃), 2.24 (q, *J*=7.6 Hz, 2H, -CH₂), 1.46 (s, 6H, -CH₃), 0.92 (t, *J*=7.6 Hz, 3H, CH₃)

¹³C NMR (100 MHz, CDCl₃) δ 153.7, 153.6, 139.7, 139.0, 138.2, 132.7, 130.7, 130.6, 108.0, 72.7, 72.0, 71.9, 70.9, 70.7, 70.6, 70.5, 69.7, 69.2, 59.0, 29.6, 17.0, 14.5, 11.6

ESI-HRMS calcd for M+Na 889.4809, found 889.4808, Δ= 0.1 ppm

2.3.7 Synthesis of Compound (26)

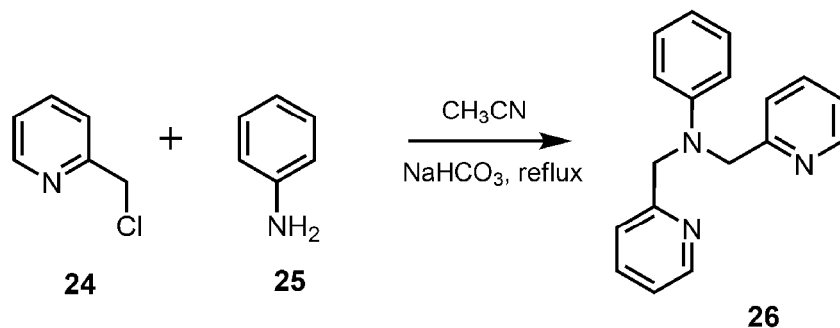


Figure 42. Synthesis of compound 26.

2-Picolyl chloride hydrochloride, **24**, (27.45 mmol, 4.5 g) and aniline, **25**, (9.15 mmol, 850 mg) were refluxed in 100 mL CH₃CN. Solvent was evaporated under reduced pressure and extracted with NaHCO₃ solution and organic phase was collected. Solvent was evaporated and compound **26** was purified by column chromatography with an eluent, CH₃OH; CHCl₃ (95; 5 v/v). Brown crystal compound (8.0 mmol, 2.20 g, 87%) ^[62]

¹H NMR (400 MHz, CDCl₃) δ: 8.47 (d, *J*=4.0 Hz, 2H), 7.50-7.47 (m, 2H), 7.16 (d, *J*=7.6 Hz, 2H), 7.07- 7.03 (m, 4H), 6.62- 6.60 (m, 3H), 4.70 (s, 4H, -CH₂)

2.3.8 Synthesis of Compound (27)

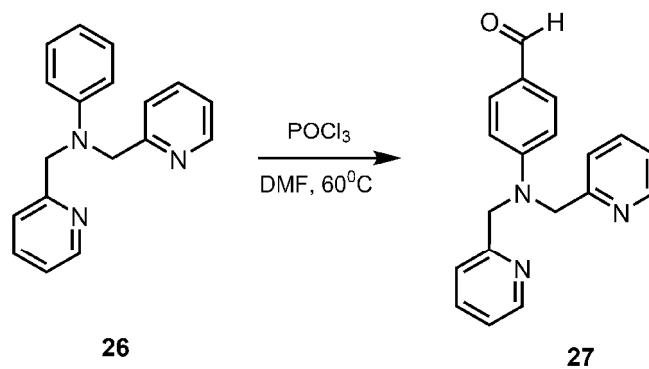


Figure 43. Synthesis of compound **27**.

To a cooled (5 °C) solution of freshly distilled anhydrous DMF (25 mL) was added POCl₃ (615 mg, 4 mmol) within 5 min. The mixture was stirred for 30 min, then **26** (1.0 g, 3.30 mmol) was added and the resulting mixture was heated for 3h at 80 °C. The mixture was hydrolyzed by slow addition of ice-cold water and then neutralized with 5 M NaOH. The product was extracted with CHCl₃ and washed with water and dried with Na₂SO₄. After evaporation of the solvent in vacuo, the product was purified by column chromatography eluting with hexane acetone (2:1) to afforded the aldehyde **27** in 80 % yield, as a viscous liquid: 810 mg.^[62]

¹H NMR (400 MHz, CDCl₃) δ: 9.60 (s, 1H, Al-H), 8.50 (d, 2H), 7.55 (m, 4H), 7.10 (m, 4H), 6.70 (d, 2H), 4.80 (s, 4H, -CH₂).

2.3.9 Synthesis of Compound (28)

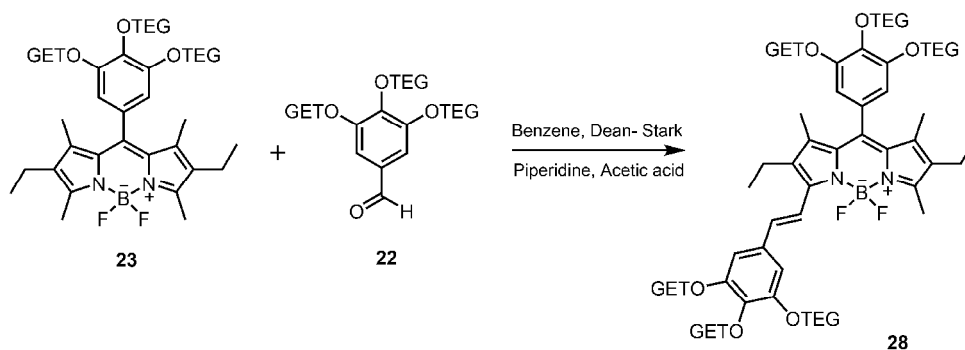


Figure 44. Synthesis of compound **28**.

Compound **23** (0.093 mmol, 90 mg) and **22** (0.186 mmol, 110.2 mg) were refluxed in a mixture of toluene (20 mL), glacial acetic acid (1.5 mL), and piperidine (2 mL). Any water formed during the reaction, was removed azeotropically by heating overnight in a Dean-Stark apparatus. Solvents were removed under reduced pressure, and the crude product was then purified by silica gel column chromatography using $\text{CHCl}_3/\text{CH}_3\text{OH}$ (95/5, v/v). The blue colored fraction was collected then the solvent was removed under reduced pressure to yield compound **28** (0.0186 mmol, 39.5 mg, 21%). Used without purification.

ESI-HRMS calcd for $\text{M}+\text{Na}$ 1463.7739, found 1463.7784, $\Delta=1.0$ ppm

2.3.10 Synthesis of Compound (29)

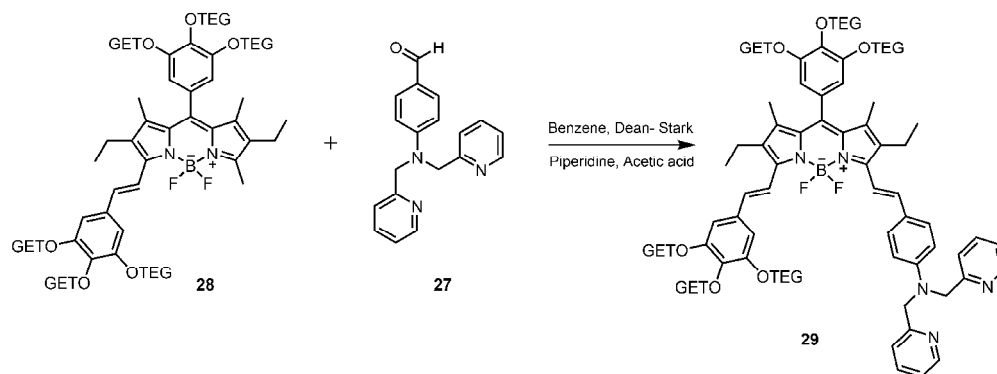


Figure 45. Synthesis of compound **29**.

Compound **28** (0.0625 mmol, 90 mg) and **27** (0.0625 mmol, 19.2 mg) were refluxed in a mixture of benzene (20 mL), glacial acetic acid (1.5 mL), and piperidine (2 mL). Any water formed during the reaction, was removed azeotropically by heating overnight in a Dean-Stark apparatus. Solvents were removed under reduced pressure, and the crude product was then purified by silica gel column chromatography using CHCl₃/CH₃OH (95/10, v/v). The green colored fraction was collected then the solvent was removed under reduced pressure to yield compound **29** (0.0186 mmol, 32.5 mg, 32%).

¹H NMR (400 MHz, CDCl₃) δ: 8.52 (d, *J*= 4.3 Hz, 2H, Ar-H), 7.58 (t, *J*=7.6 Hz, 2H, Ar-H), 7.55 (d, *J*= 16.5 Hz, 2H, ethylene H), 7.37 (d, *J*=8.4 Hz, 2H, Ar-H), 7.20-7.07 (m, 4 H, Ar-H), 7.01 (d, *J*=16.5 Hz, 2H, ethylene H), 6.77 (s, 2H, Ar-H), 6.67 (d, *J*=8.4 Hz, 2H, Ar-H), 6.50 (s, 2H, Ar-H), 4.80 (s, 4H, -CH₂), 4.20-4.02 (m, 10H), 3.80-3.23 (m, 80 H), 2.50 (q, *J*=7.4 Hz, 4H, -CH₂), 1.48 (s, 6H, -CH₃), 1.08 (t, *J*=7.4 Hz, 6H, -CH₃)

¹³C NMR (100 MHz, CDCl₃) δ: 157.2, 152.6, 151.8, 151.3, 148.7, 147.8, 147.6, 138.4, 138.0, 136.0, 135.9, 133.6, 133.1, 132.3, 131.5, 130.1, 128.1, 125.6, 124.3, 121.3, 120.0, 118.9, 115.0, 111.7, 109.0, 107.5, 71.8, 71.5, 71.0, 70.9,

69.9, 69.8, 69.6, 69.5, 68.5, 68.3, 68.2, 57.9, 56.2, 30.9, 28.6, 28.3, 21.7, 17.4,
17.3, 13.3, 13.1, 12.9, 10.5, 10.4.

ESI-HRMS calcd for M+Na 1748.9065, found 1748.9050, $\Delta = 0.9$ ppm

CHAPTER 3

RESULTS AND DISCUSSIONS

3.1 Solid state emissive BODIPY dyes with bulky substituents as spacers⁷²

Although solid state emissive dyes are highly valuable in diverse applications, in the literature, there are few examples of emissive solids. It is well-known that bright fluorescent dyes in solution undergo quenching of emission in the solid state or amorphous solid phase because of the close packing. Considering this point, we proposed a solution to this problem. This solution involves appropriate locating of very bulky groups on the BODIPY core and with this placement, π - π stacking of the chromophore can be minimized. Therefore, we used p-tert-butylphenyl and 3,5-di-tert-butylphenyl substituents to keep π -systems of the fluorophore separate.

With these considerations, we synthesized five compounds. For simplicity, the focus will be on Compound **3** and **6**, and then Compound **9**, **11**, **15** will be discussed.

For the Compound **3** and **6**, we used the standard BODIPY synthesis procedures corresponding to the reactions of appropriate aryl aldehydes and pyrroles. We obtained **3** and **6** in reasonable yields.

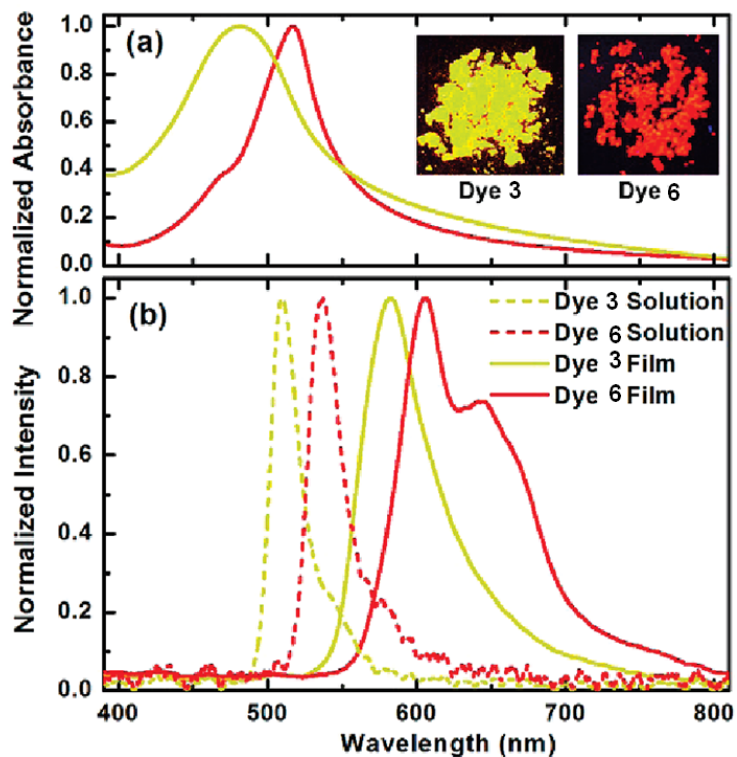


Figure 46. Absorption spectra of the thin films (top) and the emission spectra (bottom) of the dyes **3** and **6** in solution and as thin films. The inset shows the powder form of the compounds under UV irradiation at 360 nm.

Compound **3** and **6** show bright luminescence in the powder form. Also, thin films of these two dyes were prepared by drop casting the solution with toluene as the solvent, on to the glass substrate, and waiting until the solution dries for the determination of emission spectra in the solid state. Concentrations of the solutions were 10.0 and 36.0 mg/mL for dye **3** and **6**, respectively. A postbaking process was carried out under rough vacuum conditions at 80 °C for 1 h. By the use of a surface texture profiler, the final BODIPY film thickness was determined to be 300 nm for dye **3** and 250 nm for dye **6**. Absorption spectra of the dye films (Figure 46, top) were measured by a spectrophotometer and the photoluminescence was characterized by exciting at 325 nm using a continuous He-Cd laser and acquiring the emission data by a fiber-coupled spectrometer.

The excited area on the films was approximately 1 mm², and the average excitation power was 4 mW. The photoluminescence for the solution phase of the dyes was acquired in the same way as the dye films. The introduction of two ethyl substituents on the 2 and 6 positions of the BODIPY core results in a red shift of approximately 30 nm, and this red shift is apparent also in the solid state. Compared to the solution spectra, there is significant red shift of the peak positions in the solid state, which is to be expected, considering stronger intermolecular interactions. Moreover, another smaller peak for compound **6** is clearly present in the spectrum of the dye film obtained using compound **6**, which is indicative of the presence aggregate structures in this compound. This is also to be expected, as 3,5-di-*tert*-butylphenyl groups are clearly superior to 4-*tert*butylphenyl groups in keeping the BODIPY units apart.

In Figure 46, absorbance and emission spectrum of Compound **3** and **6** both in solution and thin films are given. We can conclude that compound **3** and **6** show fluorescence not only in solution, but also in thin film forms. This proves that our design to get solid state emission is satisfactory. After studying spectroscopic properties of our compounds, we made some calculations. It is clear from Table 2 that Stokes shifts of our dyes are comparatively large, 428.8 and 727.1 cm⁻¹ for Compound **3** and **6**, respectively.

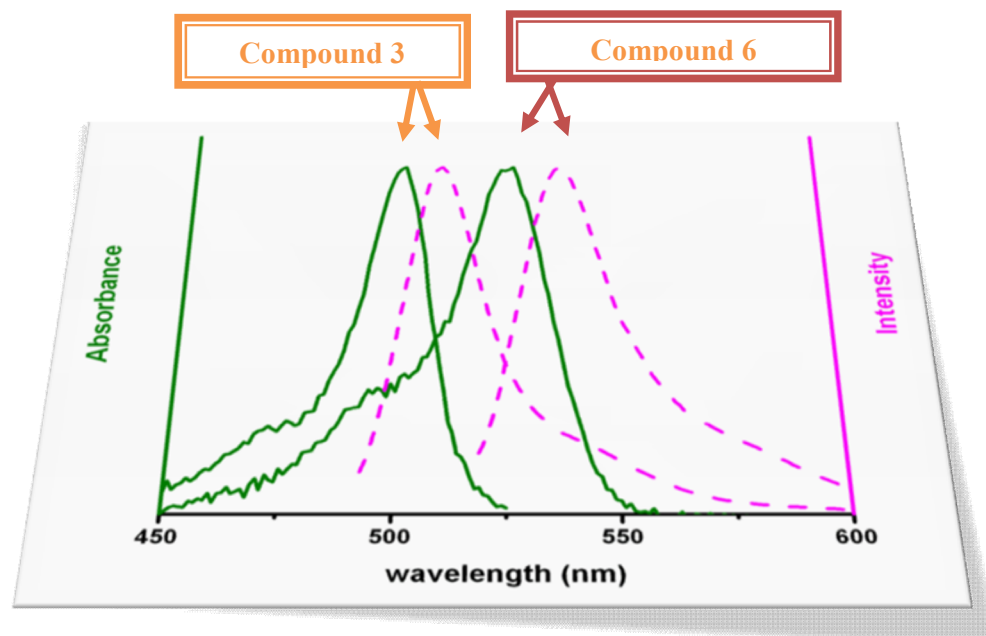


Figure 47. Absorbance and emission spectra of Compound **3** and **6** in CHCl_3 .

Table 2. Quantum yield, max. absorbance, max. emission and Stokes shifts of Compound **3** and **6**.

COMPOUNDS	QUANTUM YIELD	Max. Absorbance (nm)	Max. Emission (nm)	Stokes Shift (cm^{-1})
Compound 3	0.83	501	512	428.8
Compound 6	0.91	527	548	727.1

Absorbance and emission spectra in organic solvents were acquired. Both dyes have high quantum yields in organic solvents ($\Phi_F = 0.83$ and 0.91 respectively, in chloroform).

In order to obtain quantitative data about the molecular structure, suitable crystals for single crystal X-ray diffraction were obtained by the slow evaporation of CHCl_3 solutions at ambient temperature. Crystal structures were as expected, with nearly orthogonal (dihedral angles were 84.3° and 79.6° for **3** and **6** respectively) 8-phenyl substituents. With a careful study of the unit cell, an interesting observation was made: the distance between the closest overlapping near parallel π -surfaces (defined as the boradiazaindacene framework, planes A in neighboring unit cells in Figures 49 and 50) in compound **3** was considerably larger (14.3 \AA) than the similar distance (10.1 \AA) in **6**. Both of them in turn are much larger compared to a reference BODIPY dye with no *meso* substituent and available crystallographic structure.

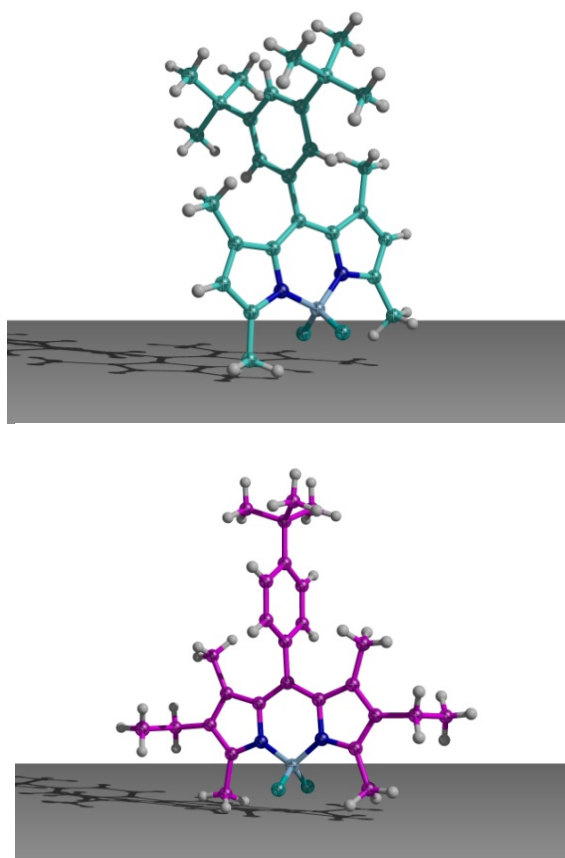


Figure 48. ORTEP drawings of compounds **3** (top) and **6** (bottom).

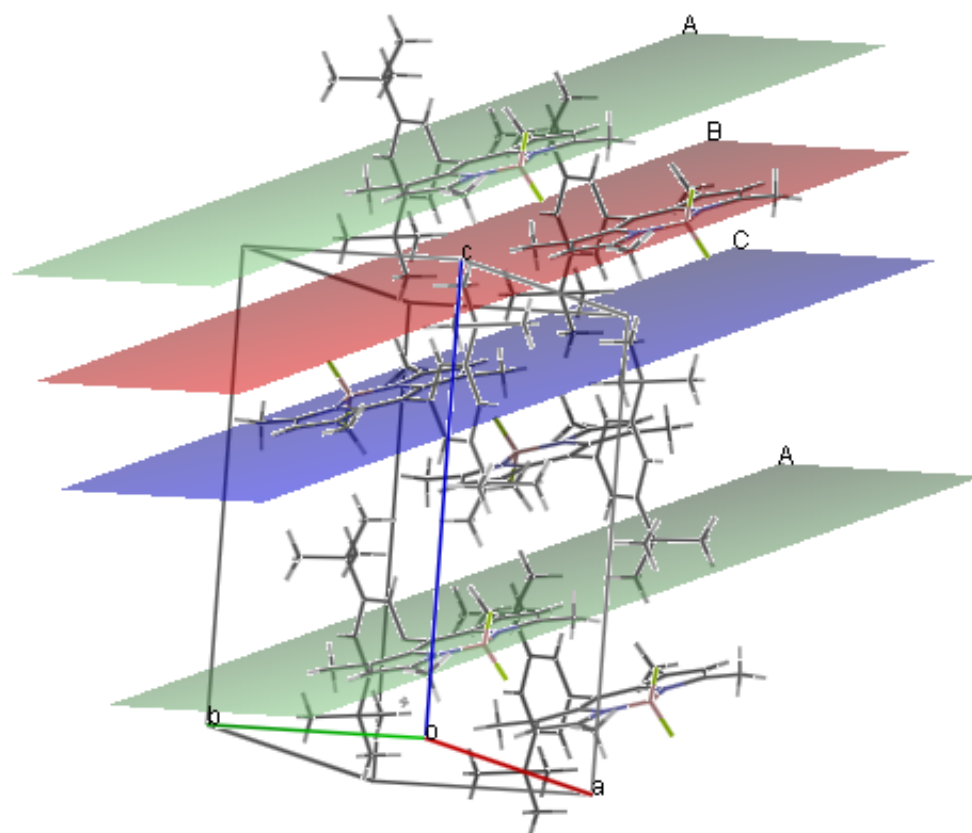


Figure 49. Packing diagram for Compound 3.

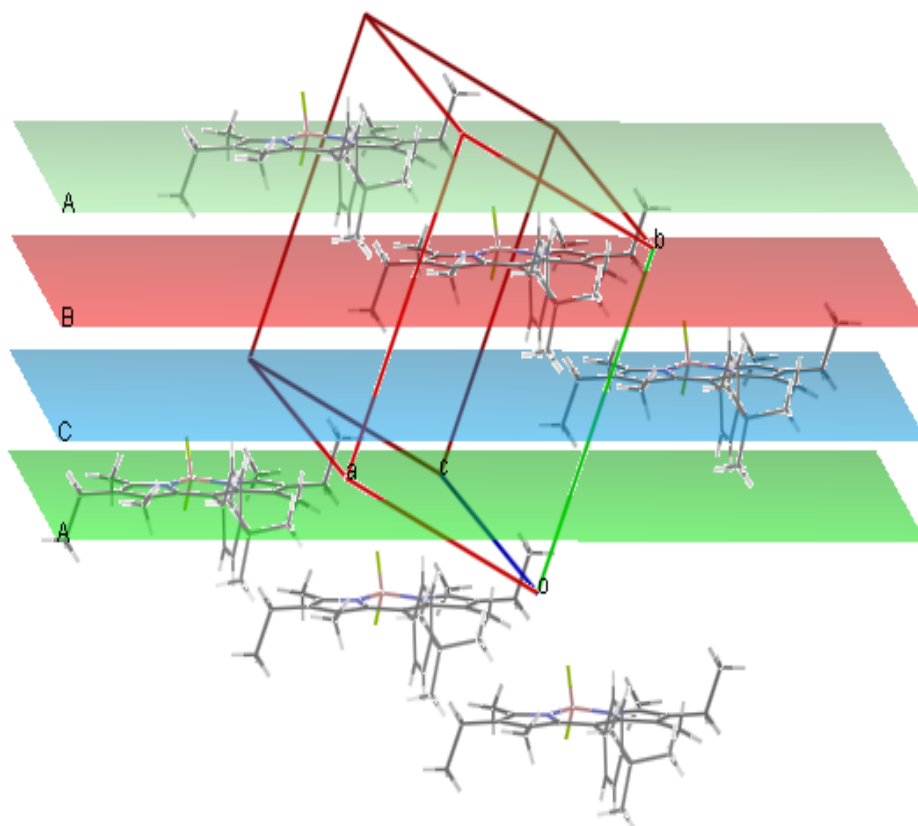


Figure 50. Packing diagram for Compound **6**.

After realizing the superiority of 3,5-di-*tert*-butylphenyl group, we tried to increase the number of this group on the BODIPY core. Therefore, we designed the molecules as shown in Figure 51. Compound **9** has a bright emission in the solid state, however, Compound **11** and **15** have semi-solid property.

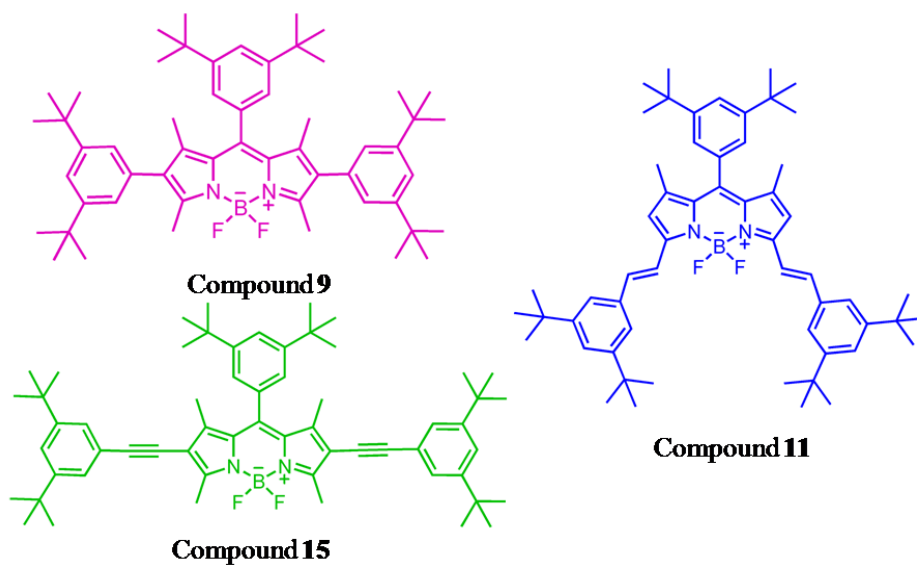


Figure 51. Structural representations of targeted dyes.

After synthesizing the compounds, we took the absorbance (Figure 52) and emission (Figure 53) spectrum in chloroform. The maximum absorbance of Compound **9** is 532 nm and Compound **11** has max. absorbance at 640 nm. Since the conjugation is extended by double bonds on the 3rd and 5th positions. Similarly, max. absorbance of Compound **15** is nearly 573 nm and by the extension of conjugation with Sonagashira coupling on 2nd and 6th positions is led to get shift to the longer wavelength. Stokes shift (red shift) is 939.8, 450.5 and 953.6 cm^{-1} for the compounds **9**, **15** and **11** respectively. This results demonstrated that our design worked successfully.

Also, quantum yields calculations showed that compound **9** and **15** have extremely high quantum yields yields in chloroform ($\Phi_F = 0.89$ and 0.86 , respectively). However, Compound **11** has a slightly low quantum yield ($\Phi_F = 0.61$). Red shifted emission in many cases result in somewhat reduced quantum yields.

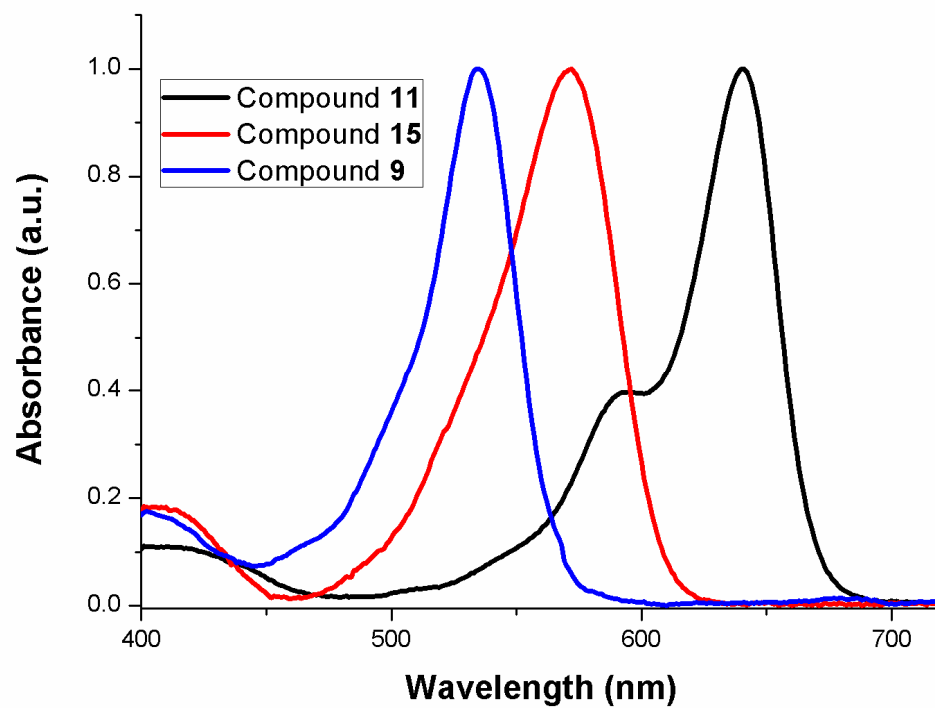


Figure 52. Absorption spectra of dyes **9**, **11** and **15** in CHCl_3 .

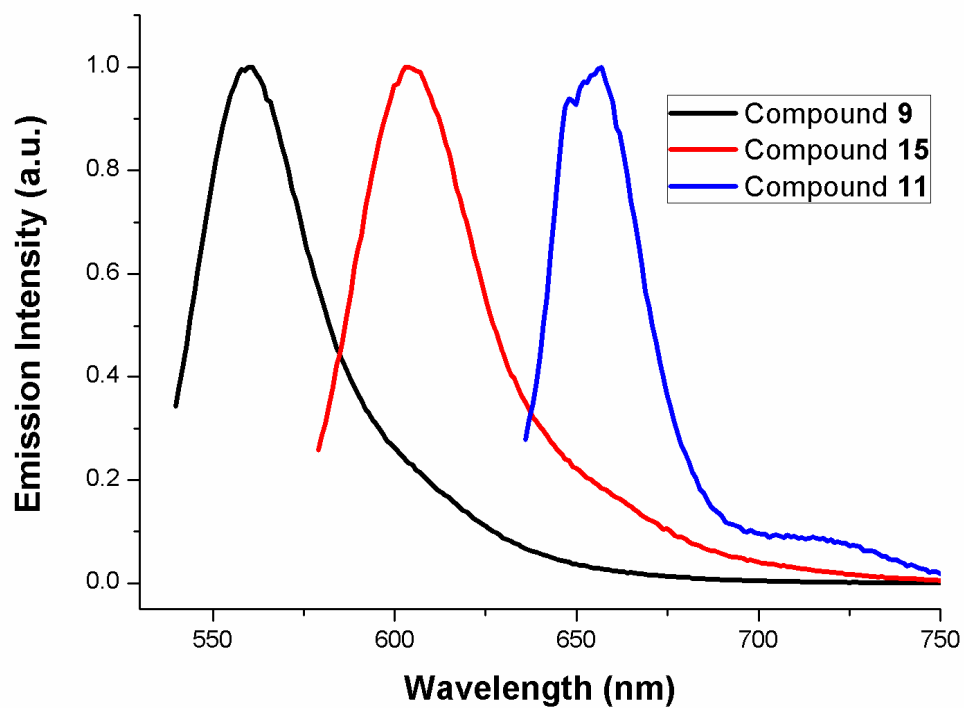


Figure 53. Absorption spectra of dyes **9**, **11** and **15** in CHCl_3 .

Table 3. Quantum yield, max. absorbance, max. emission and Stokes shifts of Compound **9**, **11** and **15**.

COMPOUNDS	QUANTUM YIELD	Max. Absorbance (nm)	Max. Emission (nm)	Stokes Shift (cm^{-1})
Compound 9	0.89	532	560	939.8
Compound 11	0.61	640	659	450.5
Compound 15	0.86	572	605	953.6

For the quantum yield measurements, we used three different references. All excitation and emission slits was both 5 nm. Compound **3** was excited at 489 nm and fluorescein was used as the reference compound. Fluorescein quantum yield is 0.95 in 0.1 M NaOH solution⁵. Compound **6** was excited at 480 nm and Rhodamine 6G was used for quantum yield calculation. Rhodamine 6G quantum yield is 0.95 in ethanol. Also, Compound **9** was excited at 488 nm and again, Rhodamine 6G was used as a reference. However, this time measurements were done in water and quantum yield of Rhodamine 6G in water is 0.95. For Compound **11** and **15**, cresyl violet⁵ was used and excitation was done 570 nm and 540 nm respectively.⁷³

3.2 A Sensitive and Selective Ratiometric Near IR Fluorescent Probe for Zinc Ions Based on the Distyryl-Bodipy Fluorophore⁷⁴,

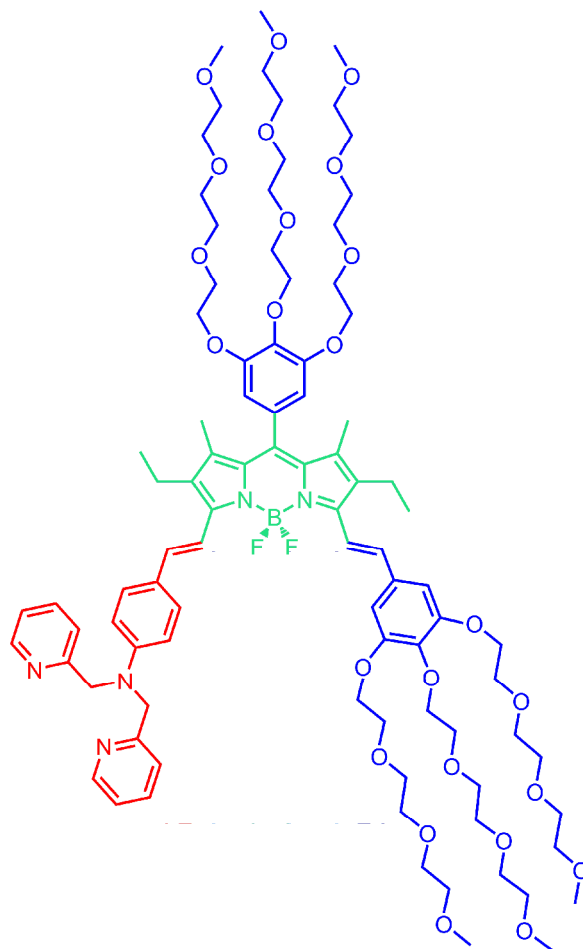


Figure 54. Representation of the modulated BODIPY fluorophore as a Zn²⁺ selective chemosensor

There are numerous examples of Zn (II) selective chemosensors in the literature. As mentioned above, some requirements must be fulfilled to have a good chemosensor. With these considerations, we designed and characterized a sensitive, selective, ratiometric, near-IR and water-soluble fluorescent chemosensor for Zn(II).

Water-solubility is one of the important parameters to obtain a properly working chemosensor. On the other hand, water-soluble chemosensors are rare in the literature and so limitations for biological applications arise. To overcome this problem, we used triethyleneglycole (TEG) groups to increase the water-solubility. TEG groups can be synthesized by starting from 3,4,5-trihydroxybenzoic acid (known as gallic acid) to get ethyl 3,4,5-trihydroxybenzoate. Ethyl 3,4,5-trihydroxybenzoate and triethylene glycol methyl ether tosylate were refluxed in acetone and using K_2CO_3 and 18-crown-6. Then, reduction with $LiAlH_4$, followed by oxidation by PCC gave the compound **22**. With this compound, firstly, 8 position on the BODIPY core was functionalized, and then we placed another three TEG groups on BODIPY core by using Knoevenagel condensation. This condensation allows the transformation acidic methyl groups on the 3,5 positions. With these functionalizations, we get totally water-soluble fluorescent chemosensor. For the absorption and emission studies, we used in 5:95 ethanol-aqueous buffer solution and chloride salts of metals.

Another problem faced while designing the well-working chemosensor is to obtain near-IR fluorophore. To surpass this problem, we used the versatile properties of BODIPY. We reached almost 700 nm emission by using Knoevenagel condensations. To obtain di-styryl BODIPY, we used two different aldehyde to modulate 3 and 5 positions. As mentioned before, near-IR dyes are very important for biological applications.

The other problem that must be overcome is to be able to have highly selective and sensitive chemosensor. For this, we used dipicolylamine (DPA) unit in which Zn(II) can easily and strongly coordinate. DPA unit was bound to BODIPY unit by Knoevenagel condensation. This moiety helped to get selective response to Zn (II) and also we can obtain ratiometric response which is crucial in chemosensors.

For proving the selectivity of Compound **29**, we took the absorption spectra with the different metal cations as seen in Figure 55. In absorption spectrum, we can interpret that Compound **29** shows a maximum at 680 nm with the extinction coefficient $72\,000\text{ M}^{-1}\text{cm}^{-1}$. Also, gradual addition of Zn(II) displayed a 15 nm blue shift and its color changed from green to blue and this color changes can be observed by naked eye. Moreover, as seen, other cations rather than Zn(II) did not alter the absorption maxima of our chemosensor.

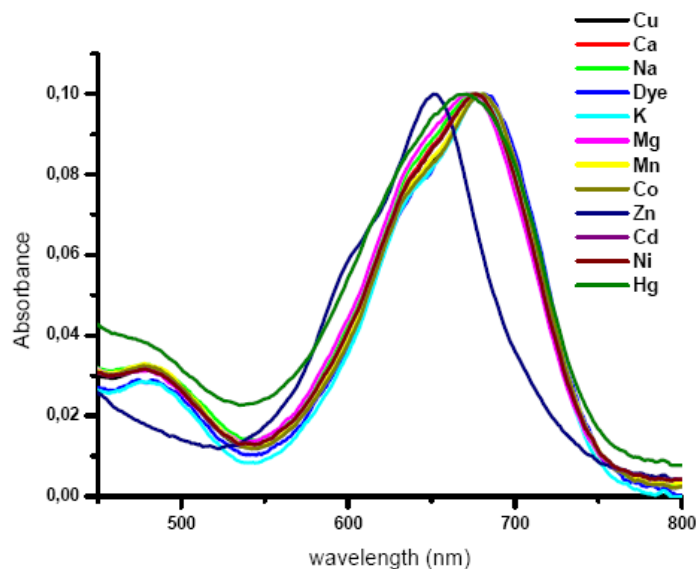


Figure 55. Absorbance change of the dye 56 (2.5 μM) in response to different metal ions (5.0 μM) in aqueous solutions. The solutions are buffered with 0.1 M HEPES pH 7.2. 5% EtOH was added as cosolvent.

From Figure 56, which shows the emission spectrum of our chemosensor in response to different cations, we can interpret that upon coordination of Zn(II), fluorescence is highly enhanced compared to other cations. Furthermore, Hg(II) and Cd(II) also shows enhancement, however, in the biological environment, these cations are negligible in living cells.

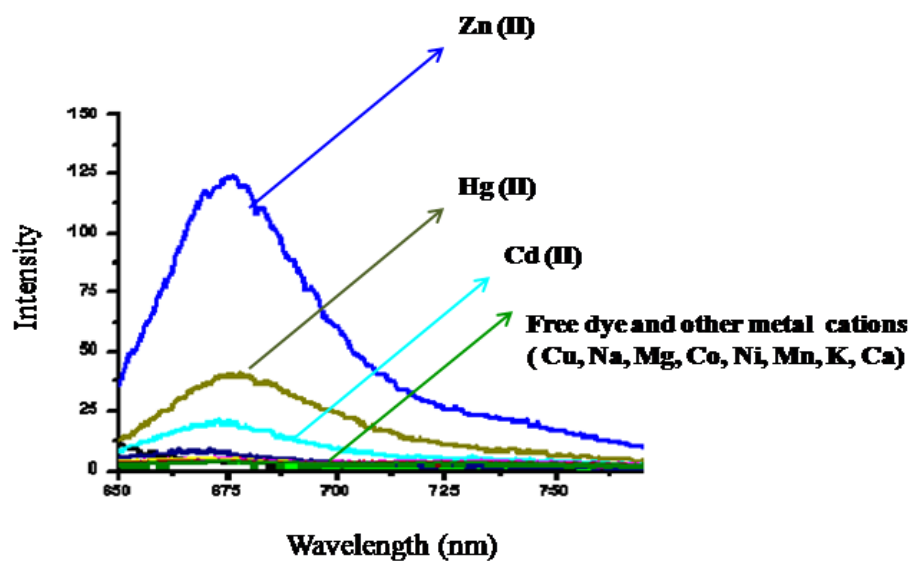


Figure 56. Change in the emission spectrum in response to different cations (100 μM) in aqueous medium at pH 7.2. Excitation was done at 630 nm. The solutions are buffered with 0.1 M HEPES pH 7.2. 5% EtOH was added as cosolvent.

Also, the absorption spectrum of Compound **29** with the increasing concentration of Zn (II) shows the blue shift and this shift helped us to observe the selectivity of our chemosensor (Figure 57).

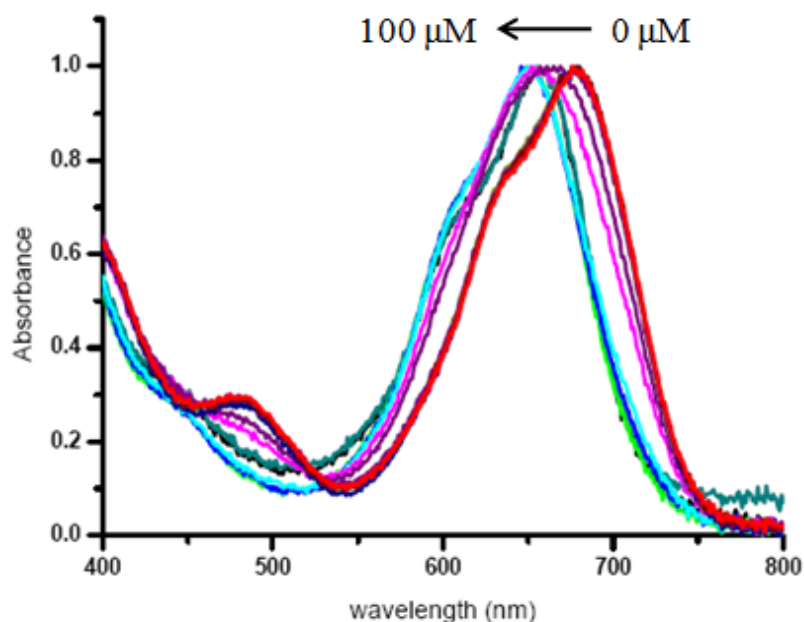


Figure 57. The change in absorption spectrum of the dye **29** ($2.5 \mu\text{M}$) as a function of increasing Zn(II) concentration. Concentration of Zn(II) is varied between 0 to $100 \mu\text{M}$.

After obtaining absorption spectra, we acquired the emission spectra of our targetted chemosensor (Figure 58). The spectra were taken in aqueous buffer solution with the help of cosolvent which is ethanol (at 5%). We excited the chemosensor at 630 nm and the compound **29** showed a peak at 726 nm. As expected, by the addition of Zn(II) gradually, we observed a blue shift approximately 50 nm. Addition of Zn(II) did not only provide a 50 nm blue shift in emission, but also increased the emission intensity. This case proves that excited-state charge transfer from the dipicolylphenyl group was hindered by the coordination of Zn(II) .

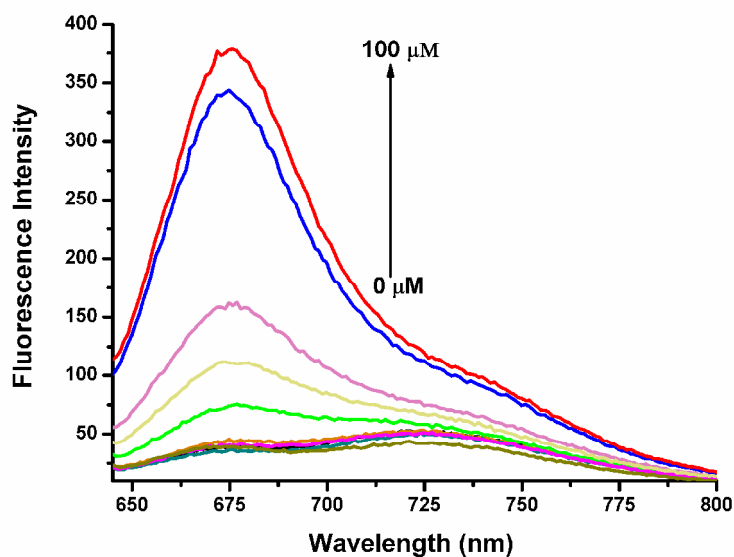


Figure 58. Change in the emission spectrum of the dye **29** (2.5 μM) in response to increasing concentrations of Zn(II) in ethanol-water mixture (5% in ethanol). Zinc concentrations were varied in the following order: 0, 0.25, 0.5, 1, 2, 5, 10, 20, 50, 100 μM . Excitation was at 630 nm, with slit widths of 5 nm.

By the analysis of Hill plot which is obtained by the titration of **29** with Zn(II), we determined a 1:1 stoichiometry (slope= 0.97) and a dissociation constant (K_d) of 2.0×10^{-5} M (Figure 59 and 61).

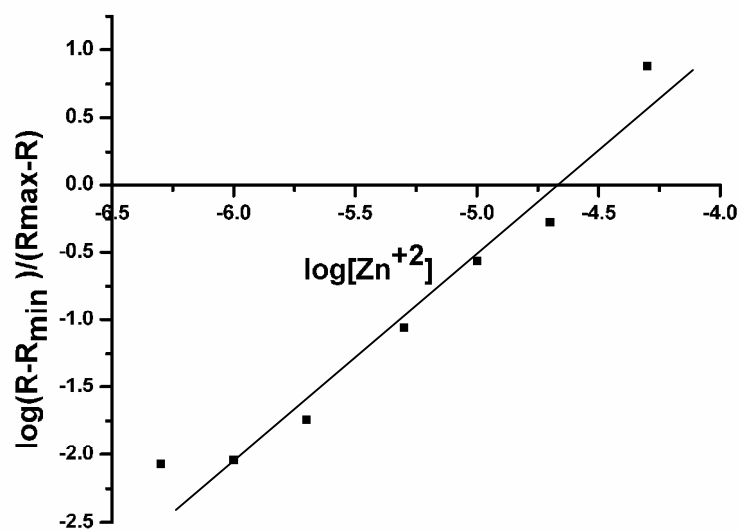


Figure 59. Fluorescence intensity ratio (F_{675}/F_{730}) of **29** versus $\log [\text{Zn}^{2+}]$. The concentration of **56** was 2.5 μM . Hill plot analysis yielded to 1:1 stoichiometry with a slope 0.97.

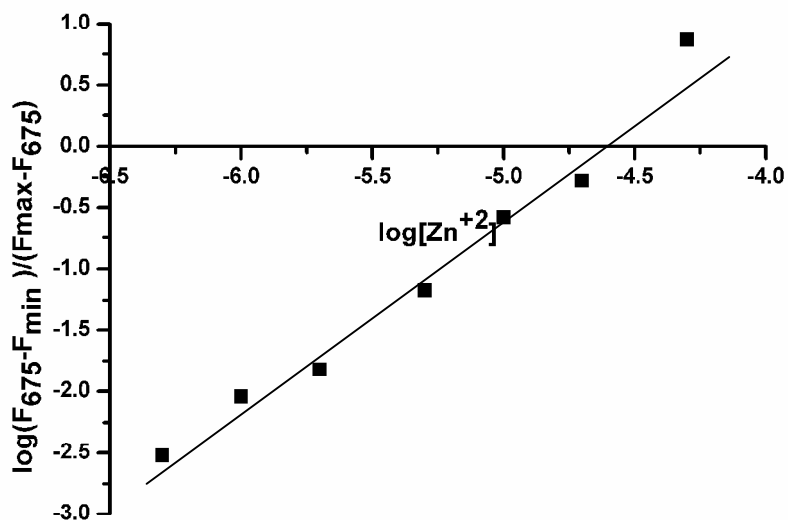


Figure 60. Logarithmic values for the fluorescence intensity of dye at 675 nm versus $\log[\text{Zn}^{2+}]$. Hill coefficients (0.938) fits with 1:1 coordination of dye- Zn^{2+}

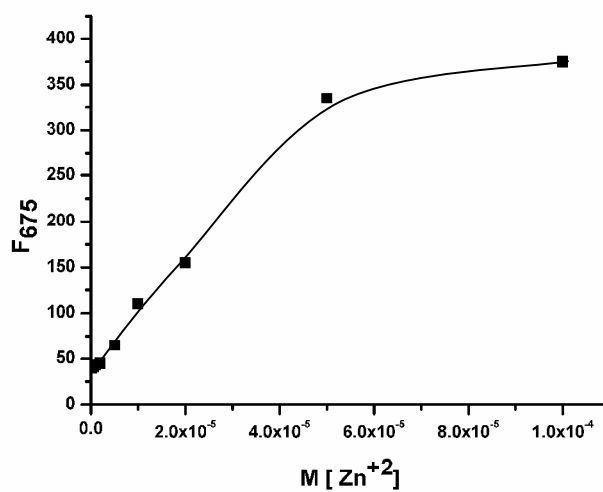


Figure 61. Curve of fluorescence intensity at 675 nm of the dye versus increasing concentration of Zn^{2+} . The concentration of the dye was 5.0 μM . Dissociation constant was calculated as 2.0×10^{-5} M.

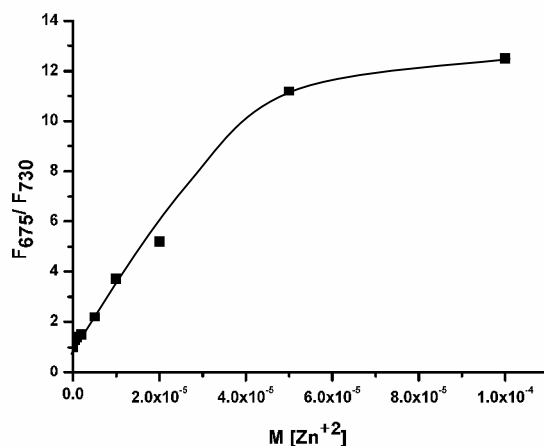


Figure 62. Curve of fluorescence ratio of the dye at 675 nm and 730 nm (5.0 μM) versus increasing concentration of Zn^{2+} .

As stated above, the absorption of dye **29** has a 15 nm blue shift and its color turned from green to blue and can be observed with naked eye. Figure 63 shows not only the color change under ambient light but also under UV light at 360 nm. This photograph was taken in ethanol-aqueous buffer mixture (5% in ethanol, HEPES 0.1 M, pH= 7.2) and our chemosensor **29** showed a bright red emission under UV light at 360 nm. Moreover, as seen, other cations except Zn (II) did not change its color in both cases.

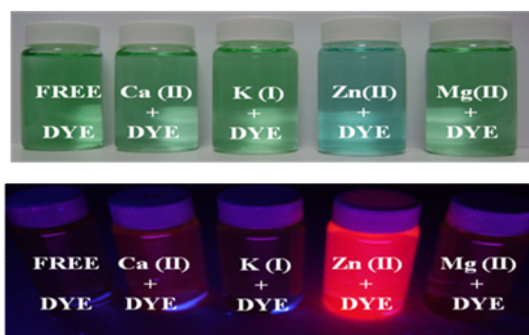


Figure 63. Digital photographs of the chemosensor solutions (5.0 μM) in the presence of different metal ions at 100 μM concentration. The upper plate is taken under ambient light, and the bottom one under UV illumination at 360 nm.

Solvent: ethanol-aqueous buffer mixture (5% in ethanol, HEPES 0.1 M, pH= 7.2).

When we plotted the bar graph of the normalized emission intensities at 680 nm which is the emission intensity of the chemosensor ($1.2 \mu\text{M}$) in the presence of selected metal ions, we showed the largest response in the presence of Zn(II) ions since the dipicolylamine ligand indicated highly supremely metal ion selectivity with this chemosensor (Figure 64). Also, coordination of Zn (II) gave brightly red fluorescence emission whereas the chemosensor itself has the emission in the visible range. On the other hand, Hg(II) and Cd(II) showed some signal. Luckily, these ions are not so common in biological samples as in the case in environmental samples. Therefore, the important parameter is to detect Zn(II) in the presence of Ca(II), K(I), Na(I), and Mg(II) because these ions are together in biological samples. Hence, our chemosensor is very selective over these ions. Then, we performed the competition experiments between Zn (II) and selected metal ions (Figure 65).

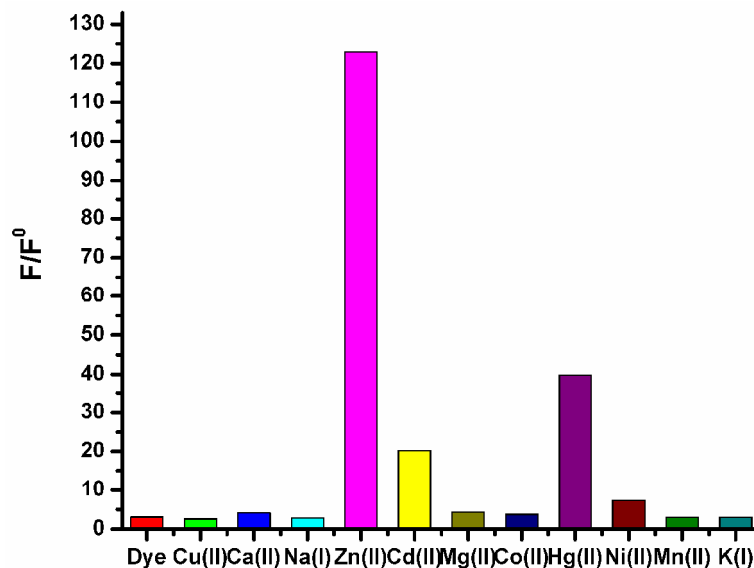


Figure 64. Normalized emission intensities at 680 nm (the emission intensity of the free dye= 1) of the chemosensor (1.2 μM) in the presence of selected metal ions (1.0 mM). Excitation was done at 630 nm with 5 nm slit widths. Solvent: ethanol-aqueous buffer mixture (5% in ethanol, HEPES 0.1 M, pH= 7.2).

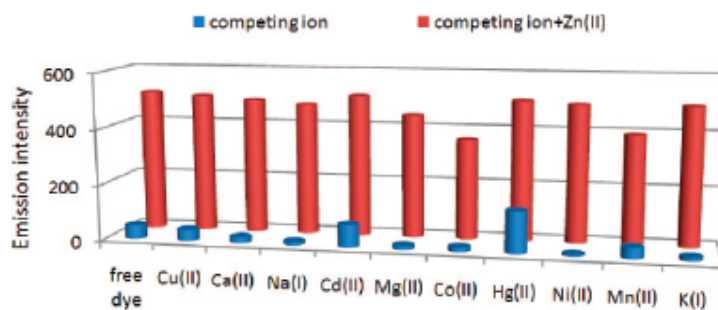


Figure 65. Results of the competition experiments between Zn (II) and selected metal ions. The free dye 29 (chemosensor) concentrations were set at 2.5 μM . Excitation was at 630 nm; emission intensity values at 680 nm were collected; and all metal ions were added at 200 μM concentration. Solvent: ethanol-aqueous buffer mixture (5% in ethanol, HEPES 0.1 M, pH=7.2).

In this thesis, the dissociation constants of the dyes were calculated by taking into consideration the appropriate metal cations with fluorescence intensity ratio in the well matched emission wavelength as illustrated in the Figures 61 and 62. The following equation was used to get these graphs.



$$K_s = [ML] / [M] [D]$$

Complexation of metal cation with dye at each concentration represented as, c_M , the fluorescence intensity monitored at two wavelengths (these wavelengths are selected as where dye is metal free and at the wavelengths where metal is complexed with dye).

$$Y(w_1) = a_{w1} [D] + b_{w1} [MD] \quad Y(w_2) = a_{w2} [D] + b_{w2} [MD]$$

The ratiometric measurements consist of R;

$$R = \frac{a_{w1} [D] + b_{w1} [MD]}{a_{w2} [D] + b_{w2} [MD]}$$

For the free dye and fully complexation of dye with metal, the values of R;

$$R_{\min} = \frac{a_{w1}}{a_{w2}} \quad R_{\max} = \frac{b_{w1}}{b_{w2}}$$

Then;

$$\frac{R - R_{\min}}{R_{\max} - R} \frac{a_{w2}}{b_{w2}} = K_s [M] \quad \Rightarrow \quad \log\left(\frac{R - R_{\min}}{R_{\max} - R}\right) = \log K_s \frac{b_{w2}}{a_{w2}} + \log [M]$$

By plotting the graphs, stability constants, K_s , and binding constants were easily obtained from the sigmoidal curves and the slopes.

CHAPTER 4

CONCLUSION

In this study, we focus on two different studies. In the first part, we report that by the modification on BODIPY core, one can design and synthesize solid state emissive dyes. With bulky groups, we prevent the quenching of fluorescence resulting from π - π stacking in the solid state. Using bulky *tert*-butyl groups, we separated the π -systems of the BODIPY, and highly bright emissive solids were obtained. The improvement of the separation achieved by the 3,5-di-*tert*-butylphenyl group is proven by single crystal X-ray analysis. From this point, we tried to increase the number of this group on BODIPY core. Stokes shifts of these dyes are larger and this property as well, leads to lower the self-absorption.

In the second part, we designed and synthesized that a selective, ratiometric and water-soluble fluorescent sensor for zinc cation. Also, we demonstrated that by utilizing the versatility of BODIPY dye, longer wavelength emission can be achieved. The changes caused by coordination of zinc cation to the receptor part (DPA), were monitored by both absorption and emission spectra. DPA was chosen because it is highly selective and strongly binds to zinc cation. From absorption spectrum, we observed a hypsochromic (blue) shift about 15 nm in 5:95 ethanol: water mixture (0.1 M HEPES pH 7.2). Similarly, emission spectrum allows us to monitor the fluorescence enhancement. Finally, with this chemosensor, water-solubility was achieved, since it is very important to study with biological samples.

In the future, we expect that BODIPY will be applicable in OLED devices with high efficiency and for chemosensor research; the sensors will be used in biological studies effectively.

REFERENCES

1. Stokes, G. G. *Philosophical Transactions of the Royal Society of London*. **1852**, *142*, 463–562.
2. Phil. Trans. R. Soc. Lond. 1853 *143*, 385-396, quote from p. 387
3. Valeur, B. *Molecular Fluorescence*, Wiley-VCH, Weinheim, **2002**, p. 10
4. <http://www.olympusmicro.com/primer/java/jablonski/jabintro/jablonskijavafigure1.jpg>
5. http://www.abdserotec.com/support/stokes_shift-737.html#
6. Lakowicz, J.R. *Principles of Fluorescence Spectroscopy*, Plenum Press, New York, **1999**.
7. Treibs A., Kreuzer F. H., *Justus Liebigs Ann. Chem.* **1968**, *718*, 208.
8. Wada, S., Ito, S., Uno, H., Murashima, T., Ono, N., Urano, T., Urano, Y. *Tetrahedron Lett.* **2001**, *42*, 6711
9. Buyukcakir, O., Bozdemir, O.A., Kolemen, S., Erbas, S., Akkaya, E.U. *Org. Lett.* **2009**, *11*, 4644.
10. López Arbeloa F., Bañuelos J., Martínez V., Arbeloa T., López Arbeloa I. *Int. Rev. Phys. Chem.* **2005**, *24*, 339–374.
11. Thoresen, L. H., Kim, H., Welch, M. B., Burghart, A., Burgess, K. *Synlett* **1998**, 1276
12. Suzuki, A. *J. Org. Chem.* *576* (1999) 147–168
13. *ACS Symposium Series*, Vol. 783 Akira Suzuki *Organoboranes for Syntheses* 14. Chapter 6, pp 80–93.
14. Matos, K., Soderquist, J. A. *J. Org. Chem.* **1998**, *63*, 461-470.
15. Hartley, F. R.; Patai, S. *The Chemistry of Metal-Carbon Bond*; Wiley: New York, **1985**; Vol. **3**.
16. Suzuki, A., Miyaura, N. *Chem. Rev.* **1995**, *95*, 2457-2483.
17. Stille, J. K., Lau, K. S. Y. *Acc. Chem. Res.* **1977**, *10*, 434.
18. Amatore, C., Jutand, A. *J. Organomet. Chem.* **1999**, *576*, 254-278.
19. Suzuki, A. *Pure Appl. Chem.* **1991**, *63*, 419.

20. Aliprantis, A. O., Canary, J. W. *J. Am. Chem. Soc.* **1994**, 116, 6985-6986.
21. Ozawa, F., Yamamoto, A. *Chem. Soc. Jpn.* **1987**, 773.
22. Cheng, F., Adronov, A. *Chem. Mater.* **2006**, 18, 5389-53
23. Blouin, N., Michaud, A., Gendron, D., Wakim, S., Blair, E., Neagu-Plesu, R., Belletete, M., Durocher, G., Tao, Y., Leclerc, M. *J. Am. Chem. Soc.* **2008**, 130, 732-742.
24. Bahl, A., Grahn, W., Stadler, S., Feiner, F., Bourhill, G., Brauchle, C., Reisner, A., Jones, P. G. *Angew. Chem. Int. Ed. Engl.* **1995**, 34, 1485.
25. Castro, C. E., Stephens, R. D. *J. Org. Chem.* **1963**, 28, 2163-2163.
26. Cassar, L. *J. Organomet. Chem.* **1975**, 93, 253-257.
27. Dieck, H. A., Heck, R. F. *J. Organomet. Chem.* **1975**, 93, 259-263.
28. Sonogashira, K., Tohda, Y., Hagihara, N. *Tetrahedron Lett.* **1975**, 16, 4467.
29. Bozdemir, O.A., Cakmak, Y., Sozmen, F., Ozdemir, T., Siemiarczuk, A., Akkaya, E.U. *Chem. Eur. J.* **2010**, 16, 6346 – 6351.
30. Miller, M. W., Johnson, C.R. *J. Org. Chem.* **1997**, 62, 1582.
31. Svoboda, J., Sedláček, M. B., Vohlídal, J. J., Balcar, H., Mav-Golež, I., Žigon, M. *Acta Chim. Slov.* **2006**, 53, 407–416.
32. Grimme, S., MPck-Lichtenfeld, C., Antony, J. *J. Phys. Chem. C.* **2007**, 111, 11199 – 11207.
33. http://en.wikipedia.org/wiki/Stacking_%28chemistry%29#Aromatic_stacking_interaction
34. Zhang, D., Yugeng, W., Xiao, Y., Yu, G., Liub, Y., Qian, X. *Chem. Commun.* **2008**, 4777–4779.
35. Mizobe, Y., Tohnai, N., Miyata, M., Hasegawa, Y. *Chem. Commun.* **2005**, 1839–1841.
36. Ooyama, Y., Yoshikawa, S., Watanabe, S., Yoshida, K. *Org. Biomol. Chem.* **2007**, 5, 1260–1269
37. Yoshida, K., Ooyama, Y., Tanikawa, S., Watanabe, S. *J. Chem. Soc., Perkin Trans. 2*, **2002**, 708–714.

38. Xu, Z., Yoon, J., Spring, D. R., *Chem. Soc. Rev.* **2010**, *39*, 1996.
39. Rurack, K., Resch-Genger, U. *Chem. Soc. Rev.* **2002**, *31*, 116–127.
40. Southall, N.T., Dill, K.A., Haymet, A.D.J. *J. Phys. Chem.* **2002**, *106*, 521-523.
41. (a) Beer, P.D., Blackburn, C., McAleer, J.F., Sikanyika, H. *Inorg. Chem.*, **1990**, *29*(3), 378. (b) Black, C.B., Andrioletti, B., Try, A.C., Ruiperez, C., Sessler, J.L. *J. Am. Chem. Soc.*, **1999**, *121*, 10438-10439.
42. Lindstrom, C.D. *Chem. Rev.* **2006**, *106* (10), 4281-4300.
43. De Silva, A.P. *Chem. Rev.* **1997**, *97*, 1515.
44. Kavarnos, G.J. *Fundamentals of photoinduced electron transfer*. VCH Publishers, New York. **1993**.
45. Valeur, B., Leray, I. *Coord. Chem. Rev.* **2000**, *205*, 3-40.
46. Kim, S. K., Yoon, J. *Chem. Commun.* **2002**, 770–771.
47. Ostaszewski, R., Klonkowski, A. M., Kledzik, K. *Supramolecular Chemistry*. **2000**, *12*, 131-134.
48. Sung, K., Fu, H.K., Hong, S.H. *J. Fluoresc.* **2007**, *17*, 383–389.
49. Cheng, T., Xu, Y., Zhang, S., Zhu, W., Qian, X., Duan, L. *J. Am. Chem. Soc.* **2008**, *130* (48), 16160–16161.
50. Maruyama, S., Kikuchi, K., Hirano, T., Urano, Y., Nagano, T. *J. Am. Chem. Soc.* **2002**, *124*, 10650-10651.
51. Valeur, B., Leray, I. *Coord. Chem. Rev.* **2000**, *205*, 3-40
52. Liu, W., Xu, Liwei., Sheng, R., Wang, P., Li, H., Wu, S. *Org. Lett.* **2007**, *9*, 3829–3832.
53. Wang, J., Qian, X., Cui, J. *J. Org. Chem.* **2006**, *71*, 4308-4311.
54. Coskun, A., Akkaya, E.U. *J. Am. Chem. Soc.* **2006**, *128*, 14474-14475.
55. Haugland, R. P. *Handbook of Fluorescent Probes and Research Chemicals*, ed. M. T. Z. Spence, Molecular Probes, Eugene, OR, 6th edn, **1996**.
56. Xue, L., Liub, C., Jiang, H. *Chem. Commun.* **2009**, 1061–1063.
57. Choi, D. W., Koh, J.-Y. *Annu. ReV. Neurosci.* **1998**, *21*, 347-375.

58. Bush, A. I., Pettingel, W. H., Multhaup, G., Paradis, M. D., Vonsattel, J.-P., Gusella, J. F., Beyreuther, K., Masters, C. L., Tanzi, R. E. *Science* **1994**, *265*, 1464-1467.
59. Maruyama, S., Kikuchi, K., Hirano, T., Urano, Y., Nagano, T. *J. Am. Chem. Soc.* **2002**, *124*, 10650-10651.
60. da Silva, J.J.R.F., Williams, R.J.P. Zinc: Lewis acid catalysis and regulation. In *The Biological Chemistry of Elements: The Inorganic Chemistry of Life*, 2nd Ed. New York: Oxford UP. **2001**.
61. Kikuchi, K., Komatsu, K., Nagano, T. *Curr. Opin. Chem. Biol.* **2004**, *8*, 182-191.
62. Weiss, J.H., Sensi, S.L., Koh, J.Y. *Trends Pharm Sci.* **2000**, *21*, 395-401.
63. de Silva, A.P., Gunaratne, H.Q.N., Gunnlaugsson, T., Huxley, A.J.M., McCoy, C.P., Rademacher, J.T., Rice, T. *Chem. Rev.* **1997**, *97*, 1515-1566.
64. Pearson, R.G. *J. Am. Chem. Soc.* **1963**, *85*, 353.
65. Ertas, N., Akkaya, E. U., Ataman, O. Y. *Talanta* **2001**, *51*, 693-699.
66. Jiang, W., Fu, Q., Fan, H., Wang, W. *Chem. Commun.* **2008**, 259
67. (a) Turfan, B., Akkaya, E. U. *Org. Lett.* **2002**, *4*, 2857-2859. (b) Harriman, A., Mallon, L. J., Stewart, B., Ulrich, G., Ziesel, R. *Eur. J. Org. Chem.* **2007**, 3191-3198.
68. Sun, W. C., Gee, K. R., Klaubert, D. H., Haugland, R. P. *J. Org. Chem.* **1997**, *62*, 6469-6475.
69. de Silva, S. A., Zavaleta, A., Baron, D. E., Allam, O., Isidor, E. V., Kashimura, N., Percarpio, J. M. *Tetrahedron Lett.* **1997**, *38*, 2237.
70. Jiang, W., Fu, Q., Fan, H., Wang, W. *Chem. Commun.* **2008**, 259.
71. Wu, Y., Peng, X., Guo, B., Fan, J., Zhang, Z., Wang, J., Cui, A., Gao, Y., *Org. Biomol. Chem.* **2005**, *3*, 1387.
72. Ozdemir, T., Atilgan, S., Kutuk, I., Yildirim, L.T., Tulek, A., Bayindir, M. and Akkaya, E.U. *Org. Lett.* **2009**, *11*, 2105.
73. Du, H., Fuh, R. A., Li, J., Corkan, A., Lindsey, J. S. *Photochem. Photobiol.* **1998**, *68*, 141.
74. Atilgan, S., Ozdemir, T., Akkaya, E.U. *Org. Lett.* **2008**, *10*, 4065-4067.

APPENDIX A
NMR SPECTRA

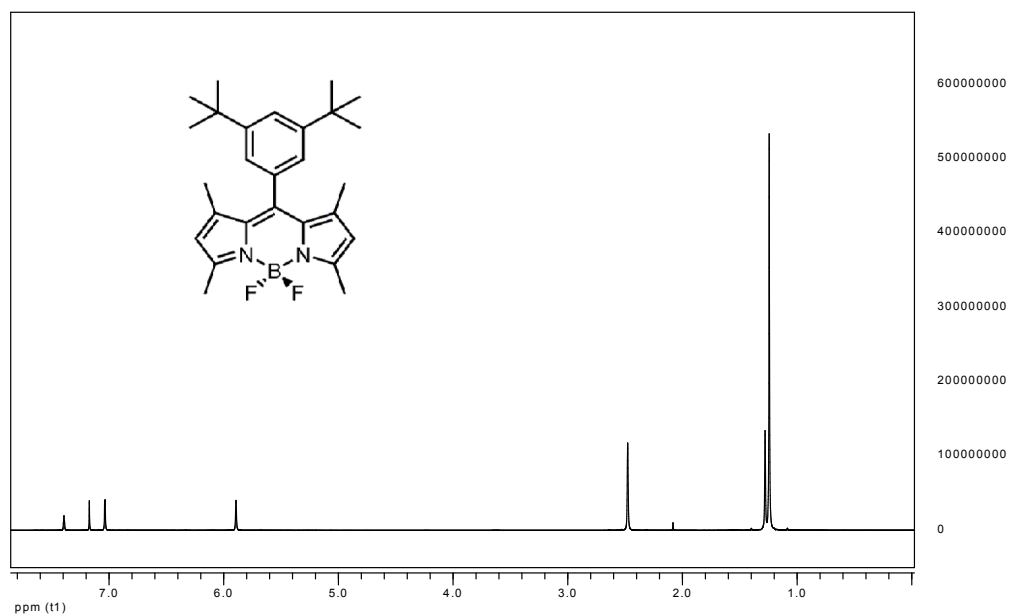


Figure 66. ¹H spectrum of Compound 3.

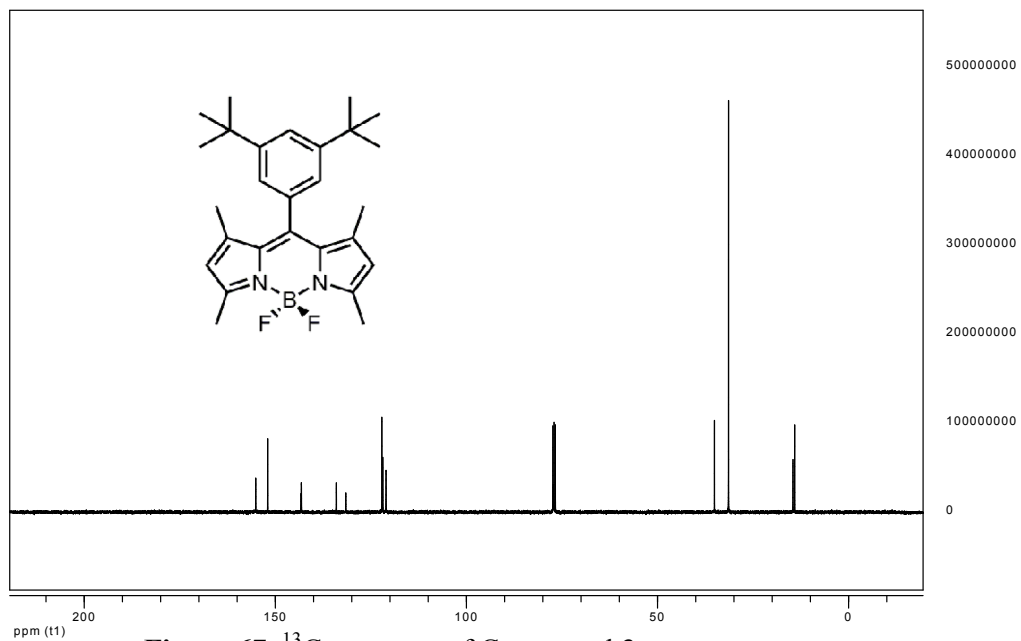


Figure 67. ¹³C spectrum of Compound 3.

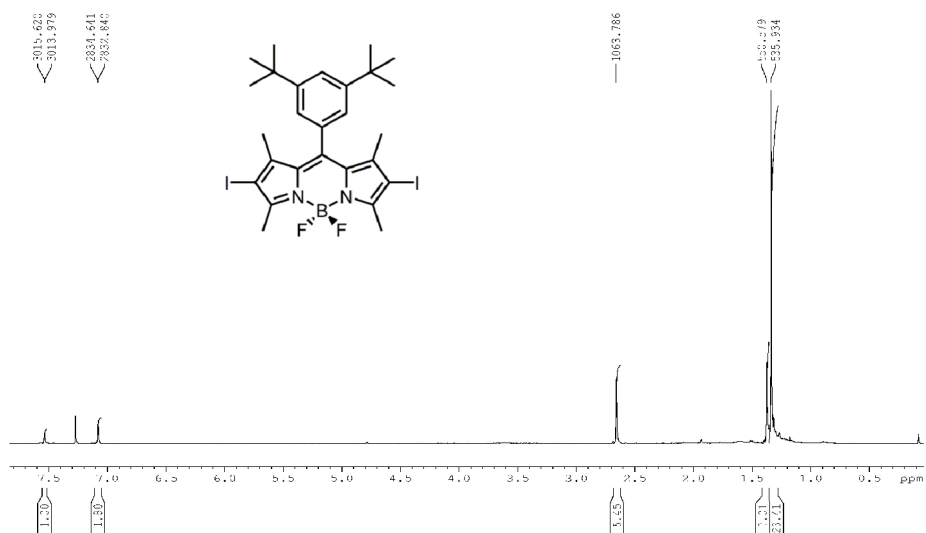


Figure 70. ^1H spectrum of Compound 7.

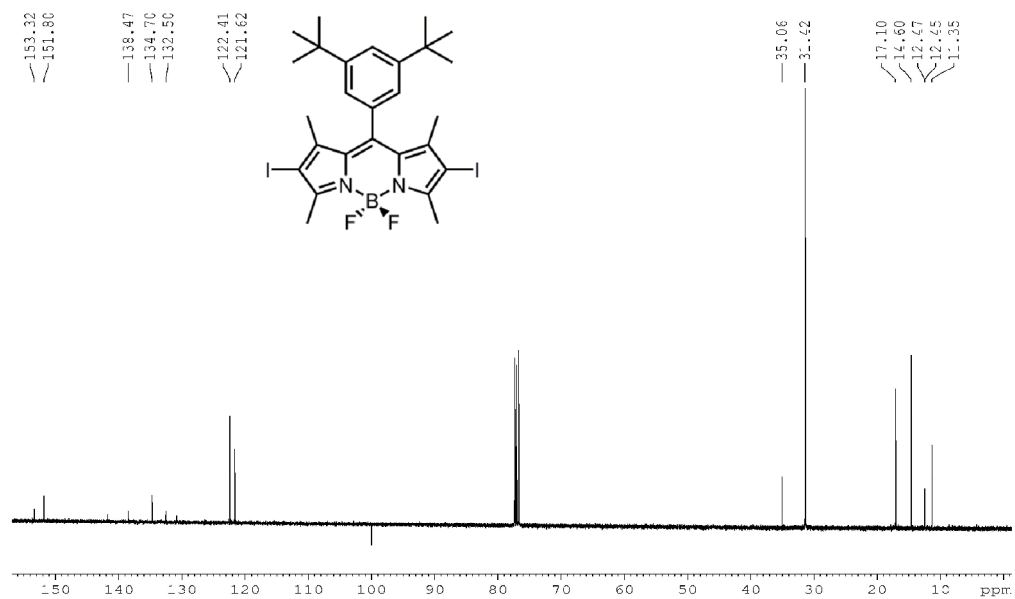


Figure 71. ^{13}C spectrum of Compound 7.

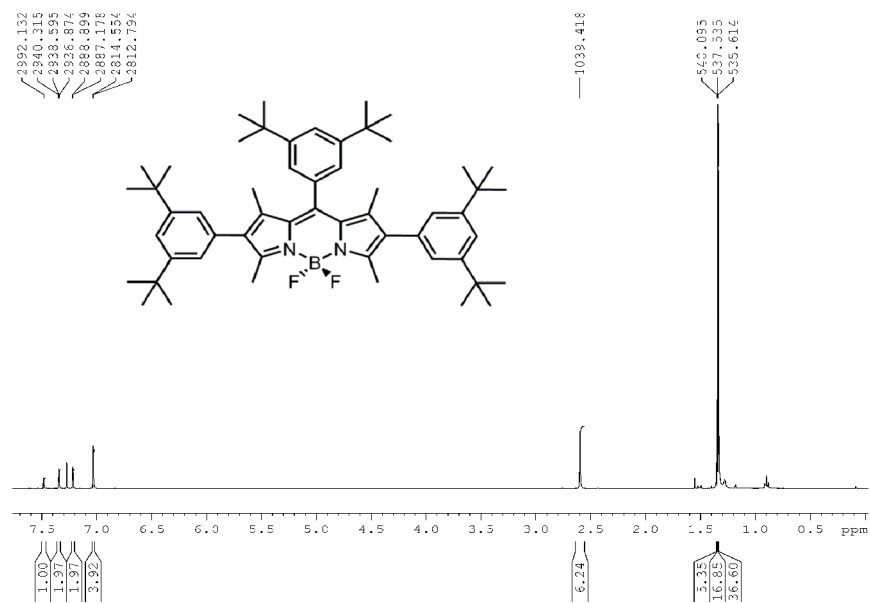


Figure 72. ¹H spectrum of Compound 9.

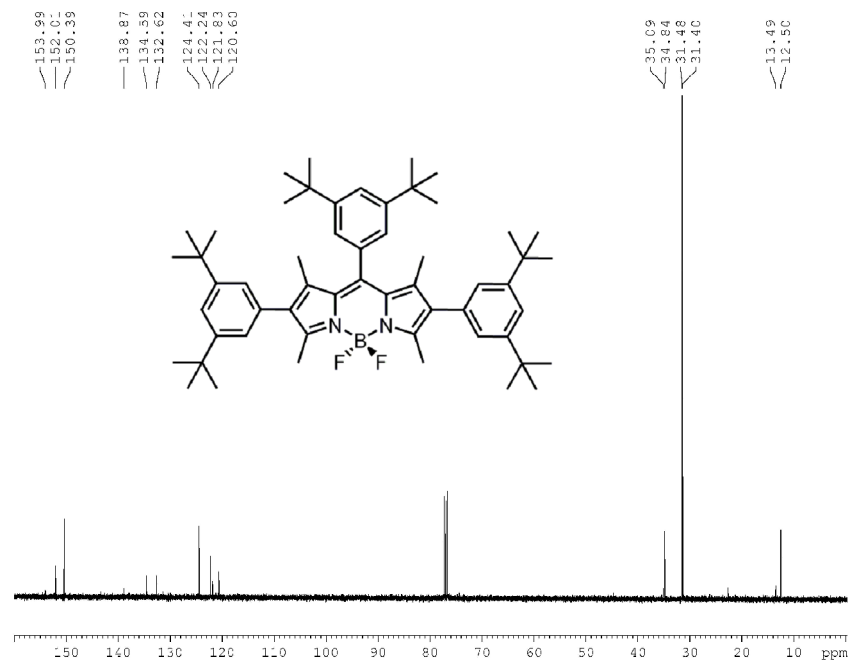


Figure 73. ¹³C spectrum of Compound 9.

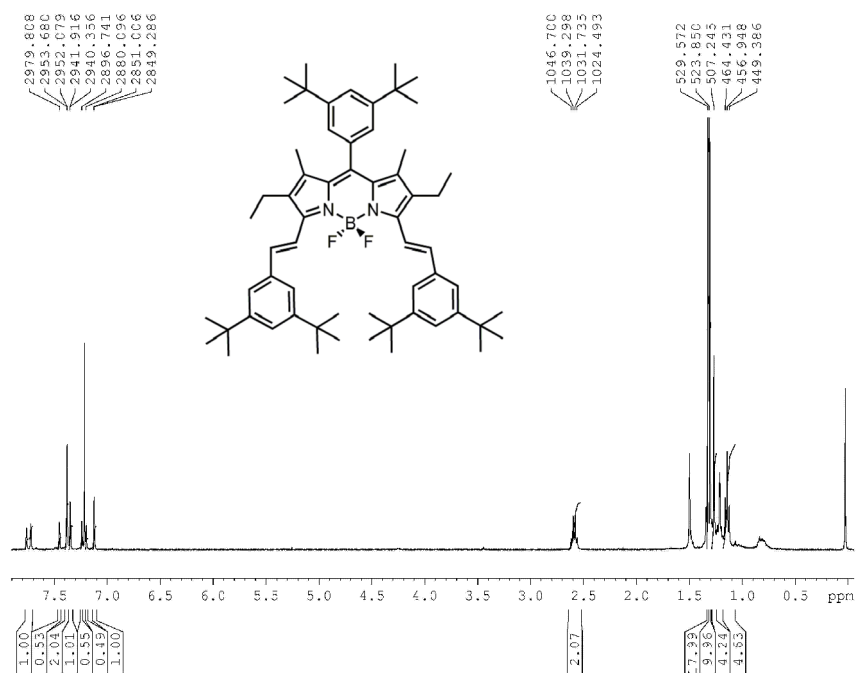


Figure 74. ^1H spectrum of Compound 11.

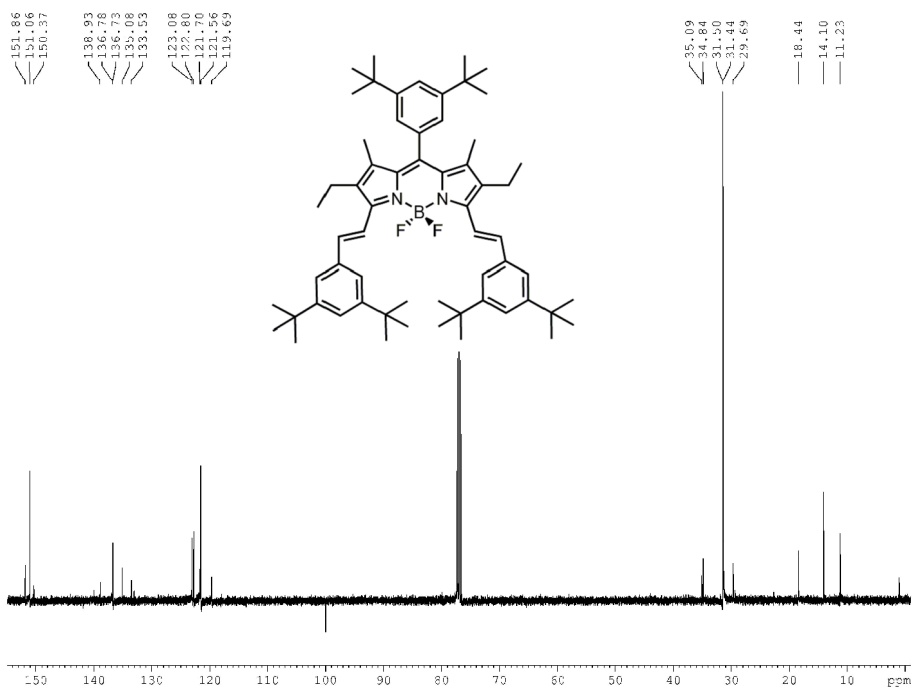


Figure 75. ^{13}C spectrum of Compound 11.

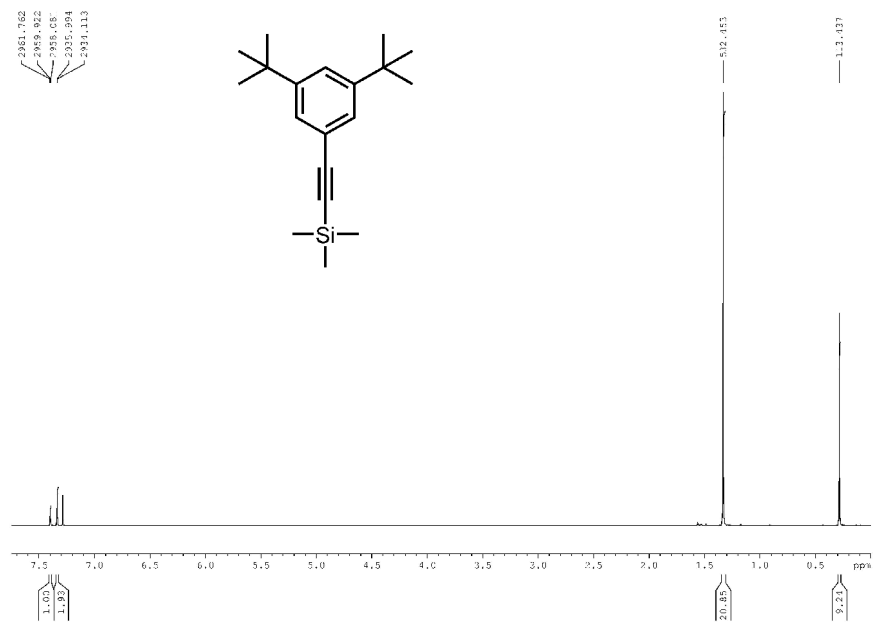


Figure 76. ¹H spectrum of Compound 13.

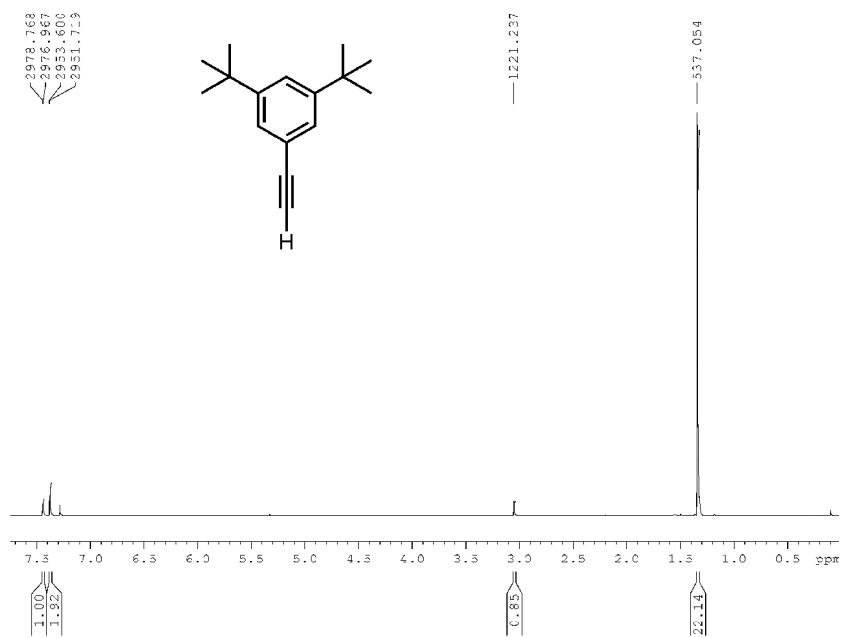


Figure 77. ¹H spectrum of Compound 14.

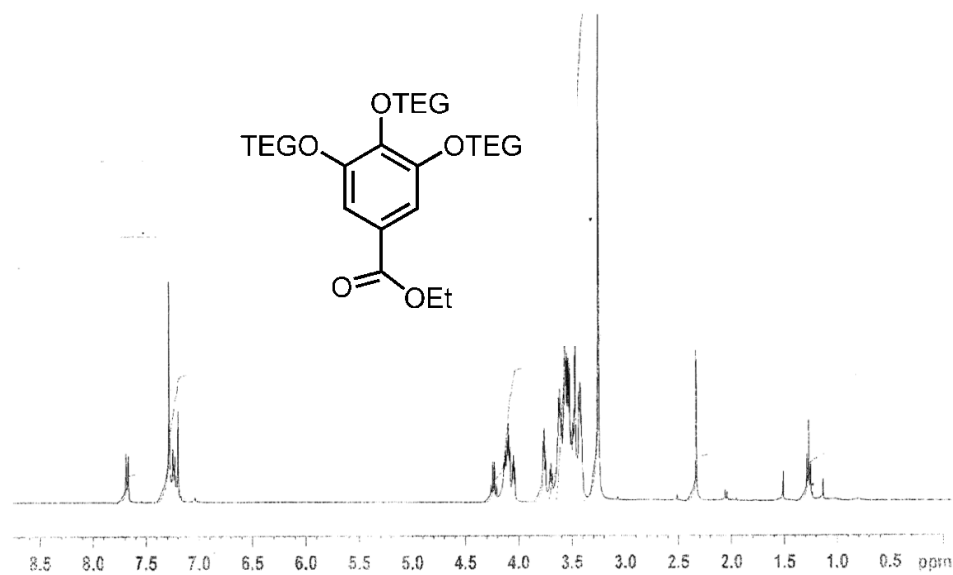


Figure 82. ¹H spectrum of Compound 20.

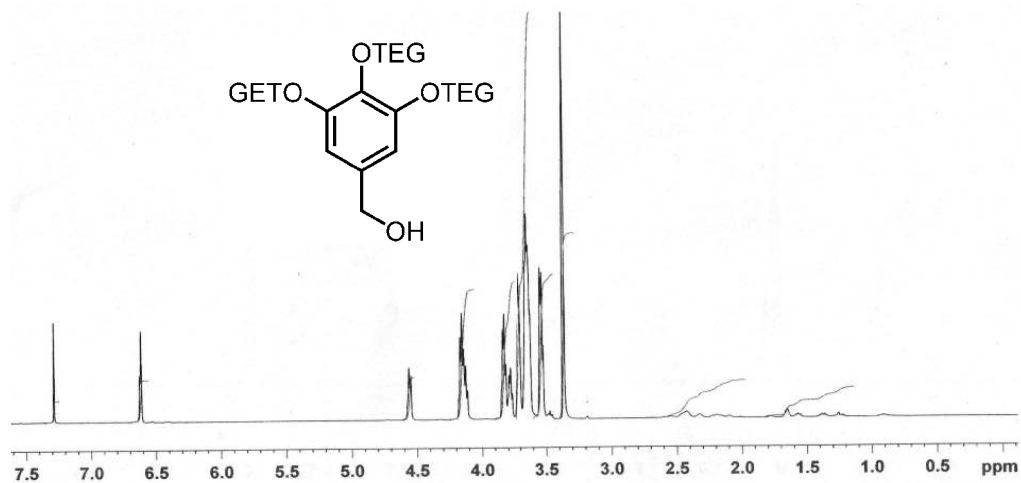


Figure 83. ¹H spectrum of Compound 21.

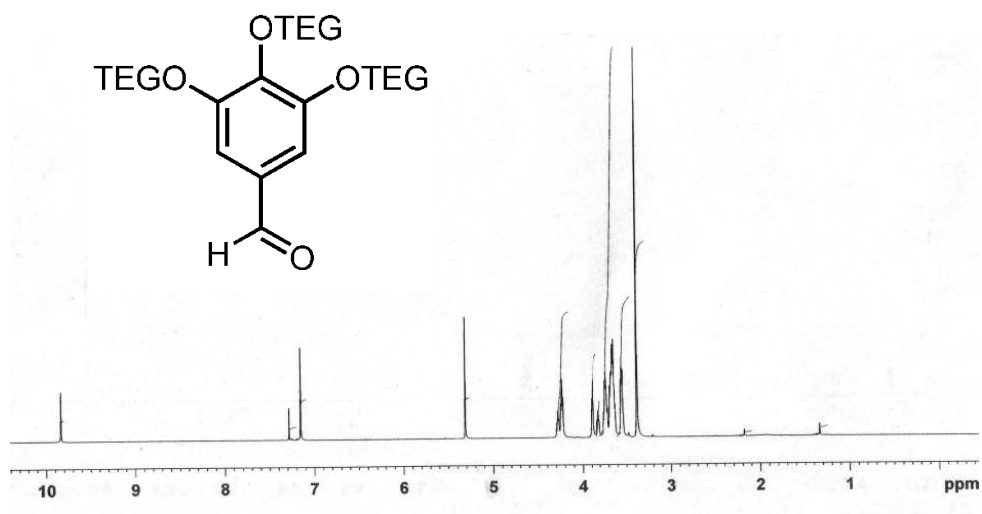


Figure 84. ¹H spectrum of Compound 22.

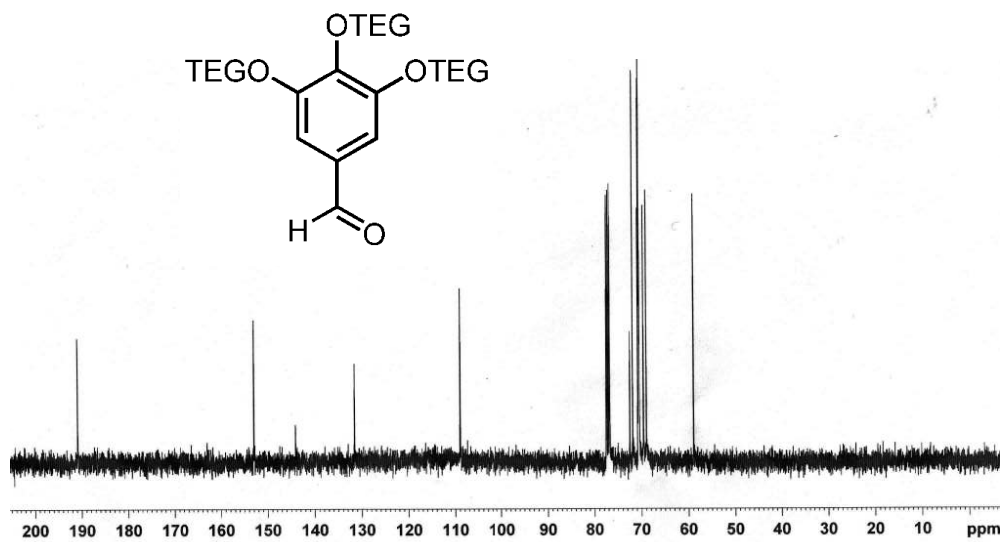


Figure 85. ¹³C spectrum of Compound 22.

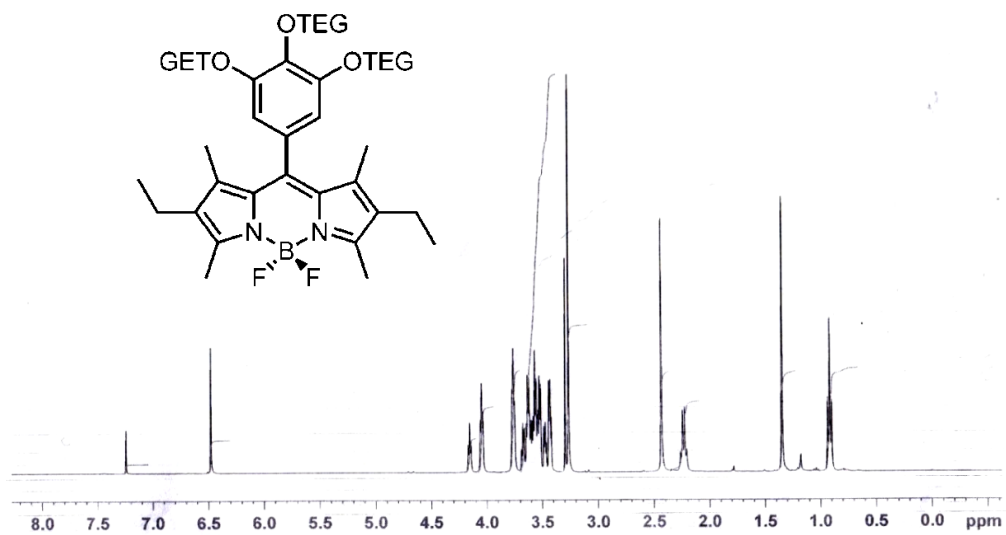


Figure 86. ¹H spectrum of Compound 23.

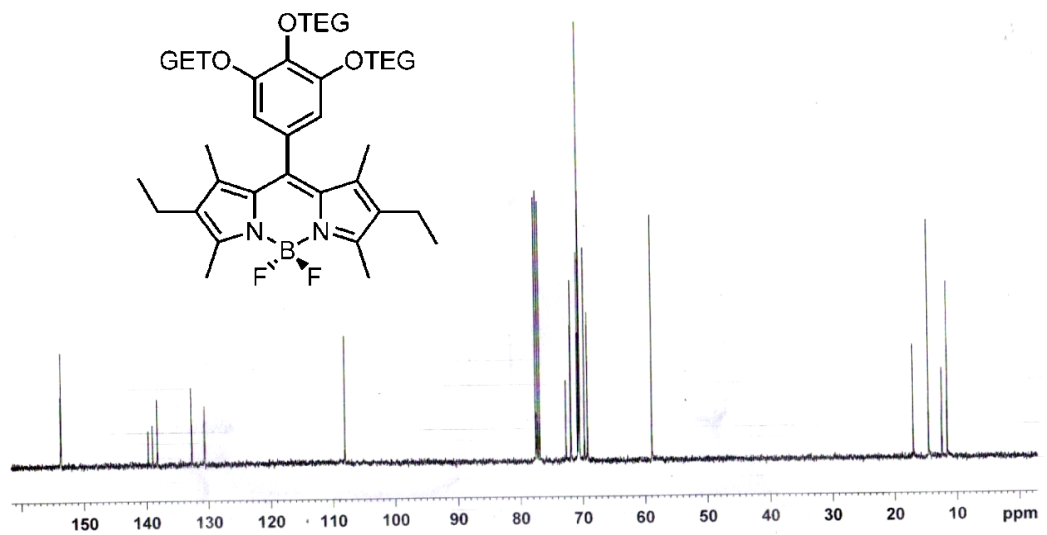


Figure 87. ¹³C spectrum of Compound 23.

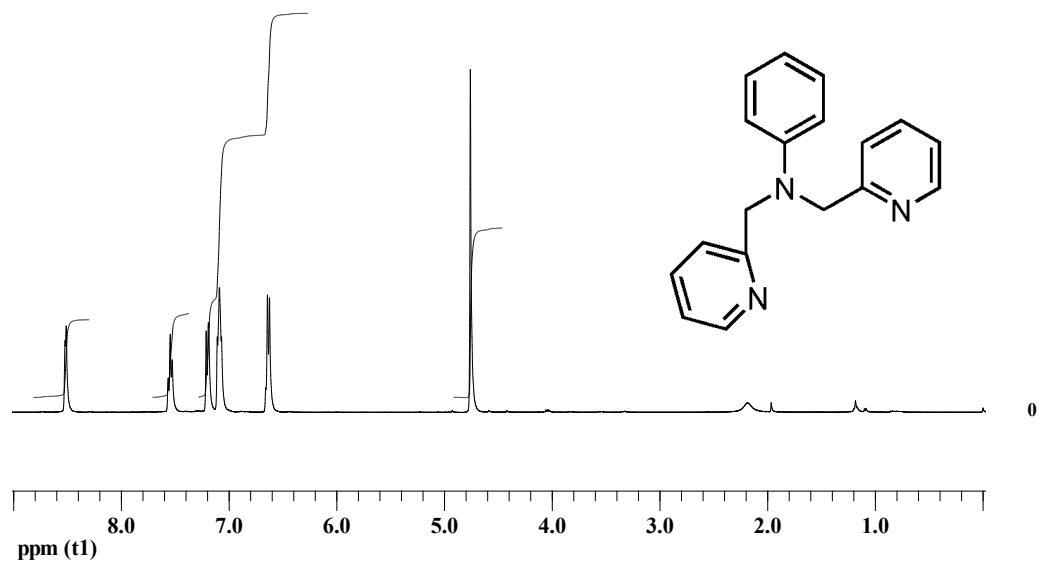


Figure 88. ¹H spectrum of Compound 26.

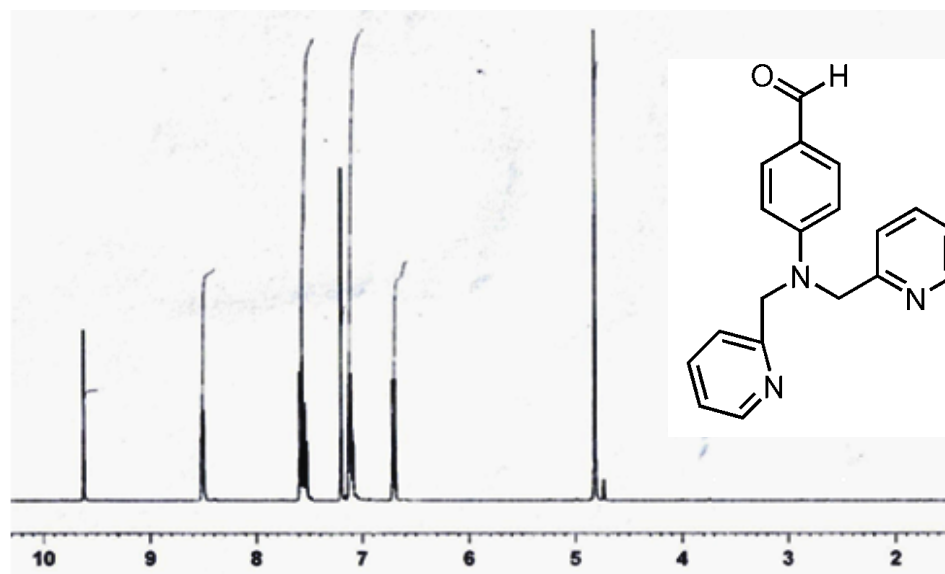


Figure 89. ¹H spectrum of Compound 27.

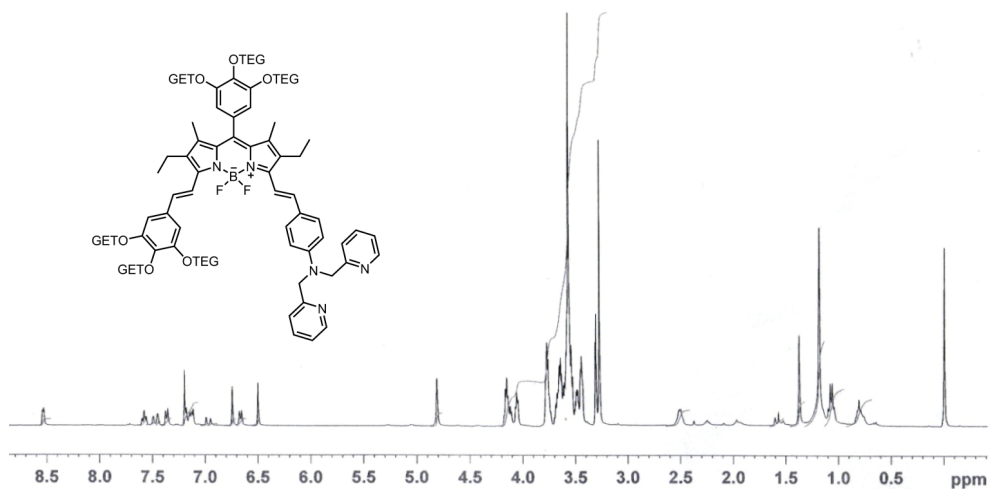


Figure 90. ¹H spectrum of Compound 29.

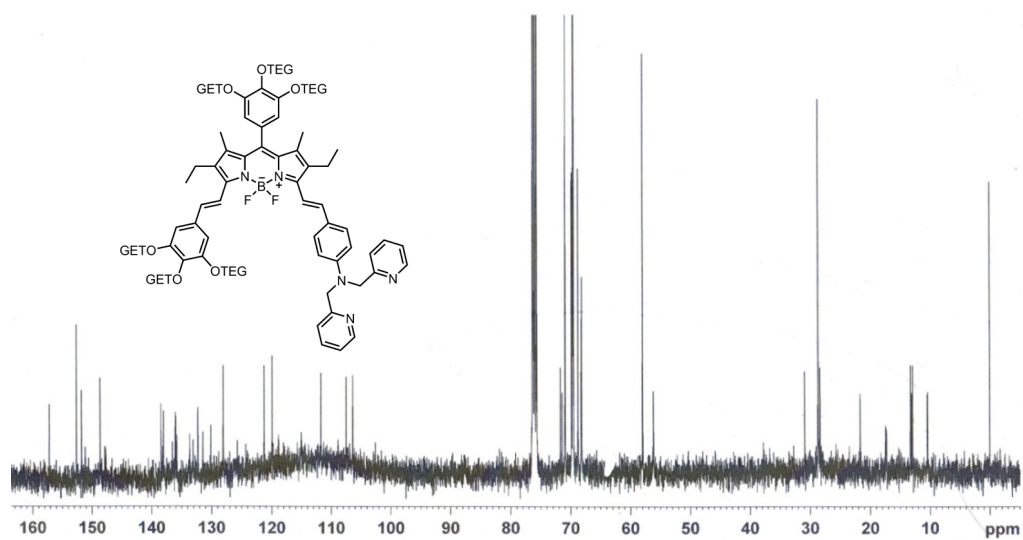


Figure 91. ¹³C spectrum of Compound 29.

APPENDIX B

MASS SPECTRA

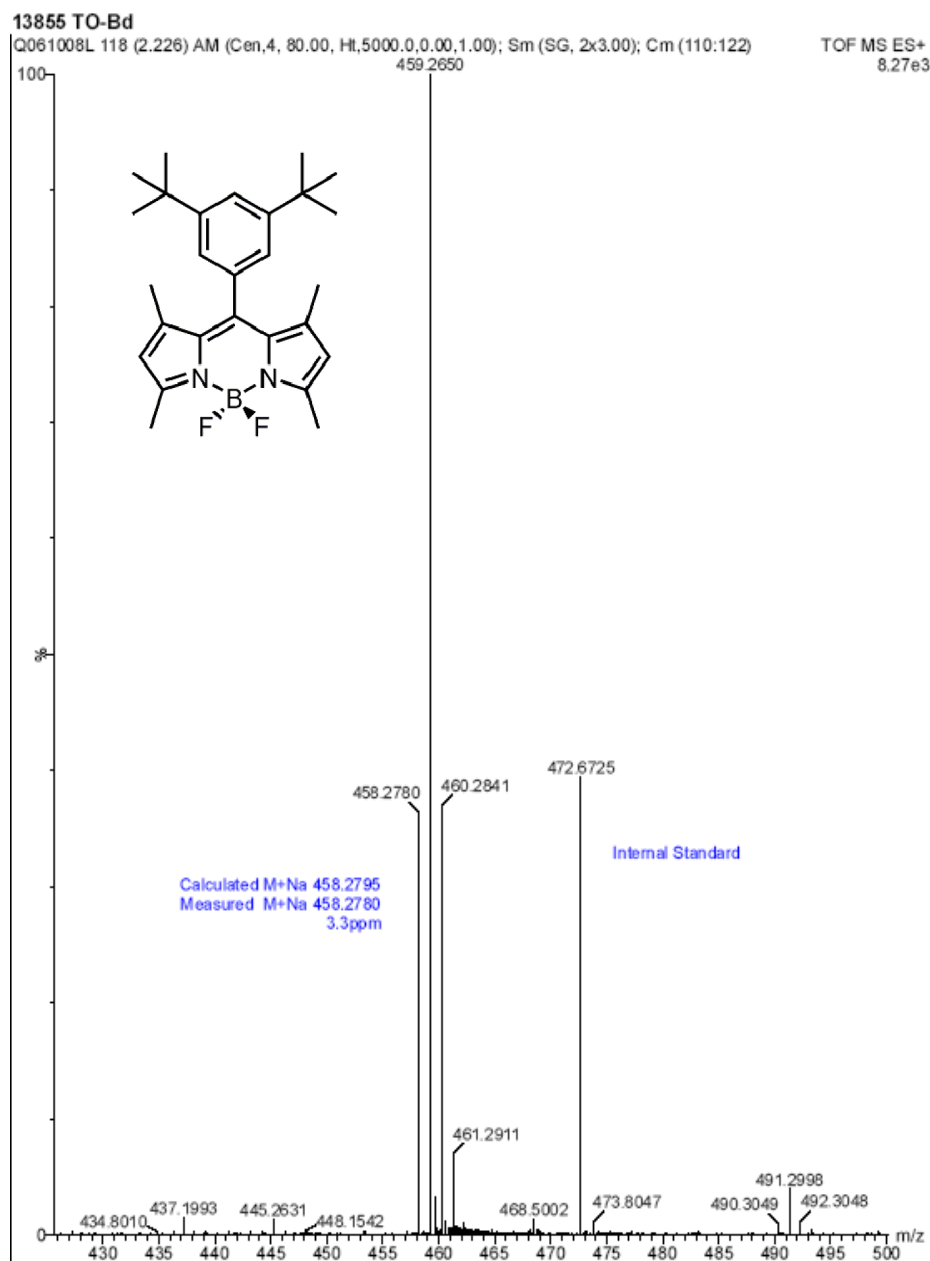


Figure 92. Mass spectrum of Compound 6.

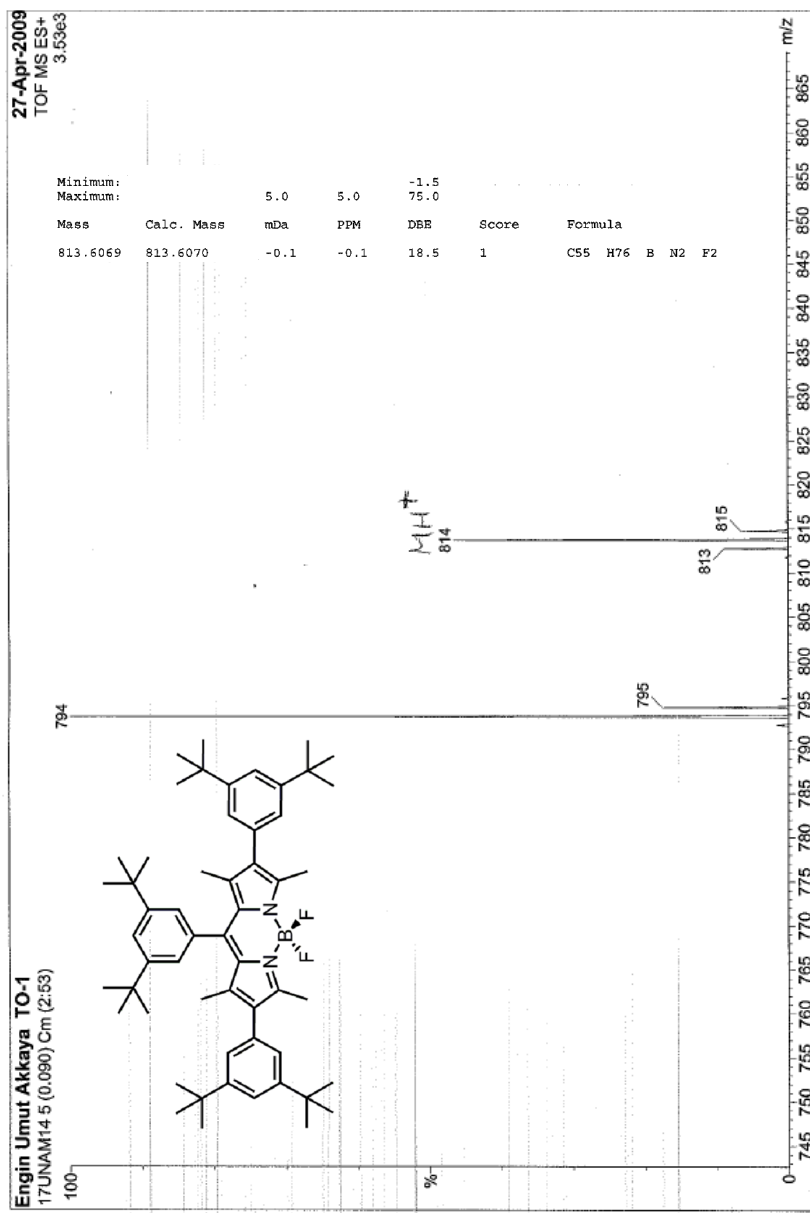


Figure 93. Mass spectrum of Compound 9.

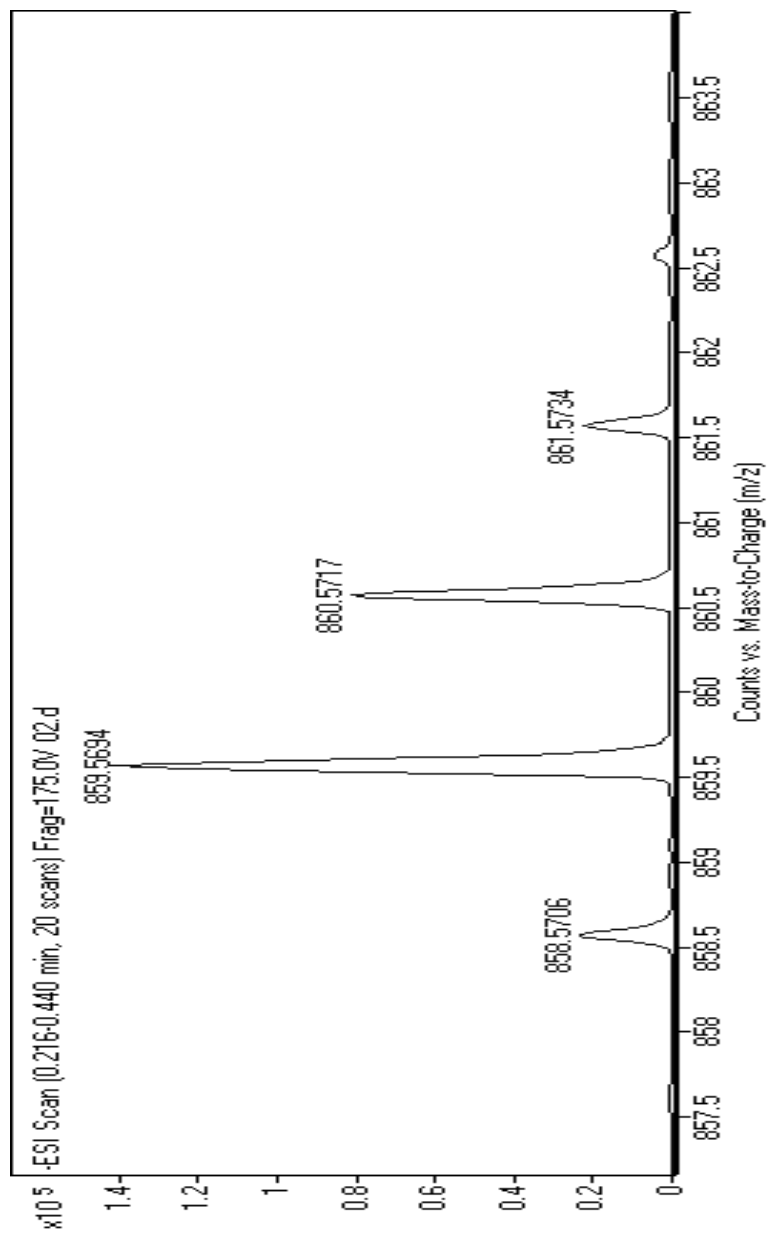


Figure 94. Mass spectrum of Compound 11.

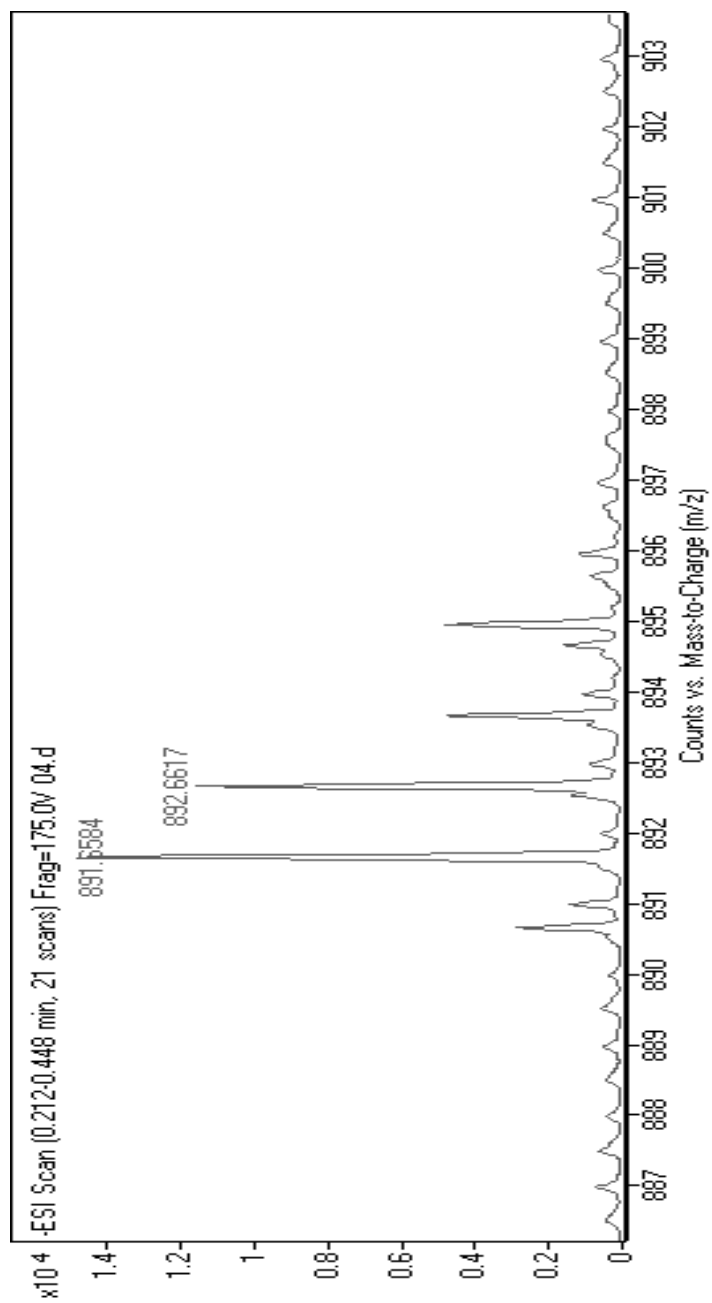


Figure 95. Mass spectrum of Compound 15.

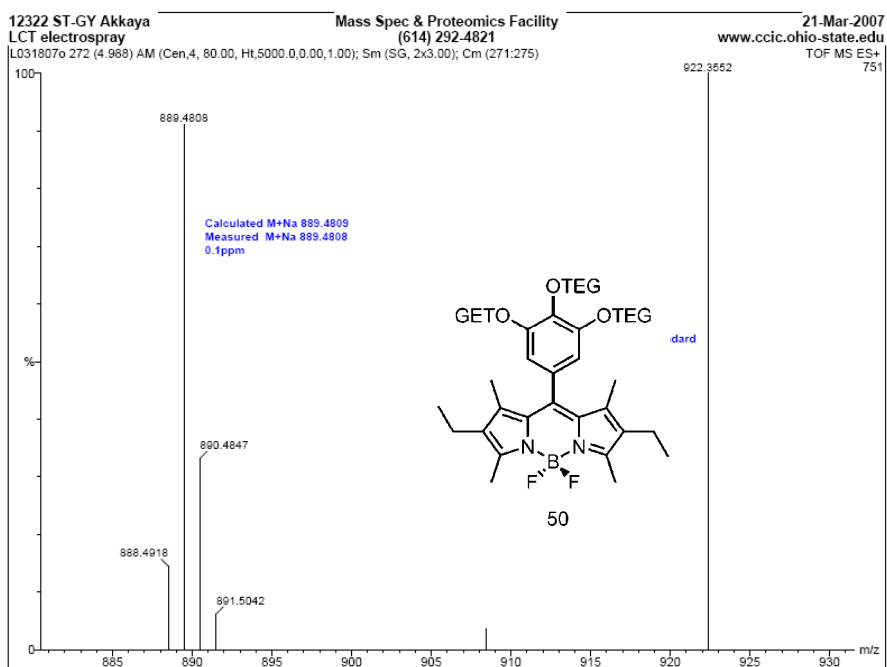


Figure 96. Mass spectrum of Compound 23.

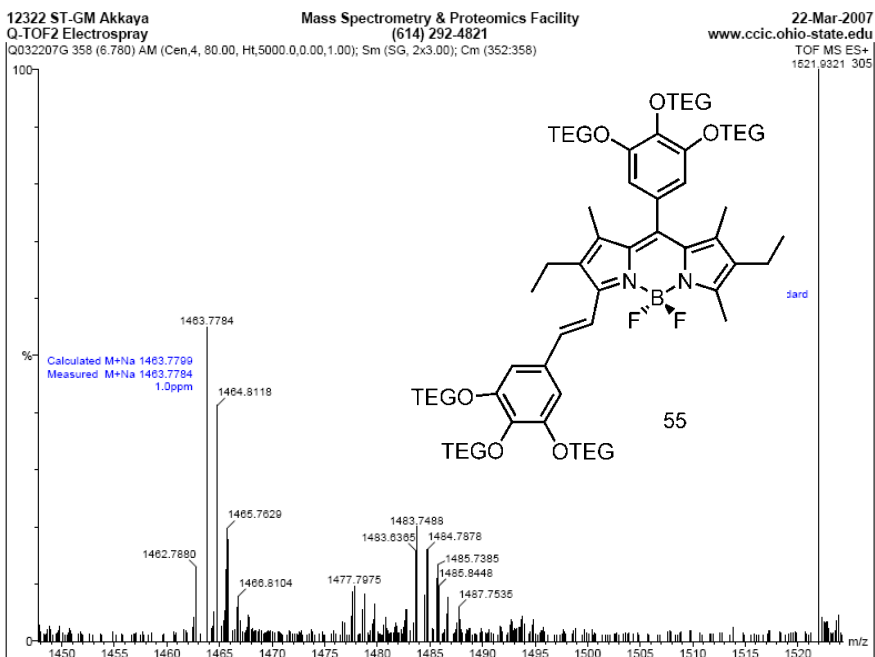


Figure 97. Mass spectrum of Compound 28.

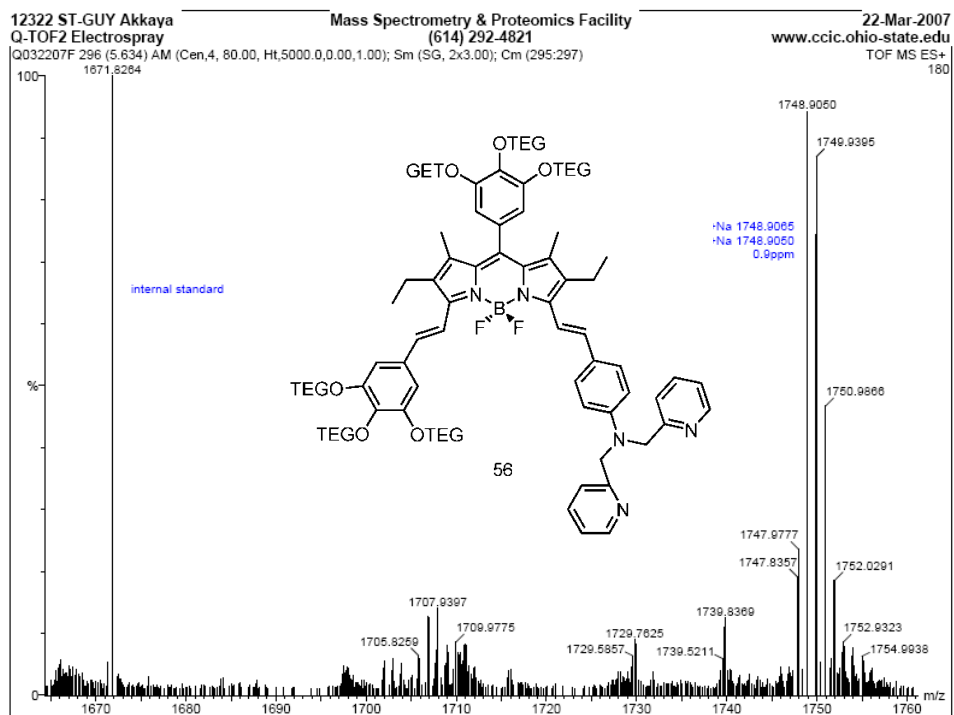


Figure 98. Mass spectrum of Compound 29.

APPENDIX C

X-RAY DIFFRACTION STRUCTURE ANALYSIS

X-ray diffraction data were obtained on an Enraf-Nonius CAD4 (κ -geometry) diffractometer operating in $\omega/2\theta$ scan mode using graphite-monochromated MoK_α radiation ($\lambda = 0.71073 \text{ \AA}$) at room temperature. The lattice parameters and their estimated standard deviations were determined by using CAD4 Express. Three standard reflections were measured every 100 reflections and their intensities showed a good stability. Data reduction was carried out using XCAD4. The structures were solved by direct methods and refined by the full-matrix least-squares refinement on F using the programs SHELXS97 and SHELXL97, respectively, in the WinGX package. Atomic scattering factors were taken from the International Tables for X-ray Crystallography. The data collection details, crystals data and refinement parameters are summarized in Table 4. Positional parameters of non-hydrogen atoms are given in Table 5.

Perspective view of molecules is given in Figure 97. Selected bond lengths and angles are given in Table 6. The molecules are held together by weak van der Waals interactions. Hydrogen bond and molecular packing geometry of the molecules were calculated with PLATON and hydrogen bonding geometry is summarized in Table 7. Packing figures (Fig 48-50) are prepared by MERCURY program.

Table 4. Crystal data and experimental details of the title compounds.

	Compound 3	Compound 6
Empirical formula	C ₂₇ H ₃₅ B F ₂ N ₂	C ₂₇ H ₃₅ B F ₂ N ₂
Formula weight	436.38	436.38
Crystal system	Monoclinic	Triclinic
Space group	P 2/c	P $\bar{1}$
Crystal shape /color	Prism/orange	Prism/red
Unit cell dimensions		
a (Å)	6.7325(10)	8.2514(10)
b (Å)	12.196(2)	11.4775(10)
c (Å)	15.301(2)	13.7766(10)
α (°)	90	73.867(8)
β (°)	101.739(10)	79.099(7)
γ (°)	90	89.638(8)
Volume (Å ³)	1230.1(3)	1229.2(2)
Z	2	2
D _{calc} (Mg/m ³)	1.283	1.179
Absorbtion coefficient (mm ⁻¹)	0.078	0.078
F(000)	468	468
<i>h, k, l</i> ranges	-8 → 0, -15 → 0, -18 → 19	-10 → 10, -14 → 0, 0 → -17
Refinement on F ²	$w = 1 / [\sigma^2 F_0^2 + (0.0893P)^2]$, P = (F ₀ ² + 2F _c ²)/3	$w = 1 / [\sigma^2 F_0^2 + (0.089P)^2]$, P = (F ₀ ² + 2F _c ²)/3
Reflections collected/unique	2635/2433 [R _{int} =0.1121]	5194/4929 [R _{int} =0.0467]
Parameters	151	309
Goodness of fit on F ²	0.883	0.951
R indices [I>2σ(I)]	R ₁ =0.0737, wR ₂ =0.1497	R ₁ =0.0615, wR ₂ =0.1427
R indices [all data]	R ₁ =0.3316, wR ₂ =0.2156	R ₁ =0.2240, wR ₂ =0.1922
(Δ/σ) _{max}	0.000	0.000
Largest difference peak and hole (e/Å ³)	0.219 and -0.261	0.199 and -0.221

Additional material available from Cambridge Crystallographic Data Center as deposition numbers: CCDC 712038, 712037.

Table 5. Atomic coordinates and equivalent isotropic displacement parameters for non-hydrogen atoms of compound **3**.

$$U_{eq} = (\frac{1}{3}) \sum_i \sum_j U_{ij} a_i^* a_j^* a_i a_j$$

Atom	x	y	z	$U_{eq} (\text{\AA}^2)$
B	0.5	0.1545(7)	0.25	0.052(2)
F	0.4398(5)	0.0887(2)	0.3133(2)	0.0977(13)
N	0.3248(6)	0.2285(3)	0.2057(2)	0.0431(11)
C1	0.1418(8)	0.1957(4)	0.1596(3)	0.0493(14)
C2	0.0227(7)	0.2876(5)	0.1317(3)	0.0588(15)
C3	0.1349(8)	0.3797(4)	0.1592(3)	0.0479(14)
C4	0.3265(7)	0.3429(4)	0.2068(3)	0.0394(12)
C5	0.0834(8)	0.0778(4)	0.1425(4)	0.0724(17)
C6	0.0593(7)	0.4943(4)	0.1384(3)	0.0644(16)
C7	0.5	0.3973(5)	0.25	0.0383(17)
C8	0.5	0.5194(5)	0.25	0.0373(17)
C9	0.4690(6)	0.5778(4)	0.3242(3)	0.0415(13)
C10	0.4677(7)	0.6916(4)	0.3260(3)	0.0422(12)
C11	0.5	0.7453(6)	0.25	0.045(2)
C12	0.4308(8)	0.7556(4)	0.4067(3)	0.0525(15)
C13	0.4325(9)	0.6833(4)	0.4877(3)	0.0674(17)
C14	0.2234(9)	0.8116(5)	0.3822(4)	0.097(2)
C15	0.5966(10)	0.8423(4)	0.4322(4)	0.086(2)

Table 6. Atomic coordinates and equivalent isotropic displacement parameters for non-hydrogen atoms of compound **6**.

Atom	x	y	z	$U_{eq}(\text{\AA}^2)$
B	0.4775(5)	0.7252(4)	0.3338(3)	0.0442(10)
F1	0.4107(3)	0.6282(2)	0.41692(14)	0.0755(7)
F2	0.5378(2)	0.8137(2)	0.36973(15)	0.0710(7)
N1	0.6164(3)	0.6831(2)	0.26225(18)	0.0408(7)
N2	0.3441(3)	0.7761(2)	0.27113(19)	0.0416(7)
C1	0.7543(4)	0.6295(3)	0.2872(2)	0.0452(9)
C2	0.8543(4)	0.6062(3)	0.2003(3)	0.0462(9)
C3	0.7728(4)	0.6465(3)	0.1188(2)	0.0426(8)
C4	0.6223(4)	0.6954(3)	0.1573(2)	0.0385(8)
C5	0.7878(7)	0.6001(5)	0.3939(3)	0.0627(12)
C6	1.0161(5)	0.5462(3)	0.2004(3)	0.0629(11)
C7	0.9967(6)	0.4082(4)	0.2334(3)	0.0887(15)
C8	0.8378(4)	0.6395(3)	0.0112(2)	0.0570(10)
C9	0.4928(4)	0.7479(3)	0.1105(2)	0.0374(8)
C10	0.3556(4)	0.7886(3)	0.1661(2)	0.0392(8)
C11	0.2091(4)	0.8413(3)	0.1385(3)	0.0446(9)
C12	0.1123(4)	0.8607(3)	0.2259(3)	0.0477(9)
C13	0.1990(4)	0.8192(3)	0.3062(3)	0.0479(9)
C14	0.1597(4)	0.8720(3)	0.0343(2)	0.0599(11)

C15	-0.0509(4)	0.9190(3)	0.2332(3)	0.0623(11)
C16	-0.0317(5)	1.0561(4)	0.2069(3)	0.0844(14)
C17	0.1446(5)	0.8170(4)	0.4173(3)	0.0654(11)
C18	0.4988(4)	0.7571(3)	-0.0001(2)	0.0388(8)
C19	0.4483(4)	0.6595(3)	-0.0283(2)	0.0472(9)
C20	0.4597(4)	0.6642(3)	-0.1311(2)	0.0513(10)
C21	0.5223(4)	0.7673(3)	-0.2102(2)	0.0464(9)
C22	0.5666(5)	0.8656(3)	-0.1794(3)	0.0565(10)
C23	0.5569(5)	0.8618(3)	-0.0775(3)	0.0528(10)
C24	0.5374(5)	0.7736(3)	-0.3243(3)	0.0554(10)
C25	0.5161(7)	0.6496(4)	-0.3401(3)	0.0985(17)
C26	0.7059(5)	0.8304(4)	-0.3862(3)	0.0917(15)
C27	0.4068(6)	0.8561(5)	-0.3683(3)	0.0994(17)

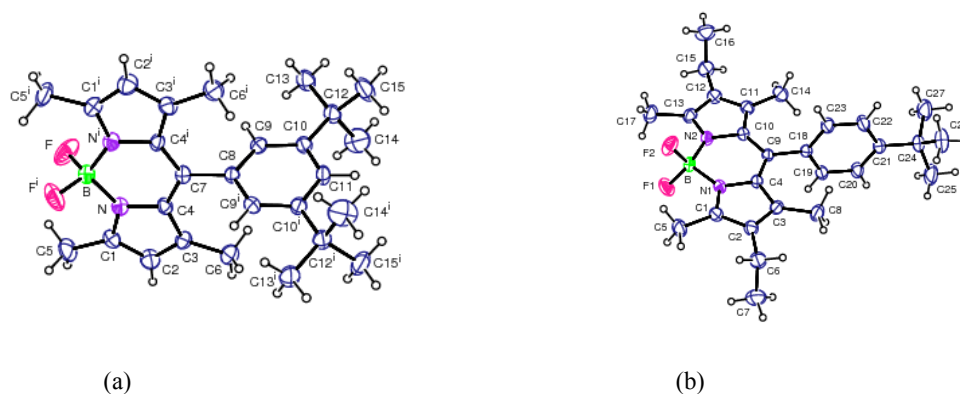


Figure 99. ORTEP drawing of the molecular structure of the title compounds with the atomic numbering scheme. a) Compound **3**, b) Compound **6**.

Table 7. Selected bond lengths (Å) and bond angles (°).

Compound 3		Compound 6	
B – F	1.381(5)	B – F1	1.384(4)
		F2 – B	1.380(4)
N – C1	1.350(5)	N1 – C1	1.346(4)
N – C4	1.395(5)	N1 – C4	1.405(3)
B – N	1.530(6)	N1 – B	1.533(4)
		N2 – B	1.538(5)
		N2 – C13	1.349(4)
		N2 – C10	1.398(4)
F – B – F ⁱ	108.9(7)	F2 – B – F1	108.9(3)
F – B – N ⁱ	110.0(2)	F2 – B – N1	110.3(3)
F – B – N	110.11(19)	F1 – B – N1	110.0(3)
		F1 – B – N2	109.8(3)
		F2 – B – N2	110.3(3)
N ⁱ – B – N	107.7(6)	N1 – B – N2	107.6(3)
B – N – C1	126.6(5)	B – N1 – C1	126.9(3)
B – N – C4	125.5(5)	B – N1 – C4	125.4(3)
		B – N2 – C10	125.3(3)
		B – N2 – C13	126.6(3)

Symmetry code i: 1-x, y, 1/2-z

Table 8. Structural parameters of hydrogen bonds between donor (D), acceptor (A) and hydrogen (H).

Compound	D – H ... A	D–H (Å)	A...H (Å)	D...A (Å)	D–H...H (°)
3	C5 – H5C...F	1.01(5)	2.55(6)	3.173(8)	120(4)
6	C5 – H5C...F1 ^a	0.98(5)	2.35(5)	3.315(4)	166(4)

Symmetry codes [a: 1-x, 1-y, 1-z]

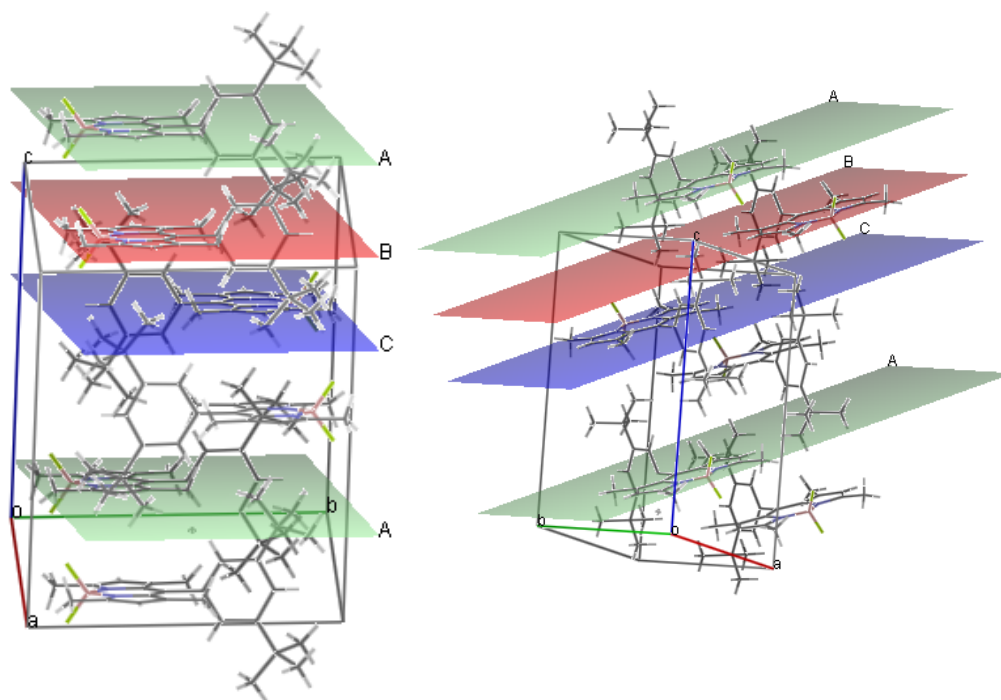


Figure 100. Two different views of the packing diagram of the title compound **3**. Planes A, B and C are the closest near parallel π -surfaces defined as the boradiazaindacene framework.

Table 9. The distance between the closest near parallel π -surfaces for compound **3**.

Number	Object1	Object2	Length
1	1  A	2  B	3.578
2	2  A	3  C	7.172
3	3  B	4  C	3.594
4	4  A	5  A	14.344

Table 10. The distance between the closest near parallel π -surfaces for compound **6**.

Number	Object1	Object2	Length
1	1  A	2  B	3.505
2	2  B	3  C	3.505
3	3  A	4  A	10.063

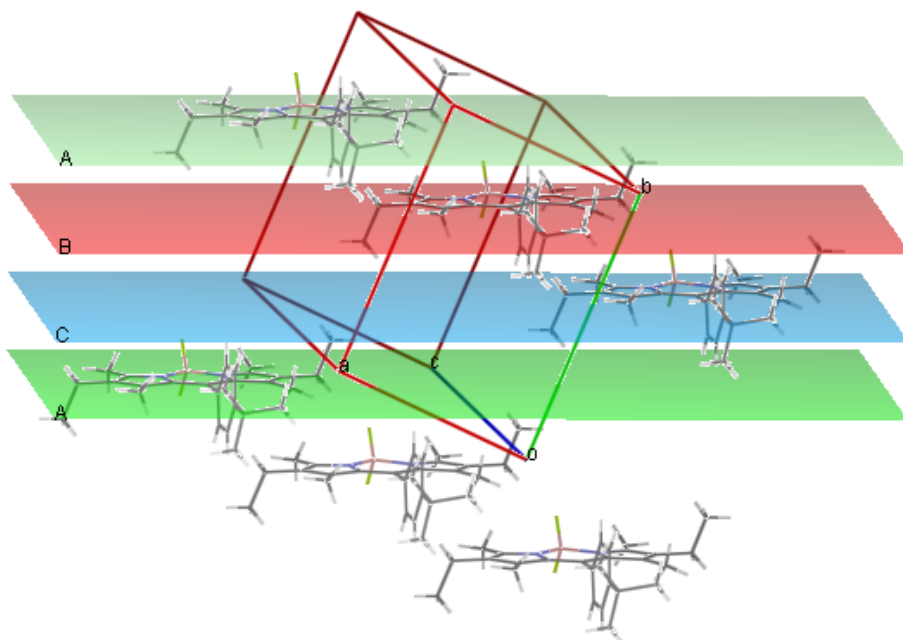


Figure 101. Packing diagram of the title compound **6**. Planes A, B and C are the closest near parallel π -surfaces defined as the boradiazaindacene framework.

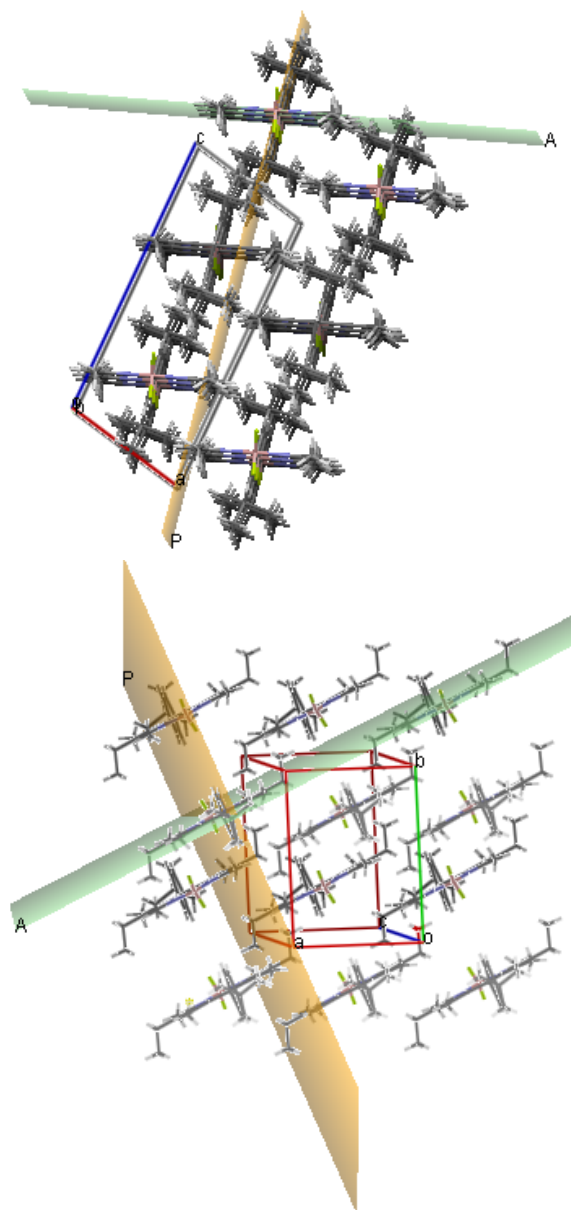


Figure 102. View of the plane defined by the bodipy π -surfaces (A) and 8-phenyl substituent (P), dihedral angle between the A and P is 84.35° and 79.56° for compound **3** and **6** respectively.

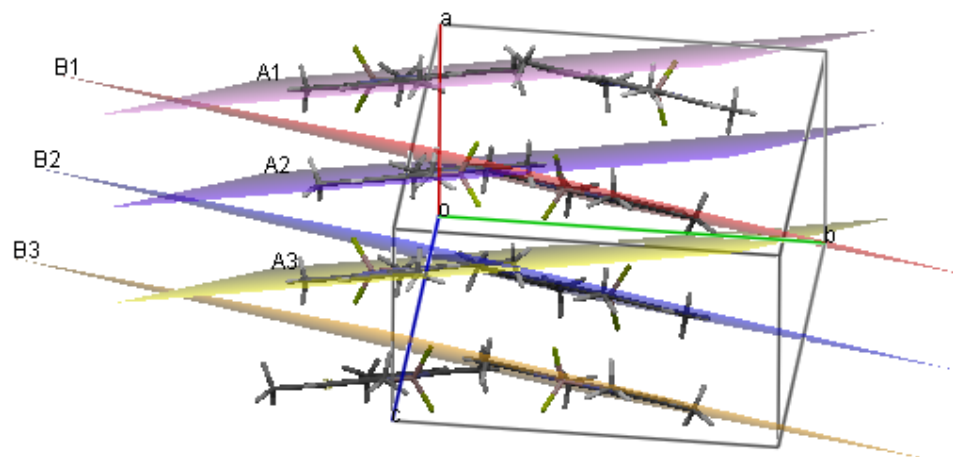


Figure 103. Packing diagram of the of the bodipy dye with no meso substituent studied as a reference. Dihedral angle between the A and B group planes is 17.90° .

Table 11. The distance between the closest near parallel π -surfaces for the reference compound.

Number	Object1	Object2	Length
1	1 ■ A1	■ A2	3.419
2	2 ■ A2	■ A3	3.505
3	3 ■ B1	■ B2	3.505
4	4 ■ B2	■ B3	3.419

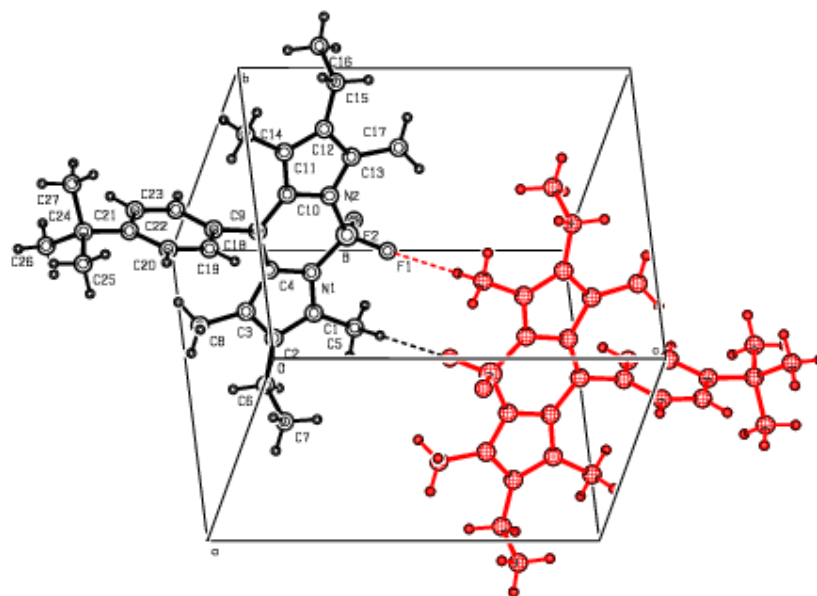


Figure 104. Hydrogen bonding geometry in compound 6.

All bond lengths (Å) and angles (°)

Compound (3)

B	F	1.381(5)
N	C1	1.350(5)
N	C4	1.395(5)
B	N	1.530(6)
C1	C2	1.394(6)
C1	C5	1.500(6)
C3	C2	1.372(6)
C3	C6	1.499(6)
C4	C7	1.389(5)
C4	C3	1.419(6)
C8	C7	1.489(8)
C9	C8	1.392(5)
C10	C9	1.388(6)
C10	C11	1.390(5)
C10	C12	1.524(6)
C12	C13	1.519(6)
C14	C12	1.531(7)
C15	C12	1.529(7)

Compound (6)

F1	B	1.384(4)
F2	B	1.380(4)
N1	C1	1.346(4)
N1	C4	1.405(3)
N1	B	1.533(4)
N2	C13	1.349(4)
N2	C10	1.398(4)
N2	B	1.538(5)
C1	C5	1.492(5)
C2	C1	1.410(4)
C2	C6	1.499(5)
C3	C2	1.385(4)
C3	C8	1.502(4)
C4	C9	1.399(4)
C4	C3	1.430(4)
C6	C7	1.522(5)
C9	C18	1.489(4)
C10	C9	1.397(4)
C10	C11	1.418(4)
C11	C12	1.385(4)

C11	C14		1.514(4)
C12	C13		1.402(4)
C12	C15		1.499(5)
C13	C17		1.505(4)
C16	C15		1.516(5)
C18	C19		1.374(4)
C19	C20		1.387(4)
C21	C22		1.384(4)
C21	C20		1.390(4)
C21	C24		1.534(4)
C23	C22		1.379(4)
C23	C18		1.383(4)
C24	C25		1.515(5)
C24	C26		1.530(5)
C27	C24		1.530(5)

Compound (3)

F	B	F ⁱ	108.9(7)
F	B	N ⁱ	110.0(2)
F	B	N	110.11(19)

N ⁱ	B	N	107.7(6)
C1	N	C4	107.9(4)
C1	N	B	126.6(5)
C4	N	B	125.5(5)
C9	C10	C11	116.9(5)
C9	C10	C12	122.1(4)
C11	C10	C12	121.0(4)
C7	C4	N	119.2(5)
C7	C4	C3	133.0(5)
N	C4	C3	107.8(4)
C13	C12	C10	112.8(4)
C13	C12	C15	108.0(5)
C10	C12	C15	109.3(4)
C13	C12	C14	108.3(4)
C10	C12	C14	108.7(4)
C15	C12	C14	109.7(5)
C10	C11	C10 ⁱ	123.7(7)
C2	C3	C4	106.5(4)
C2	C3	C6	123.8(5)
C4	C3	C6	129.7(5)
C10	C9	C8	122.0(5)

N	C1	C2	109.2(4)
N	C1	C5	123.7(5)
C2	C1	C5	127.1(5)
C9	C8	C9 ⁱ	118.5(6)
C9	C8	C7	120.7(3)
C4	C7	C4 ⁱ	122.8(6)
C4	C7	C8	118.6(3)
C4 ¹	C7	C8	118.6(3)
C3	C2	C1	108.6(4)

Symmetry code i: 1-x, y, 1/2-z

Compound (6)

F2	B	F1	108.9(3)
F2	B	N1	110.3(3)
F1	B	N1	110.0(3)
F1	B	N2	109.8(3)
F2	B	N2	110.3(3)
N1	B	N2	107.6(3)
B	N1	C1	126.9(3)
B	N1	C4	125.4(3)

B	N2	C10	125.3(3)
B	N2	C13	126.6(3)
C1	N1	C4	107.7(3)
N1	C1	C2	110.4(3)
N1	C1	C5	122.4(3)
N1	C4	C9	120.0(3)
N1	C4	C3	107.6(3)
N2	C10	C9	120.3(3)
N2	C10	C11	107.2(3)
N2	C13	C12	110.1(3)
N2	C13	C17	122.3(3)
C13	N2	C10	108.1(3)
C1	C2	C6	124.8(3)
C2	C1	C5	127.3(4)
C2	C3	C4	107.1(3)
C2	C3	C8	124.5(3)
C2	C6	C7	113.0(3)
C3	C2	C1	107.2(3)
C3	C2	C6	128.0(3)
C4	C3	C8	128.4(3)
C4	C9	C18	119.3(3)

C9	C4	C3	132.4(3)
C9	C10	C11	132.5(3)
C10	C11	C14	128.2(3)
C10	C9	C4	121.3(3)
C10	C9	C18	119.3(3)
C11	C12	C13	106.8(3)
C11	C12	C15	127.0(3)
C12	C11	C10	107.8(3)
C12	C11	C14	124.0(3)
C12	C13	C17	127.7(3)
C12	C15	C16	112.3(3)
C13	C12	C15	126.1(3)
C18	C19	C20	121.2(3)
C19	C18	C23	117.8(3)
C19	C18	C9	120.3(3)
C19	C20	C21	121.9(3)
C20	C21	C24	122.5(3)
C21	C24	C27	109.1(3)
C22	C21	C20	115.6(3)
C22	C21	C24	121.9(3)
C22	C23	C18	120.4(3)

C23	C18	C9	121.9(3)
C23	C22	C21	123.0(3)
C25	C24	C26	108.4(3)
C25	C24	C21	112.3(3)
C25	C24	C27	109.3(3)
C26	C24	C21	110.7(3)
C26	C24	C27	106.9(3)